AD-A064 530 UTAH STATE UNIV LOGAN CENTER FOR ATMOSPHERIC AND SPA--ETC F/G 4/1
STUDIES OF THE DYNAMICS OF THE HIGH LATITUDE IONOSPHERE.(U)
OCT 78 W J RAITT F19628-77-C-0011

UNCLASSIFIED AFGL-TR-78-0261 NL

| OF |
AD A064530

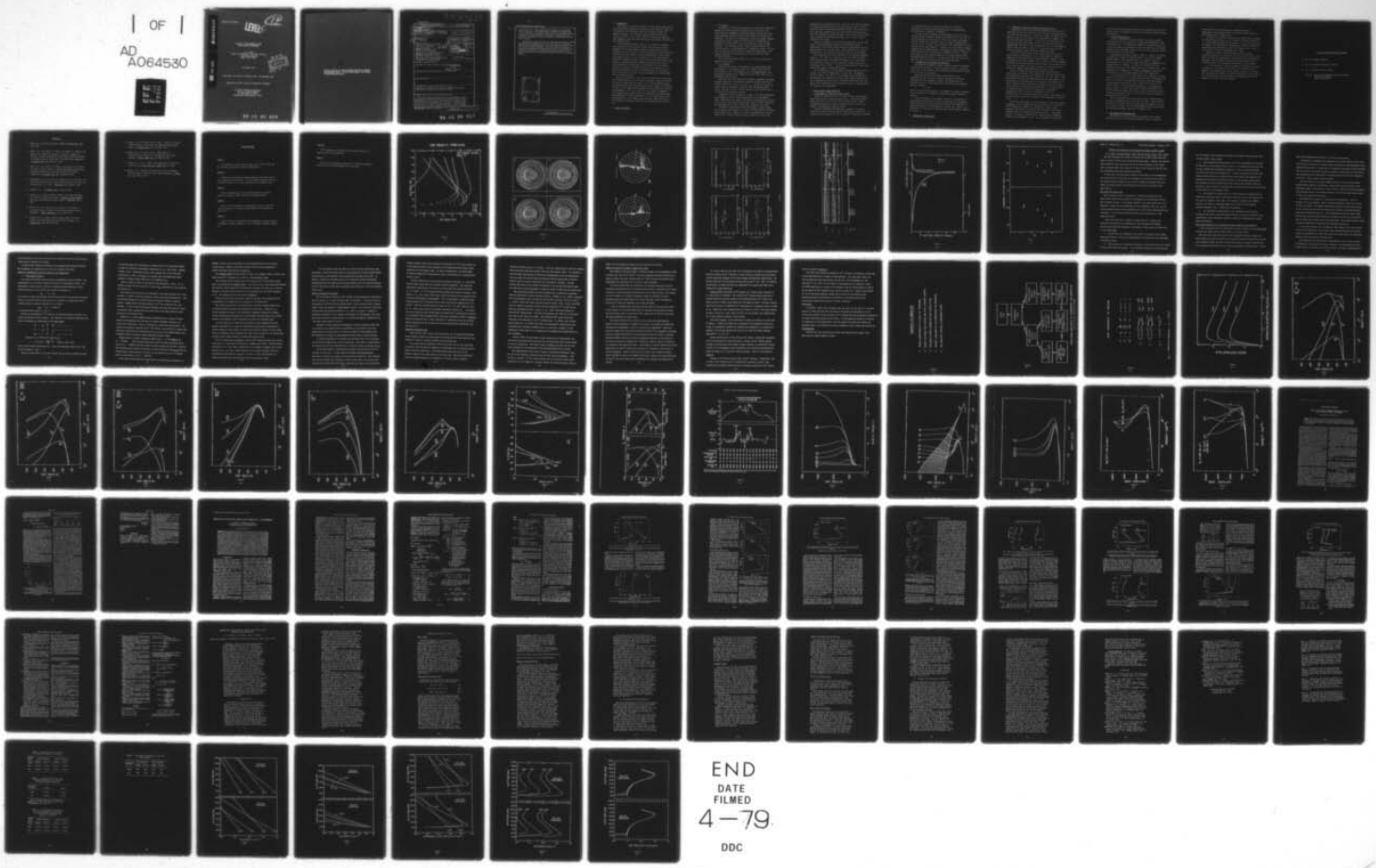

END
DATE FILMED
4-79
DDC

AFGL-TR-78-0261

LEVEL II

12 NW

STUDIES OF THE DYNAMICS OF THE HIGH LATITUDE IONOSPHERE

W. J. RAITT
Center for Atmospheric and Space Sciences
Utah State University
Logan, Utah, 84322

26 October 1978

Final Report for Period 11 November 1976 - 30 September 1978

Air Force Geophysics Laboratory
Air Force Systems Command
United States Air Force
Hanscom AFB, Massachusetts 01731

(9) Final rept. 11 Nov 76-30 Sep 78,

Unclassified

SECURITY CLASSIFICATION OF THIS PAGE (When Data Entered)

REPORT DOCUMENTATION PAGE	READ INSTRUCTIONS BEFORE COMPLETING FORM
(19) 1. REPORT NUMBER (18) AFGL-TR-78-0261	2. GOVT ACCESSION NO. 3. RECIPIENT'S CATALOG NUMBER
4. TITLE (and Subtitle) (6) STUDIES OF THE DYNAMICS OF THE HIGH LATITUDE IONOSPHERE.	5. TYPE OF REPORT & PERIOD COVERED Final, 11/11/76-9/30/78
	6. PERFORMING ORG. REPORT NUMBER
7. AUTHOR(s) (10) W. J. Raitt	8. CONTRACT OR GRANT NUMBER(s) (15) F19628-77-C-0011 new
9. PERFORMING ORGANIZATION NAME AND ADDRESS Center for Atmospheric & Space Sciences Utah State University Logan, UT 84322 411067 NW	10. PROGRAM ELEMENT, PROJECT, TASK AREA & WORK UNIT NUMBERS (16) 61102F 2311G2AC (17) G2
11. CONTROLLING OFFICE NAME AND ADDRESS Office of Naval Research University of California, Berkeley Berkeley, California 94720	(11) 12. REPORT DATE 26 Oct 1978 13. NUMBER OF PAGES 87
14. MONITORING AGENCY NAME & ADDRESS (if different from Controlling Office) Air Force Geophysics Laboratory Hanscom AFB, Massachusetts 01731 Monitor/R. C. Sagalyn/I HR	15. SECURITY CLASS. (of this report) Unclassified
	15a. DECLASSIFICATION/DOWNGRADING SCHEDULE

16. DISTRIBUTION STATEMENT (of this Report)

Approved for public release; distribution unlimited.

(12) 88p.

17. DISTRIBUTION STATEMENT (of the abstract entered in Block 20, if different from Report)

18. SUPPLEMENTARY NOTES

19. KEY WORDS (Continue on reverse side if necessary and identify by block number)

Ionosphere, F-Region, High Latitude, Dynamics Polar Wind
Magnetospheric Convection, Electric Fields.

20. ABSTRACT (Continue on reverse side if necessary and identify by block number)

The report surveys theoretical and experimental studies of ionospheric dynamics made during the contract period. Two major aspects of this topic were studied; the outflow of He^+ from the earth's ionosphere, and the effect of magnetospheric convection on the high latitude ionosphere. Model programs were written to study the general characteristics of the outflow

He (4)

CONT'

DD FORM 1 JAN 73 1473 EDITION OF 1 NOV 65 IS OBSOLETE

Unclassified

SECURITY CLASSIFICATION OF THIS PAGE (When Data Entered)

411 067

79 02 09 029

He(+) N(+)

Cont

of He^+ and also to make quantitative estimates of the escape flux of this ion. An existing model program for studying the effect of convection electric fields on the F-region was updated and the N^+ ion was included in the model. Initial work was started to incorporate realistic convection trajectories in the model program.

Experimental data from the S3-2 satellite was used to compare with theoretical predictions of both the variation of plasma density with perpendicular electric field and the onset of light ion outflow at high latitudes. While the light ion outflow showed good agreement with theory, the effects of perpendicular electric fields did not and provided further stimulus to incorporate the effect of convection trajectories in our ionospheric models.

1. INTRODUCTION

This report is a survey of work done on the dynamic nature of the near earth plasma forming the ionosphere at high latitudes, which for the purpose of this study was taken to be poleward of about 45^{o} magnetic latitude. The work done largely concerned theoretical studies of aspects of the dynamic nature of this plasma. However, some comparisons were made with experimental observations from the Air Force Satellite S3-2.

The two dominant dynamic effects of the ionospheric plasma at high latitudes are the outflow of light ions from the near earth ionosphere to the magnetosphere, and the convection motion of the plasma as the result of the $\bar{E} \times \bar{B}$ force resulting from electric fields which map into the ionosphere from the magnetosphere. Both effects are thought to play role in the formation of a very characteristic night time ionospheric feature known as the mid-latitude trough. This feature is commonly observed by numerous techniques, but, as yet, a fully satisfactory explanation of its formation is not available. Besides the intrinsic scientific interest in this feature it is of practical significance in that its characteristics are variable to such an extent that its effect on radio propagation in high latitude regions is unpredictable.

Most of the studies of light ion outflow made under this contract were directed towards He^{+}, an ion which is known to exist but has not been widely studied with the respect to its outflow characteristics. An important application of the results of these studies is related to the use of He^{+} in mapping the plasmasphere and in particular locating the plasmapause. He^{+} is the only ion at the distance plasmapause which enables optical observation of this boundary to be made using the phenomenon of resonant scattering. He^{+} is a very useful ion for this purpose since the resonant scattering wave length of 304 $\mathring{A}$ is a very strong solar emission line due to the abundance of He^{+} in the sun.

2. LIGHT ION OUTFLOW

2. H^+ Outflow

Our studies of H^+ outflow made under this contract were limited to improving our model program developed earlier to include a term representing the phenomenon of diffusion-thermal conductivity in the energy transport equation of the H^+ ions flowing out through an O^+ background. The effect of including this term in the energy transport equation was found to reduce the high altitude H^+ temperature of 3000-4000^o K by about 600^o K above altitudes of the order of 1000 kilometers. The diffusion-thermal effect therefore proved to be a significant factor in determining the H^+ temperature profile. We feel that the addition of this term was a significant improvement in our computer model for the distribution of H^+ in and above the high latitude ionosphere.

This work was published (Schunk et al., 1977) and a reprint is appended to this report.

2.2 He^+ Outflow

During the early part of the contract, we started work on the development of a new program to model the outflow of He^+ from the source region in the low ionosphere out to the magnetosphere. The program was developed on the assumption that He^+ was a minor ion, an experimently observed fact.

The model solves the coupled He^+ continuity, momentum and energy transport equations in a background ionosphere computed from our H^+ - O^+ model referred to earlier in section 2.1. For our first study we used the neutral atmosphere of Jacchia (1964) modified by Walker (1965). The source of He^+ is photo ionization of He and the loss is in reactions with molecular nitrogen.

A parametric study was made for a range of He^+ outflow velocities and ionospheric electric fields perpendicular to the geomagnetic field. Additionally the change in He density reflecting the so called "winter bulge " and changes in N_2 density typical of those observed at high latitudes during active periods were included in the study.

The general conclusions were that He^+ density profiles showed similar general characteristics to those of H^+ when the He^+ is flowing away from the earth. However, the effect of perpendicular electric fields on He^+ is quite different from the effect on H^+ due to the

different source mechanisms for the He^+ ions. The velocity profiles also differ considerably, He^+ increasing from near zero to its full outflow velocity at much higher altitudes than H^+. This results in a much less Joule heating for the He^+ ions thereby resulting in much lower He^+ temperatures at high altitudes. More details of this study can be found in the published paper (Raitt et al., 1977) which is appended to this report.

During our studies of He^+ outflow described above, we were made aware of some experimental observations by Hoffman (Private communication, 1977) which showed substantial disagreement with the absolute value of our escape fluxes. This prompted us to look into improvements in the quantitative results of our He^+ outflow model.

We incorporated the latest MSIS model of the neutral atmosphere (Hedin et al., 1977a, b), used more recent He^+ photo ionization cross sections (Stewart and Webb, 1963, Baker et al, 1961) and the solar EUV fluxes measured on the atmospheric explorer satellites (Hinteregger et al., 1978). Also, we allowed for solar zenith angle changes from summer to winter hemispheres.

The incorporation of the new model atmosphere enabled realistic account to be taken of summer/winter, solar cycle, and magnetic activity effects. The effect of the parameters were studied and it was found that the computed He^+ outward fluxes showed substantially better agreement with the results of Hoffman (1978) and we feel that these results represent the best theoretical basis for predicting the He^+ content of the plasmasphere.

3. HIGH LATITUDE PLASMA CONVECTION

3.1 Improvements to Multi-Ion F-Region Model

During the latter part of the contract, we have been working on improving the multi-ion model derived earlier. This model computes height profiles of O^+, O_2^+, NO^+, N_2^+ by solution of the coupled continuity and momentum transport equations for these ions in the presence of perpendicular electric fields.

We first incorporated the MSIS model atmosphere, revised UV fluxes and the most recently published chemical rate coefficients. In addition we have extended the code to compute N^+ densities in response

to recent observations of regions of enhanced N^+ densities, particularly in high latitude locations where the perpendicular electric fields is found to be enhanced.

We were currently working on this program at the end of the contract period to generate steady state profiles of O^+, O_2^+, NO^+, N^+, and N_2^+ densities for the range of solar cycle, season and magnetic activity conditions encountered, and for a range of perpendicular electric fields. We have a minor problem in the convergence of the N^+ solution at the upper boundary. A typical set of ion density profiles computed from the improved multi-ion program is shown in figure 1, but the N^+ density profile should not be considered as final. A paper describing this work has been submitted to the Fall meeting of the American Geophysical Union. It is anticipated that this work will be continued under a new contract currently being negotiated.

3.2 Incorporation of Ionospheric Convection

The important ionospheric dynamic condition known as ionospheric convection was referred to in the introductory section. During the latter part of the contract period ground work was started to include this in the multi-ion program.

Some work was done in surveying current models of the equipotential over the polar cap which represent the convection trajectories of the ionospheric plasma. The magnitude of the convection velocity is determined by $\bar{E} \times \bar{B}$ and $\bar{E}$ can be determined from the relation

$$E = \nabla \emptyset$$

where 0 is the electric potential. An example of a simple convection pattern in which the co-rotation field has been added is shown in figure 2.

At the termination of the contract we were at the position of using E and the direction of $\bar{E} \times \bar{B}$ to follow packets of ionospheric plasma through the convection pattern to start on the generation of a comprehensive model of ionization over the polar cap. Again it is hoped that this work will be continued under the new contract referred to earlier.

4. EXPERIMENTAL OBSERVATIONS

4.1 Comparison of Electric Fields and Plasma Densities

During the course of the contract period we received data from AFGL taken from the S3-2 satellite from instruments measuring electric field and electron densities. We selected a number of passes over the Northern polar cap in different local time planes for magnetically quiet and disturbed conditions. The data was received mainly in the form of plots from AFGL examples of which for quiet and disturbed noon/midnight variations of the perpendicular electric field along the orbital track are shown in figure 3. In addition, some data was received on magnetic tapes for further computer analyses.

The electric field plots and their associated drift velocity plots show the characteristics of the plasma convection pattern in common with other observations of these phenomena. However, it must be remembered that these passages over the polar cap are not snapshots and during the 30 minute period required to make a trans-polar section of the orbit as shown in the plots in figure 3 there may have been substantial changes in the perpendicular electric field.

One of our objectives was to relate these observations to predictions of the effect of the perpendicular electric field and the electron density published earlier (Schunk et al., 1975, 1976). This was attempted for quiet and disturbed days in the noon/midnight local time plane for the daytime sector of the passes. The results are shown in figure 4 where the measured perpendicular electric field is plotted against the measured electron density. It can be seen that the expected reduction of electron density with increasing perpendicular electric field is not apparent. This is in contradiction to the published theoretical studies of the steady state electron density profiles as a function of the perpendicular electric field.

We feel sure the reason for the discrepancy is that this a direct consequence of not incorporating convection correctly in our models, and not making due allowance for perpendicular electric field components that are not in the east/ west direction. These latter components result in north/south plasma drift with the consequent transport of plasma in altitude due to induced velocity components parallel to the geomagnetic field. It is experimental observations

such as this and similar observations by other workers that lead us to believe that it is important to pursue our convection studies outlined in section 3.2.

4.2 H+ S3-2 Outflow Data

The S3-2 instrument designed to measure ion drifts provides a useful monitor of the location of the region where substantial light ion outflow occur. The mechanism by which the instrument detects this is from the depth of the modulation of the ion current as the entrance aperture of the instrument rotates in and out of the satellite wake as the satellite spins in its orbit.

An example of the data is shown in figure 5. When H^+ is dominant the modulation is small as shown in region A, but when O^+ becomes dominant there is very deep modulation as is shown in region B. Unfortunately, in the center of region B the data is degraded by local charging effects. However, the onset of H^+ outflow is not so affected, and because of the rapid reduction of H^+ density above 1000 kilometers as it changes from diffusive equilibrium to even slow outflow there is a very rapid change in the H^+/O^+ compisition.

It is interesting to note that there is little change in electron density at this point, this verifies the theorectical predictions from Raitt et al.,(1977) which are shown in figure 6 where the change of electron density and the O^+/H^+ ratio is shown as a function of H^+ outflow velocity at 1500 kilometers altitude for no perpendicular electric field. It can be seen that O^+ becomes the dominant ion at outflow velocities greater than 1 km/sec, while the electron density changes by less than a factor of 2 from zero H^+ outflow velocity to 1 km/sec H^+ outflow velocity.

The relationship of this outflow start point to magnetospheric processes is emphasized by the plot shown in figure 7 which shows the variation of invariant latitude of this point with magnetic activity for the group of orbits near the noon/midnight meridian which covered both quiet and disturbed conditions in December, 1975.

5. CONCLUSIONS AND RECOMMENDATIONS

The problems of our understanding and predicting the dynamic characteristics of the high latitude ionosphere are of continuing

interest both from understanding the coupling between the magnetosphere and ionosphere and from practical aspects related to high frequency radio communication.

The degree of scientific interest can be judged by the attendance at sessions involving this topic at scientific conferences which the P.I. has attended including the presentation of a review on "Positive Ion Changes in the Thermasphere During Magnetic Storms" which the PI presented at the IAGA Meeting in Seattle in August, 1977, a copy of the transcript of which is appended to this report.

Theoretical studies and experimental studies have shown sufficient divergence to convince us that there is still much to learn about the effect of magnetospheric convection from the high latitude ionosphere, and we strongly recommend continuing support of both theoretical models and experimental observations of this problem.

It is not possible to come to any general conclusions in a topic as broad as is the subject of the contract, particularly as only segments of the whole problem can be studied. However, it is hoped that the material published, the review transcript and the content of this report provide a few more pieces in the complex puzzle of the dynamics of the high latitude ionosphere.

Scientists Contributing To Research

1. Dr. P. M. Banks, Professor

2. Dr. R. W. Schunk, Associate Professor

3. Mr. L. Pearson, Graduate Student

All at: Center for Atmospheric and Space Sciences
Utah State University
Logan, Utah 84322

References

1. Baker, D.J., D.E. Bedo, and Ditt, Tomboulian, Phys. Rev., 124, 1471, 1961

2. Hedin, A.E., J.E. Salah, J.V. Evans, C.A. Reber, G. P Newton, N.W. Spencer, D.C. Kayser, D. Alcayde°, P. Bauer, L. Cogger, J.P. McClure, A global thermospheric model based on mass spectrometer and incoherent scatter data, MSIS 1, N_2 density and temperature, J. Geophys. Res., 82, 2139-2147, 1977a.

3. Hedin, A.E., C.A. Reber, G.P. Newton, N.W. Spencer, H.C. Britan, H.G. Mayr, and W.E. Plotter, A global thermospheric model based on mass spectrometer and incoherent scatter data, MSIS 2, Composition, J. Geophys. Res., 82, 2148-2156, 1977b.

4. Hinteregger, H.E., D.E. Bedo, J.E. Manson, and D.B. Stillman, EUV flux variations with solar rotation observed during 1974-1976 from AE satellites, C, D, and E, Space Res., 17, in press, 1978.

5. Hoffman, J.H., J. Geophys. Res., in press, 1978.

6. Jacchia, L.G., Static diffusion models of the upper atmosphere with empircal temperature profiles. Research in Space Science, Spec Rep. 170, Smithson Astrophys. Observ., Cambridge, Mass., 1964.

7. Raitt, W.J., R.W. Schunk, and P.M. Banks, The influence of convection electric fields on thermal proton outflow from the ionosphere, Planet. Space Sci., 25, 291-301, 1977.

8. Schunk, R.W., W.J. Raitt, and P.M. Banks, Effect of electric fields on the daytime high-latitude E- and F- regions, J. Geophys. Res., 80, 3121-3130, 1975.

9. Schunk, R.W., P.M. Banks, and W.J. Raitt, Effects of electric fields and other processes upon the nighttime high-latitude F-layer, J. Geophys. Res., 81, 3271-3282, 1976.

10. Schunk, R.W., W.J. Raitt, and A.F. Nagy, Effect of diffusion-thermal processes on the high-latitude topside ionosphere, Planet. Space Sci., 26, 189-191, 1978.

11. Stewart, A.L., and T.G. Webb, Photo-ionization of helium and ionized lithium, Proc. Phys. Soc. London, 82, 532, 1963.

12. Walker, J.C.G., Analytic representation of upper atmosphere densities based on Jacchia°s static diffusion models, J. Atmos. Sci., 22, 462-463, 1965.

FIGURE CAPTIONS

Figure 1

Ion composition profiles for the ions O^+, O_2^+, NO^+, N^+, N_2^+ and He^+, the He+ profiles were computed independently.

Figure 2

Convection trajectories of thermal plasma over the polar cap in one inertial frame of reference. The four panels show the effect of a 12^o dipole offset at 6, 12, 18, and 24 hours local magnetic time.

Figure 3

Plots of perpendicular electric fields measured by the S3-2 satellite (courtesy of AFGL, Electrical processes branch).

Figure 4

Plots of S3-2 measurements of perpendicular electric field and electron density for a quiet day (orbit 188) and a disturbed day (orbit 310).

Figure 5

Plots of the S3-2 ion density probe showing the transition from an H^+ dominant ionosphere (Region A) to an O^+ dominant ionosphere (Region B).

Figure 6

O^+/H^+ composition ration and electron density plotted as a function of H^+ outflow velocity.

Figure 7

Variation of equatorward boundary of H^+ outflow with magnetic activity in the noon and midnight local time zones.

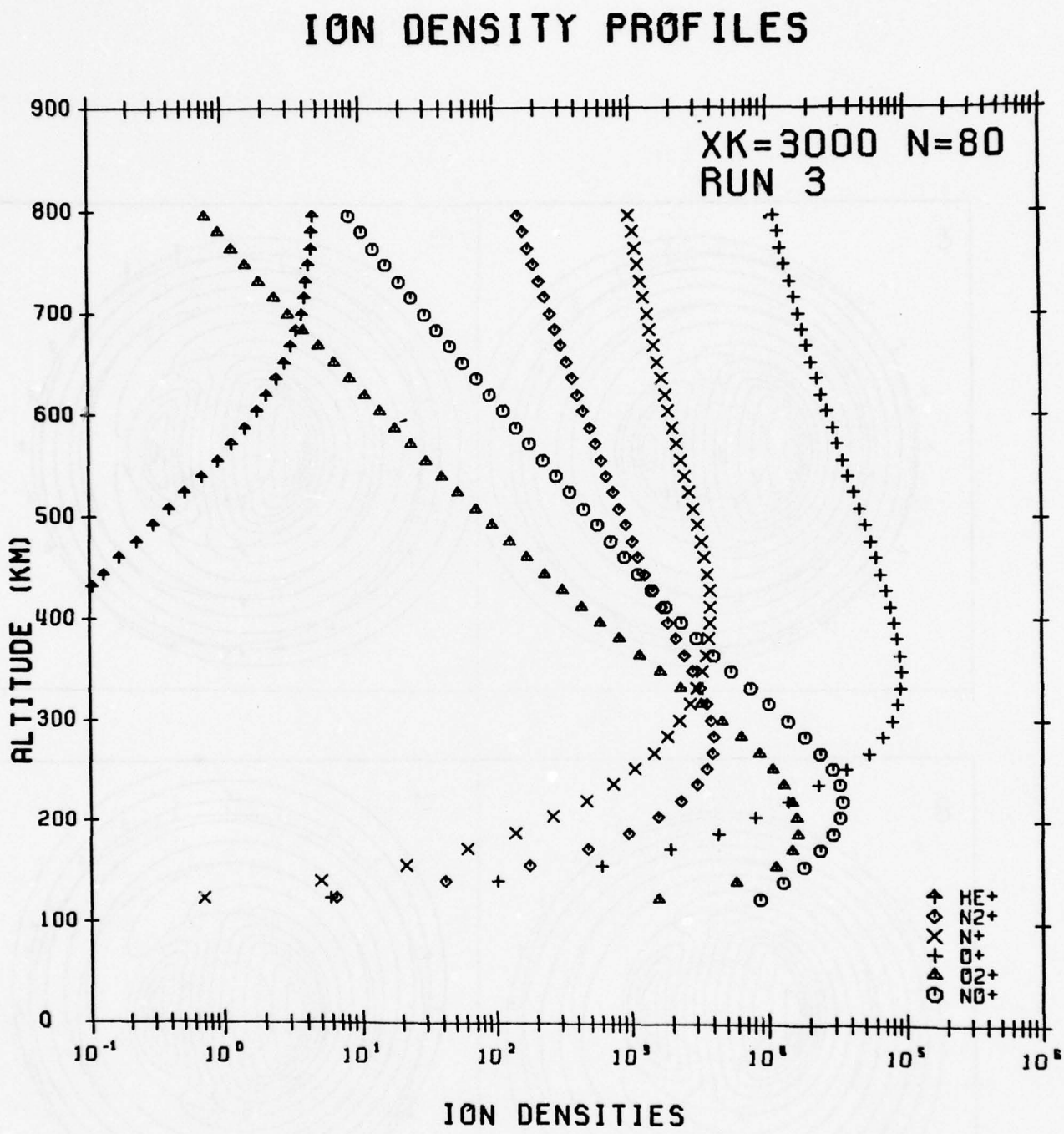
ION DENSITY PROFILES
XK=3000 N=80
RUN 3
ALTITUDE (KM)
ION DENSITIES
900
800
700
600
500
400
300
200
100
0
10⁻¹
10⁰
10¹
10²
10³
10⁴
10⁵
10⁶
HE+
N2+
N+
O+
O2+
NO+

Figure 1

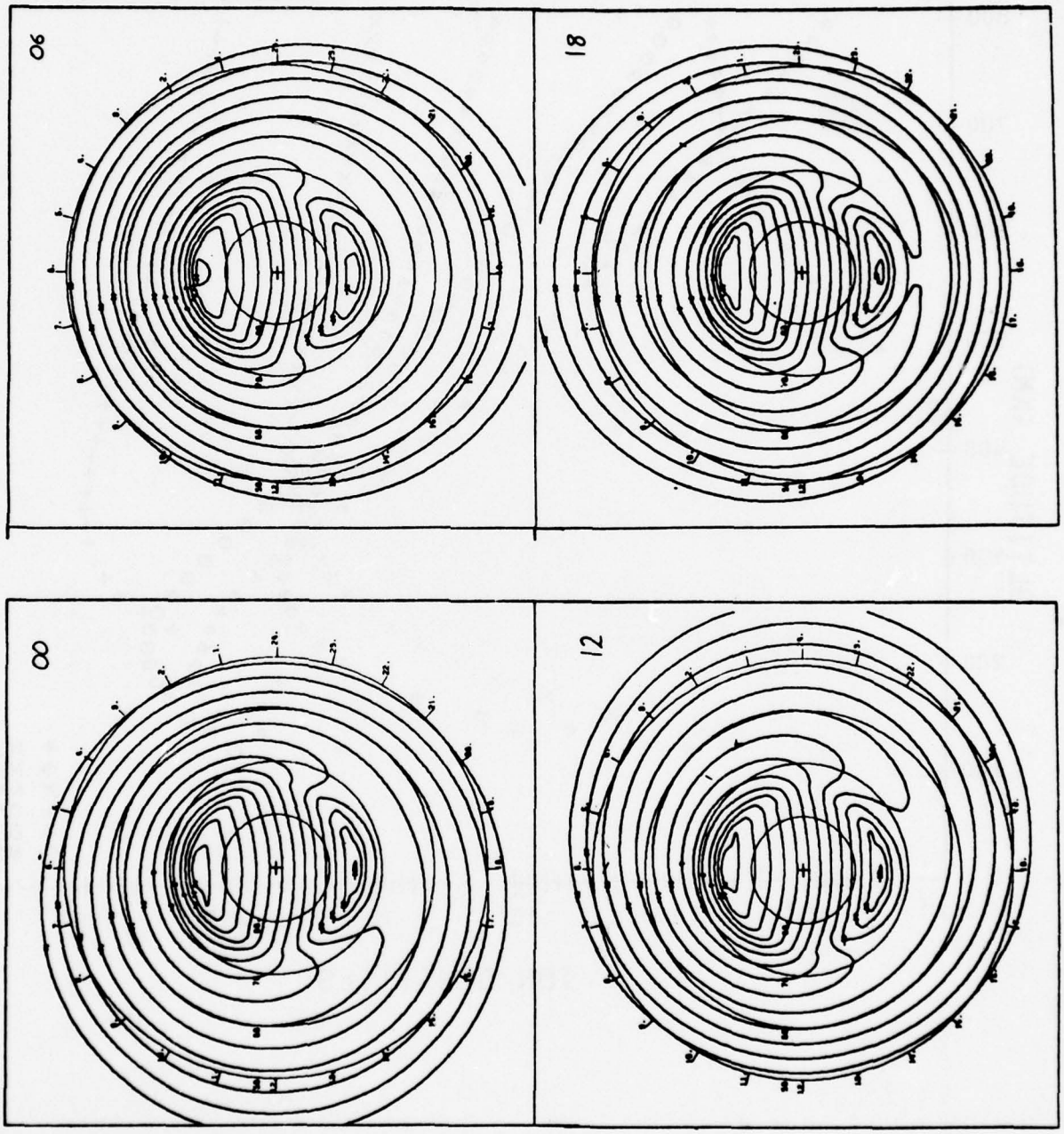

Figure 2

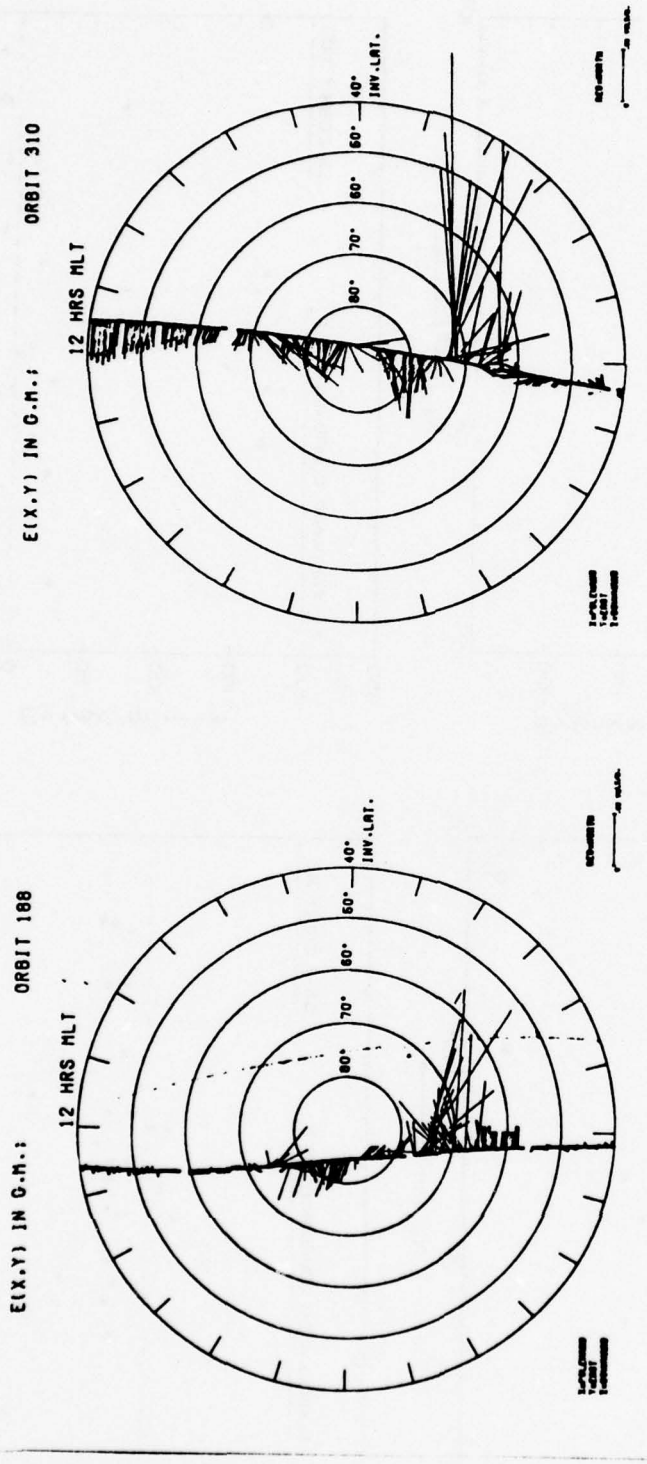
E(X,Y) IN G.M.:
12 HRS MLT
ORBIT 310
40°
INV.LAT.
50°
60°
70°
80°
E(X,Y) IN G.M.:
12 HRS MLT
ORBIT 188
40°
INV.LAT.
50°
60°
70°
80°

Figure 3

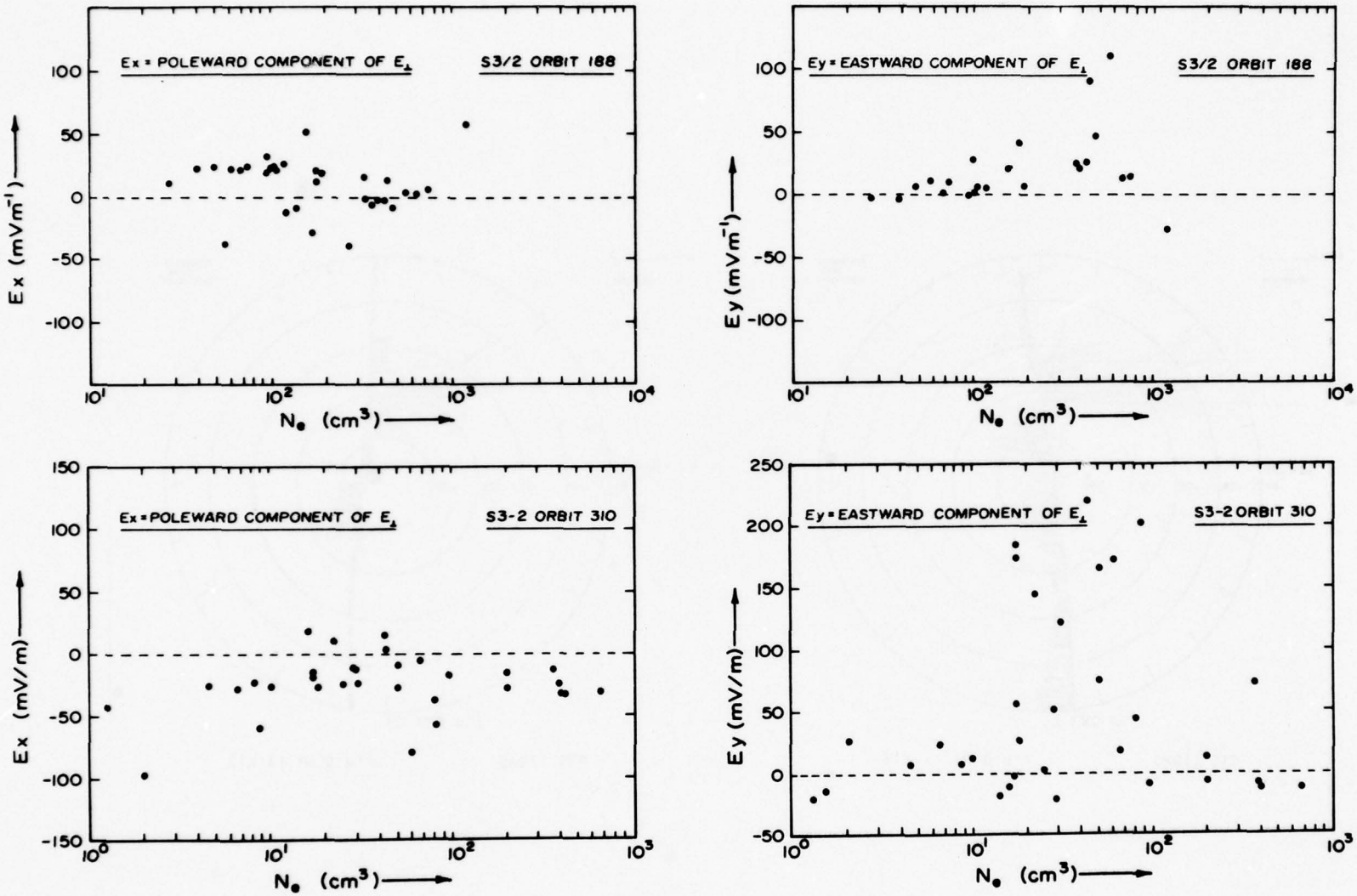
Ex = POLEWARD COMPONENT OF E⊥
S3/2 ORBIT 188
Ex (mVm⁻¹)
100
50
0
-50
-100
10¹
10²
10³
10⁴
N₀ (cm³)
Ey = EASTWARD COMPONENT OF E⊥
S3/2 ORBIT 188
Ey (mVm⁻¹)
100
50
0
-50
-100
10¹
10²
10³
10⁴
N₀ (cm³)
Ex = POLEWARD COMPONENT OF E⊥
S3-2 ORBIT 310
Ex (mV/m)
150
100
50
0
-50
-100
-150
10⁰
10¹
10²
10³
N₀ (cm³)
Ey = EASTWARD COMPONENT OF E⊥
S3-2 ORBIT 310
Ey (mV/m)
250
200
150
100
50
0
-50
10⁰
10¹
10²
10³
N₀ (cm³)

Figure 4

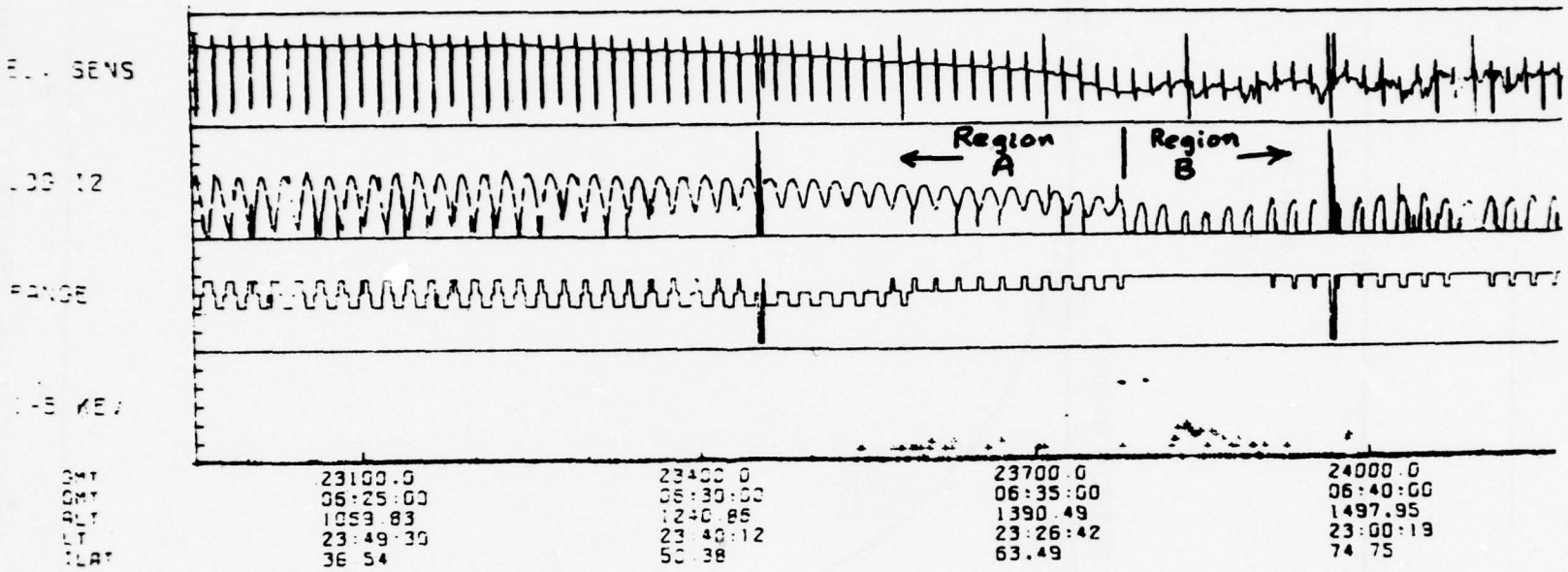
E.. SENS
.00 12
RANGE
1-5 KE/
Region A
Region B
GMT 23100.0 23400.0 23700.0 24000.0
GMT 06:25:00 06:30:00 06:35:00 06:40:00
ALT 1059.83 1240.86 1390.49 1497.95
LT 23:49:30 23:40:12 23:26:42 23:00:19
ILAT 36.54 50.38 63.49 74.75

Figure 5

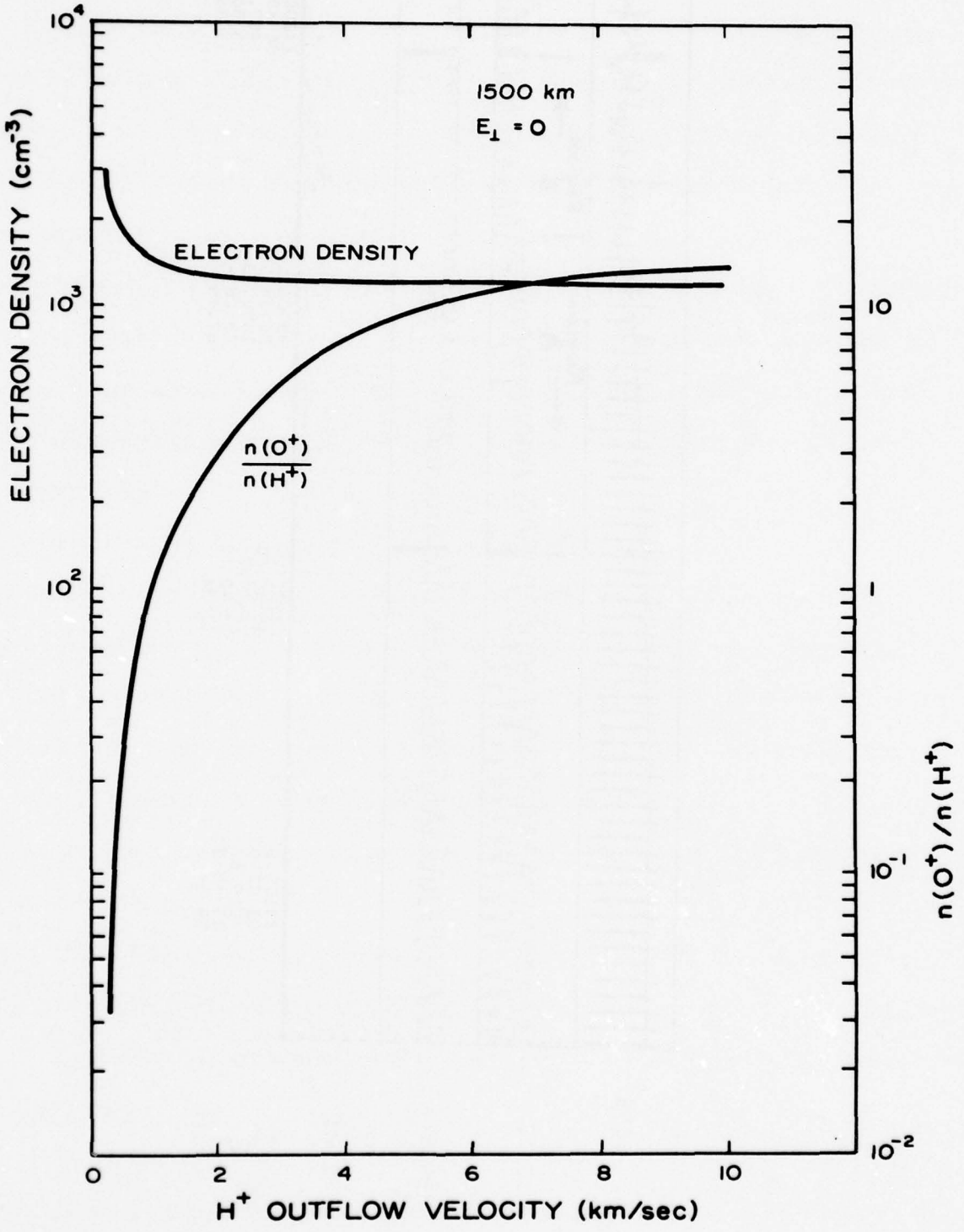
1500 km
$E_\perp = 0$
ELECTRON DENSITY
$\frac{n(O^+)}{n(H^+)}$
ELECTRON DENSITY (cm^{-3})
$n(O^+)/n(H^+)$
H^+ OUTFLOW VELOCITY (km/sec)
10^4
10^3
10^2
10
1
10^{-1}
10^{-2}
0
2
4
6
8
10

Figure 6

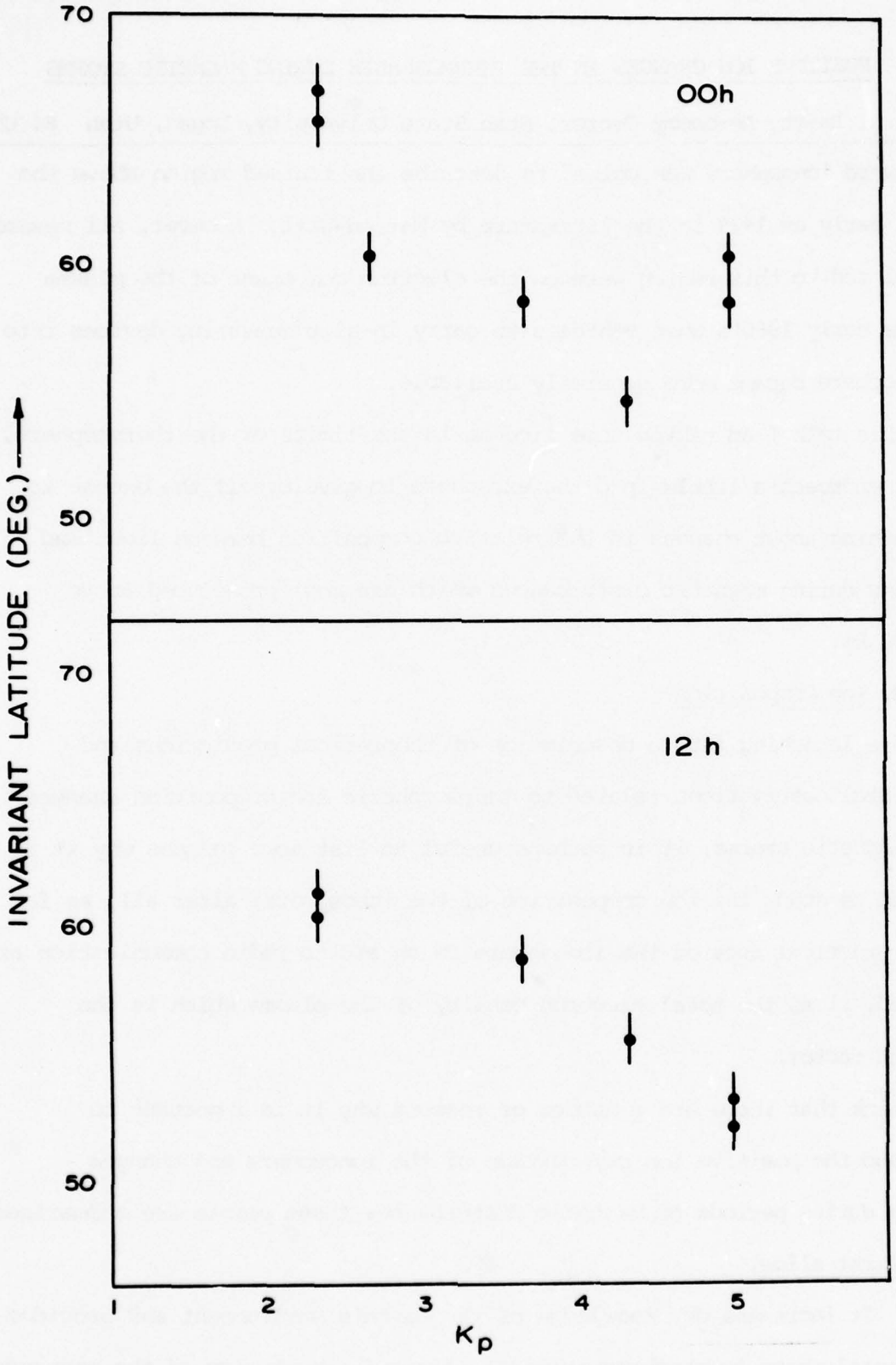

Figure 7

POSITIVE ION CHANGES IN THE THERMOSPHERE DURING MAGNETIC STORMS

W. J. Raitt, Aeronomy Center, Utah State University, Logan, Utah 84 322

The word ionosphere was coined to describe the ionised region above the earth as early as 1929 in the literature by Watson-Watt. However, all measurements related to this region were on the electron component of the plasma until the early 1960's when vehicles to carry in-situ measuring devices into the ionosphere became more generally available.

In this talk I am taking some license in the limits of the thermosphere, and will encroach a little into the exosphere to give myself the excuse to say something about changes in the relative composition between light and heavy ions during magnetic disturbances which are most pronounced above about 800 km.

Why Study Ion Composition?

Before launching into a description of theoretical predictions and experimental observations related to thermospheric ion composition changes due to magnetic storms, it is perhaps useful to list some reasons why it is important to study the ion composition of the ionosphere; after all, as far as most practical uses of the ionosphere as an aid to radio communication are concerned, it is the total electron density of the plasma which is the important factor.

I think that there are a number of reasons why it is important to understand the positive ion composition of the ionosphere and changes occuring during periods of magnetic disturbance: these points are summarised in the first slide.

1. It increases our knowledge of the earth's environment and provides experimental tests to check our understanding of the physics of the unbounded ionospheric plasma.

2. The ion mass is an important parameter in controlling the scale height of the plasma above the F_2 peak. It is therefore important in considerations

of, for example, wave propagation through the ionosphere involving the total electron content along a path.

3. The propagation characteristics of certain wave modes in the plasma - ion acoustic, ion cyclotron, plasma acoustic - is strongly influenced by the ion mass through such fundamental parameters as the ion plasma frequency ω_{pi} and the ion cyclotron frequency ω_{ci}. Closely associated with these wave modes are the generation of instabilities in the thermal ion plasma by the presence of hot plasma or by the $\underline{E} \times \underline{B}$ drift of the thermal plasma itself. The existence of such instabilities affects the current systems flowing in the plasma, and can lead to the generation of anomalous resistivity and electric fields parallel to the magnetic field.

4. The topside ion composition is a fairly sensitive indicator of ion temperature gradients, that is an inflow of heat in the ion gas from further out along the magnetic field line. For example, a gradient of $0.5^{o}K/km.$ results in an order of magnitude change in the O^{+}/H^{+} ratio at 400 km. altitude (compared to $T_{\infty} = 1200^{o}K$ with no gradient).

5. Ion composition measurements in the ionosphere can be used in conjunction with other measured plasma parameters to test ion chemistry rate coefficients in the unbounded ionospheric plasma for comparison with ground based measurements.

What Causes Changes in Ion Composition During a Magnetic Disturbance?

I have illustrated the main mechanisms and their effects on the second slide, referring the causes back to their origin in the solar wind.

When the solar wind interacts with the geomagnetic field it causes two major effects, an electric field is set up by the plasma flowing in the presence of the magnetic field, and this electric field sets up currents which distort the geomagnetic field into the well known magnetospheric configuration. Within

this field configuration particles are stored and energised.

In relation to ionospheric ion composition, the main effects of the cross-tail electric field are i) to cause erosion of plasma at the plasmapause in the equatorial plane and ii) to map down to ionospheric altitudes at high latitudes. The main effect of particle storage in relation to the subject of this talk is the precipitation of large fluxes of energetic particles into the atmosphere from time to time, again at high latitudes.

The three facets of the magnetosphere referred to earlier show marked changes during magnetic disturbances, particularly during the short lived phenomenon known as the substorm. Both electric fields and particle precipitation increase during the substorm resulting in the three major effects shown in the lowest boxes on the diagram.

The reduction in pressure at the equatorial plasmapause - that is a movement of the plasmapause causes increased outflow of light ions to move to lower latitudes. The mapped perpendicular electric fields cause heating of the ions by friction with the neutral gas resulting in altered chemical processes and diffusion effects. The precipitating particles mainly cause neutral gas heating through ionisation processes occuring at around 100 km., that is below the altitude range being considered. The neutral heating results in neutral composition changes and wind systems being set up.

In fact the processes are not distinct, they interact, the main channels of interaction being from the electric field heating which on the one hand effects the production of light ions, and on the other hand is an additional, important heat source for the neutral gas.

The diagram is not intended to be comprehensive, but, in the interests of simplicity, to represent the major processes. One magnetospheric storm effect which is not shown is the SAR-arc which is related to magnetospheric

particle storage in the ring current and the conduction of heat in the electron fluid down to ionospheric altitudes.

In view of the extensive influence of the perpendicular electric field on the ionospheric ion composition we will first consider this topic.

Effect of Perpendicular Electric Fields on Ion Composition

1. Theoretical Studies:

We should first define what we mean by perpendicular electric fields. The perpendicular is, of course, defined relative to the geomagnetic field. As a consequence of this electric field the ionospheric plasma acquires a drift velocity relative to the neutral gas (assumed stationary) of

$$\underline{V_d} = \underline{E_\perp} \times \underline{B}$$

As a result of collisions between the drifting positive ions and the neutral gas there is frictional heating resulting in an increased ion temperature for O^+ drifting through O given by (Schunk et. al., 1975): -

$$T_{eff} = T_n + 0.329\, E_\perp^2$$

in altitude regions where $\nu_i / \Omega_i \ll 1$

Within the thermosphere O^+ is normally the dominant positive ion and O, O_2 and N_2 the dominant neutral species. The important ion reactions dominating the lower thermosphere are summarised on the third slide.

$$O^+ + N_2 \xrightarrow{k_1} NO^+ + N \quad \text{-------} \quad 1.$$

$$O^+ + O_2 \xrightarrow{k_2} O_2^+ + O \quad \text{-------} \quad 2.$$

$$NO^+ + e \xrightarrow{k_3} N + O \quad \text{-------} \quad 3.$$

Reaction 3. is influenced largely by T_e

$$k_3 = 4.6 \times 10^{-7} \left(\frac{300}{T_e}\right)^{0.8} \quad \text{(Walls \& Dunn, 1974)}$$

but T_e is not greatly affected by $E_\perp$, hence the dominating effect of $E_\perp$ lies in the reactions 1. and 2.

Until the early 1970's it had been thought that k_1 and k_2 remained constant

or even decreased with increasing ion temperatures in the range 600-2,000°K. A number of laboratory measurements (McFarland et. al., 1973, 1974; Johnsen & Biondi, 1973; Rutherford & Vroom, 1971) showed that in fact the rate coefficients k_1 and k_2 increased very rapidly with ion temperature after reaching a minimum around 750°K for k_1 and 1800°K for k_2.

The net result of this, as can be seen from equations 1. and 2., is to greatly increase the loss rate for O^+ ions as T_{eff} increases by, for instance, the effect of $E_\perp$.

One further point which must be addressed is the decay distance of O^+ from reaction 1., which is the more important, after the plasma encounters $E_\perp$. This is relevant because of the limited extent of electric fields in auroral regions. Slide 4 shows the decay distance of O^+ as a function of $E_\perp$ and altitude. It can be seen that typical distances are less than 1000 km. which is generally small compared with the scale size of the major electric field structure in the auroral zone.

Schunk et. al. (1975) applied these considerations to a study of thermospheric ion composition for the case of a sunlit ionosphere and for $E_\perp$ in a North-South direction. That is resulting in an East-West plasma drift. The coupled ion transport equations for O^+, NO^+ and O_2^+ were solved for steady state solutions using neutral gas densities for O_2, N_2 and O for 1000°K based on the atmospheric model of Jacchia (1964) modified by Walker (1965).

Slide 5 shows a typical ionospheric model for $E_\perp = 0$ and Slide 6 for $E_\perp = 100$ mV/m. The increased importance of NO^+ to higher altitudes can be seen for $E_\perp = 100$mV/m with the transition height moving from 220 km. to 320 km. The increased scale heights can be seen, and the structure of the N_e profile has changed from a normal F_2 peak at 300 km. in the absence of $E_\perp$ to an F-region peak at around 180 km. for $E_\perp = 100$ mV/m.

At the time of performing the calculations we tentatively increased $E_\perp$ to

200mV/m since at that time fields of that magnitude had not been reported to any extent. However, since then electric fields of this magnitude or greater have been measured more frequently.

The seventh slide shows the dramatic effect of a 200mV/m electric field on the model where NO^+ is dominant up to 600 km. and presumably higher.

The increase in NO^+ concentration and decrease in O^+ concentration caused by $E_\perp$ are summarised in Slides 8 and 9. The effect on N_e is less pronounced because the electric field changes one ion species for another, but there is an overall decrease in electron density because of the greater loss rate of NO^+ compared to O^+. The change in N_e is summarised in Slide 10.

Thus we can see that the general result of electric field effects on the thermospheric ion composition is to deplete O^+ and enhance NO^+.

The results presented so far have been for the more straightforward case of constant photo-ionisation and steady state conditions. Schunk et. al. (1976) extended the study to the night-time ionosphere allowing for changes in photo-ionisation and changes in $E_\perp$ which might be encountered as the plasma drifts in the typical 2-cell convection structure over the polar caps.

In this study it was found that perturbation to the composition as the plasma co-rotated into a region of significant $E_\perp$ when photo-ionisation was absent produced a rapid change in composition while $E_\perp$ existed, but the normal decay of ionisation soon caused the ion composition to revert to its unperturbed profiles within about one hour of leaving the region of $E_\perp$.

This is illustrated in Slide 11, where the NO^+ density profiles for various times from t = 0 when photo ionisation is stopped are plotted. The NO^+ density increases at t = 2 hrs. when a meridional $E_\perp$ of 100mV/m is applied for 15 mins. However, by t = 2.5 hrs. the NO^+ density is not greatly different from the pre-electric field profile, and by t = 4 and t = 6 hrs. the profiles are nearly identical with those computed without any electric field.

In the nightime study the effects of zonal electric fields were also considered. These E-W fields result in N-S plasma flow causing induced plasma flow parallel to the magnetic field provided the dip angle is not 90°. In general, however the overiding effect of O^+ depletion and NO^+ enhancement predominates, but the shape of the profiles differs with an E-W field compared to a N-S field due to the effect of plasma being driven up or down the magnetic field lines.

Effect of Neutral Gas Heating

One of the major effects of heat transfer from magnetospheric processes to the neutral gas is to cause the O/N_2 ratio to decrease. It turns out that at thermospheric altitudes the N_2 density shows a large increase while O changes rather little in response to magnetospheric storms. The reasons for this have recently been discussed by Jacchia et. al. (1977) in terms of a change in exospheric temperature and a change in the height of the homopause (the level below which turbulent mixing results in a uniform atmospheric composition for the major constituents ≈ 95 km.).

Reference to the dominating thermospheric chemical equations shows that an increase in N_2 concentration is equivalent to an increase in the rate coefficient k_1 and thus this is a process by which O^+ can be depleted and NO^+ enhanced in response to magnetospheric energy input at high latitudes.

A further mechanism for increasing the reaction rate k_1 is to increase the vibrational temperature of the N_2 molecules. The result is equivalent to increasing the effective temperature by frictional heating resulting from $E_\perp$.

During magnetospheric disturbances we expect the population of N_2^* to increase in two areas. In the region of precipitating magnetospheric particles, inelastic non-ionizing collisions can increase N_2^*, this combined with overall neutral gas temperature increase can result in a neutral wind carrying the vibrationally excited N_2 away from the region of precipitation.

Schunk and Banks (1975) have discussed the depletion of O^+ by this process as a contributing factor to the formation of the nightside mid-latitude trough equatorward of the auroral oval. In these circumstances, one would expect to observe enhanced NO^+ concentrations even in the absence of a perpendicular electric field.

Another mechanism for vibrationally exciting N_2 molecules is collisions with the high energy tail of a thermal electron population. The effective vibrational temperature of N_2 due to a given T_e has been studied by Newton et. al. (1974). It is an experimentally observed fact (Norton & Findlay, 1969; Roble et. al., 1971; Raitt, 1974) that within SAR arcs T_e can be enhanced from its normal 2000-3000°K to 5000-6000°K. This is sufficient to generate significant numbers of N_2^* molecules and so affect the relative composition of O^+ and NO^+. This was studied using the triple ion (O^+, O_2^+, NO^+) model by Raitt et. al. (1975) using typical T_e profiles expected in an SAR arc. We showed that both during the day and the night the enhanced N_2^* concentration resulted in increased NO^+ and increased O^+/NO^+ transition altitudes as shown in Slide 12. While the conversion of O^+ to NO^+ resulted in a reduction in N_e, the electron density depletion was not as great as had been predicted by considering only the loss of O^+.

Experimental Observations

There have not been a great many observations of ion composition changes during magnetic storms; of those reported the majority have been specific case studies of a pass or a group of passes over the polar cap.

The reasons for the scarcity of the observations are not too surprising. In general, high latitude ion composition measurements must be made by in-situ probes carried on satellites. The experimenters must then rely on the satellite being in the right place at the right time. This can be difficult since the typical duration of a substorm is $\approx$ 30 mins. while a typical

satellite orbital period is $\approx$ 90 mins. This fact emphasises the need for missions having multiple satellites spaced around the same orbital track. In contrast to the few direct observations of storm time disturbances to the ion composition, there are many more ground based observations during storms which in general measure only the electron density at the latitudes of interest. We have already seen that for the effects considered so far the electron density does not show such a strong dependence on magnetic storms as does the ion composition.

The observations which have been published are in qualitative agreement with the theoretical studies discussed earlier. Hoffman et. al. (1974) presented ISIS-2 measurements taken at 1400 km. showing NO^+ densities $\approx 10^3$ cm^{-3} with O^+ $\approx 10^4$cm^{-3} during the severe magnetic storm of August, 1972. Such a low O^+/NO^+ ratio at 1400 km. could well result from the conversion of O^+ to NO^+ by the processes discussed earlier. Taylor et. al. (1975) identified regions of enhanced NO^+ concentration from OGO-6 measurements near 1000 km. on the poleward side of the light ion trough. These enhanced NO^+ regions were well correlated with decreases in the O^+ concentration. On another set of OGO-6 passes Taylor et. al. (1975) found that the enhanced NO^+ concentration also coincided with increased broadband noise, an indication, perhaps, of the importance of the effect of ion composition on wave/particle instabilities in the ionosphere.

Brinton (1975) has published a direct observation of enhanced NO^+ concentration associated with increased $E_\perp$ by utilising data from in-situ probes on the AE-C spacecraft. The data is shown in Slide 13 on which can be seen clear evidence of the enhanced NO^+ with enhanced plasma drift velocity.

The published data still leave a number of questions unanswered, since not all of the relevant parameters have yet been presented together. Thus we need to see NO^+ , O^+, N_2, O densities, T_e and soft particle fluxes simultaneously to try to judge the interplay between the three processes acting to

change the ion composition which have been discussed previously.

Effect of Erosion of Plasma in Equatorial Plane

The concept of the polar wind or outflow parallel to the geomagnetic field of light ions, that is H^+ and He^+, from the ionosphere has been accepted for a number of years, and more recently direct H^+ bulk velocity measurements have established the existence of H^+ outflow at high latitudes.

It is well known that the transition from diffusive equilibrium for H^+ to dynamic equilibrium with H^+ flowing outwards causes a reduction in H^+ concentration at a given altitude starting from as low as about 700 km. The changes in the H^+ outflow as a result of magnetic storms is therefore a factor determining the ion composition at the upper boundary of the thermosphere, leading to O^+ being the dominant ion to high altitudes.

I wish to conclude this talk by describing some of the more recent work on the changes in H^+ outflow which might be expected during magnetic storms, and just briefly refer to some very recent studies on He^+ outflow which have just been submitted for publication.

One of the effects of an increase in the cross tail magnetospheric electric field discussed by Chappell and others is to erode the plasma from the equatorial plasmapause; that is to shrink the plasmasphere. When this occurs we expect that the pressure gradient between H^+ at ionospheric altitudes along the magnetic field line to the equatorial plane will result in greatly increased outflow velocity as shown in Slide 14, where we see the effect on the outflow velocity of changes in H^+ density at 3000 km. which is related to its density at the equatorial plane. This change in outflow velocity has direct repercussion on the H^+ density down to quite low altitude as can be seen in the next Slide 15. Both of these slides are taken from a paper by myself, Schunk and Banks in which the coupled continuity, momentum and energy equations for the H^+ ions were solved self-consistently for subsonic and supersonic H^+ outflow.

In a later study we also took into consideration the effect of perpendicular electric fields on the H^+ outflow in a way in which we allowed for ion heating and the associated changes in the scale heights and diffusion coefficients. We did not allow for the increased reaction rate in the $O^+ + N_2 \rightarrow NO^+ + N$ reaction consistently, but made provision for depleted O^+ by running the model with a range of O^+ F_2 peak densities.

Slide 16 shows the effect on H^+ density for a fixed outflow velocity as $E_\perp$ varies from 0 to 100mV/m. The increase in H^+ concentration being due to reduced diffusion velocity caused by the increased amount of O^+ when it is hotter and has a larger scale height for the higher $E_\perp$ cases. We have, however, seen that for an $E_\perp$ of 100mV/m the O^+ concentration is reduced by about a factor of 10. Taking this into consideration the results in the H^+ flux being reduced by about a factor of 2 and, since the flow is flux limited, the concentration for a given outflow velocity is also halved.

Thus under magnetic storm conditions we expect two effects to reduce the H^+ density. Firstly the reduction in pressure at the equatorial plane will result in increased H^+ outflow and secondly the ionospheric $E_\perp$ increase will deplete O^+ and thereby deplete the source of H^+ from the change exchange reaction $H^+ + O \rightleftarrows H + O^+$.

Recent calculations of the outflow of He^+ within a background ionosphere of O^+ and outflowing H^+ have shown that $E_\perp$ affects the He^+ density mainly through ion heating and scale height changes resulting in reduced He^+ concentration in the thermosphere with increased $E_\perp$ and increased concentration at higher altitudes for a given He^+ outflow velocity. This is illustrated in Slide 17.

Changes in O^+ density mainly effect the He^+ diffusion coefficient, and a factor of ten reduction in O^+ concentration resulted in the He^+ ions becoming more strongly outflowing with a consequent reduction in He^+ concen-

tration as shown in Slide 18.

The final storm effect we studied for He^+ ions was to increase N_2 selectively as has been observed by a number of experimenters. The surprising result was that although the main loss process for the He^+ in the thermosphere is the reaction $H^+ + N_2 \rightarrow N_2^+ + He$ the effect of increasing the N_2 temperature alone to 1500°K resulting in a factor of 50 increase in the N_2 concentration at 600 km. was to reduce the He^+ escape flux by a factor of only 1.5. Study of the balance of the H^+ continuity equation showed this to be due to the density being determined mainly be production and diffusion at altitudes where the N_2 concentration showed the greatest increases in density.

Conclusions.

In summary I would like to propose that the topic of this talk is a fruitful subject of study and urge that more data be collected and presented on all of the factors involved in the variation of ion composition during magnetic disturbances to enable theoretical models to be tested. If the models are found to be wanting in comparison to the observations, then the experimental data will enable the boundary values to be adjusted to improve attempts to match theory and observation.

Acknowledgment.

Material for this review was collected and condensed with support from AFGL contract number F19628-77-C-0011.

IONOSPHERIC ION COMPOSITION

- IMPROVE UNDERSTANDING OF PHYSICS OF IONOSPHERE.
- EFFECT ON PLASMA SCALE HEIGHT AND TOTAL ELECTRON CONTENT.
- INFLUENCE ON WAVE PROPAGATION AND INSTABILITIES.
- INDIRECT INDICATOR OF ION TEMPERATURE AND GRADIENTS.
- ION CHEMISTRY STUDIES IN UNBOUNDED PLASMA.

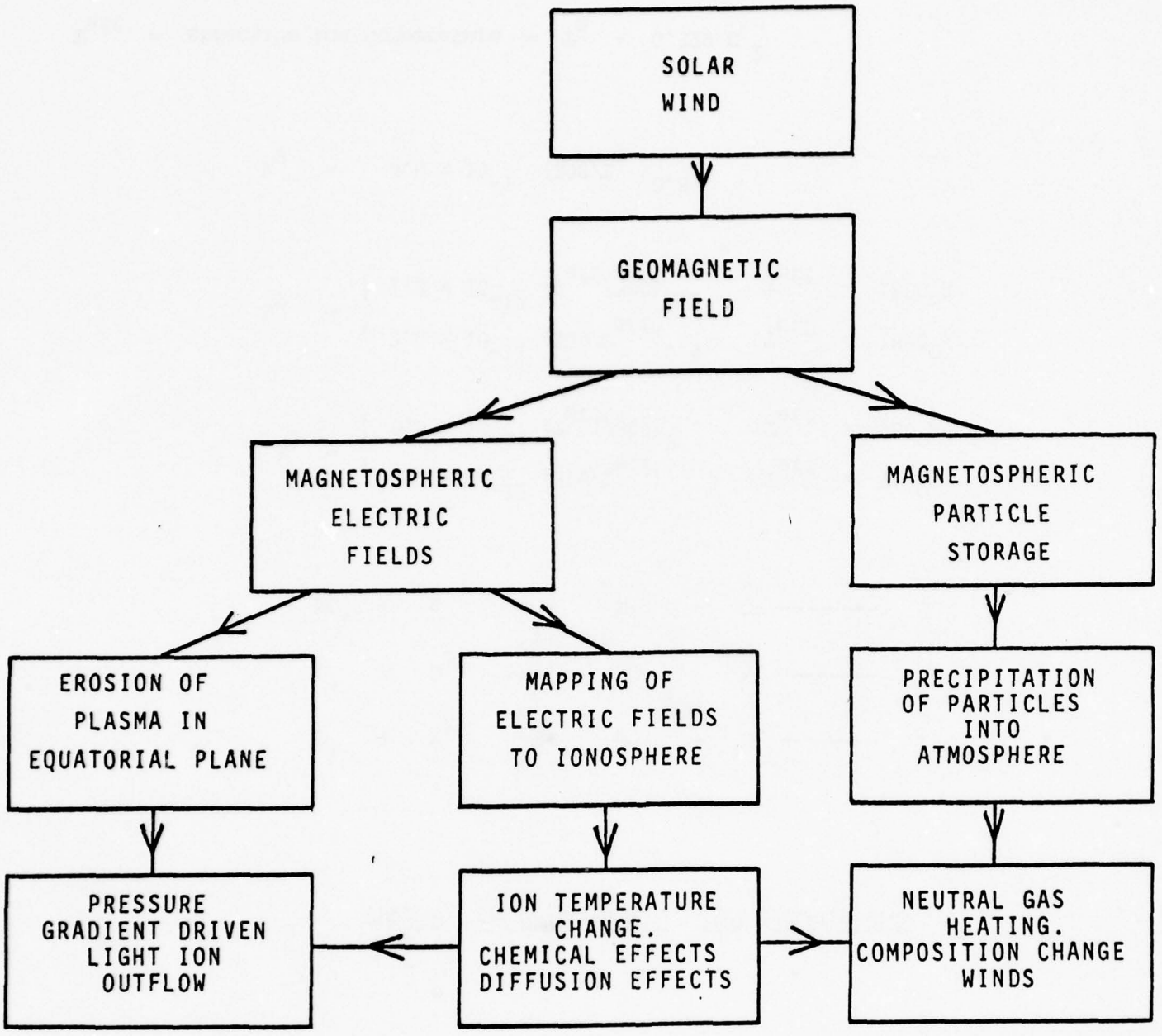

MAJOR CAUSES AND EFFECTS OF THERMOSPHERIC ION COMPOSITION CHANGES DURING MAGNETIC STORMS

MAJOR THERMOSPHERIC ION REACTIONS

$$O^+ + N_2 \xrightarrow{k_1} NO^+ + N \quad \text{-------} \quad 1.$$

$$O^+ + O_2 \xrightarrow{k_2} NO^+ + N \quad \text{--------} \quad 2.$$

$$NO^+ + e \xrightarrow{k_3} N^* + O^* \quad \text{--------} \quad 3.$$

$$k_1 = \begin{cases} 1.2 \times 10^{-12} \, (300/T_{eff}) & T_{eff} < 750^{\circ}K \\ 8.0 \times 10^{-14} \, (T_{eff}/300)^2 & T_{eff} > 750^{\circ}K \end{cases}$$

$$k_2 = \begin{cases} 2.0 \times 10^{-11} \, (300/T_{eff})^{0.4} & T_{eff} < 1800^{\circ}K \\ 1.3 \times 10^{-12} \, (T_{eff}/300)^{1.2} & T_{eff} > 1800^{\circ}K \end{cases}$$

$$k_3 = 4.6 \times 10^{-7} \, (300/T_e)^{0.8}$$

T_{eff} = effective ion temperature = $T_n + 0.329 \, E_\perp^2$

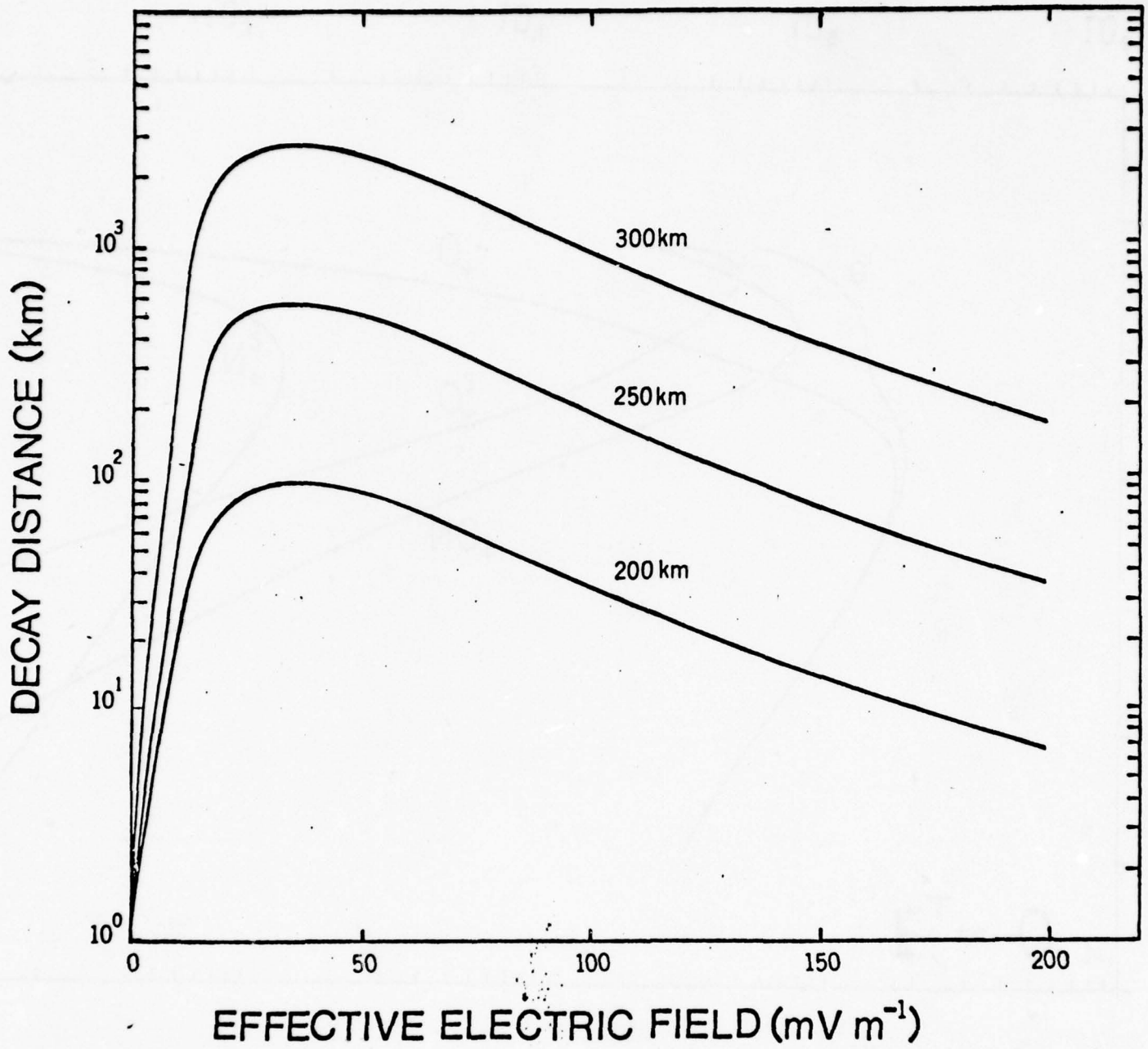
DECAY DISTANCE (km)
10^3
10^2
10^1
10^0
300km
250km
200 km
0
50
100
150
200
EFFECTIVE ELECTRIC FIELD (mV m^{-1})

SLIDE 4

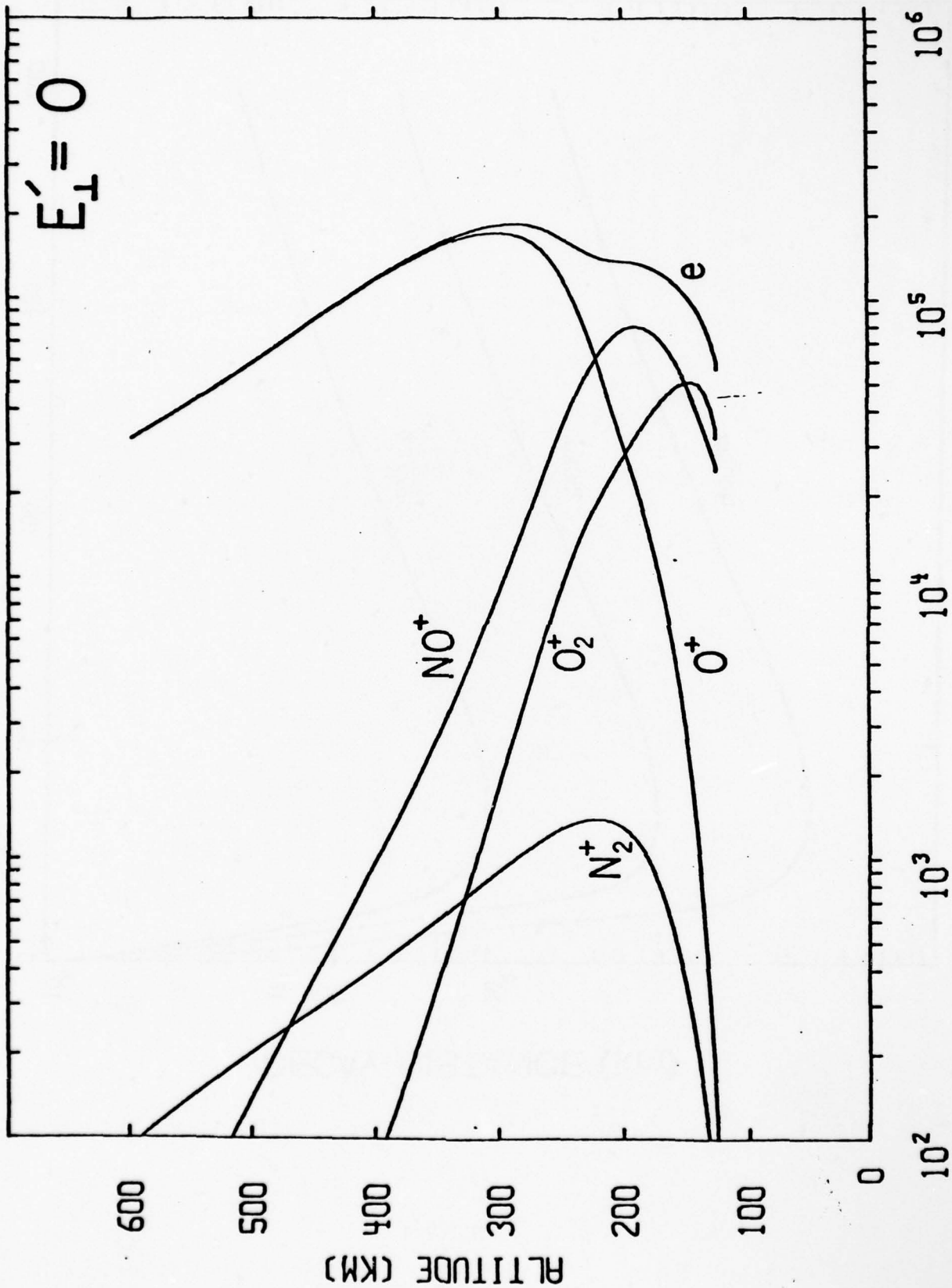
$E_\perp' = 0$
e
NO^+
O_2^+
O^+
N_2^+
ALTITUDE (KM)
600
500
400
300
200
100
0
10^2
10^3
10^4
10^5
10^6
DENSITY (CM-3)

SLIDE 5

SLIDE 6

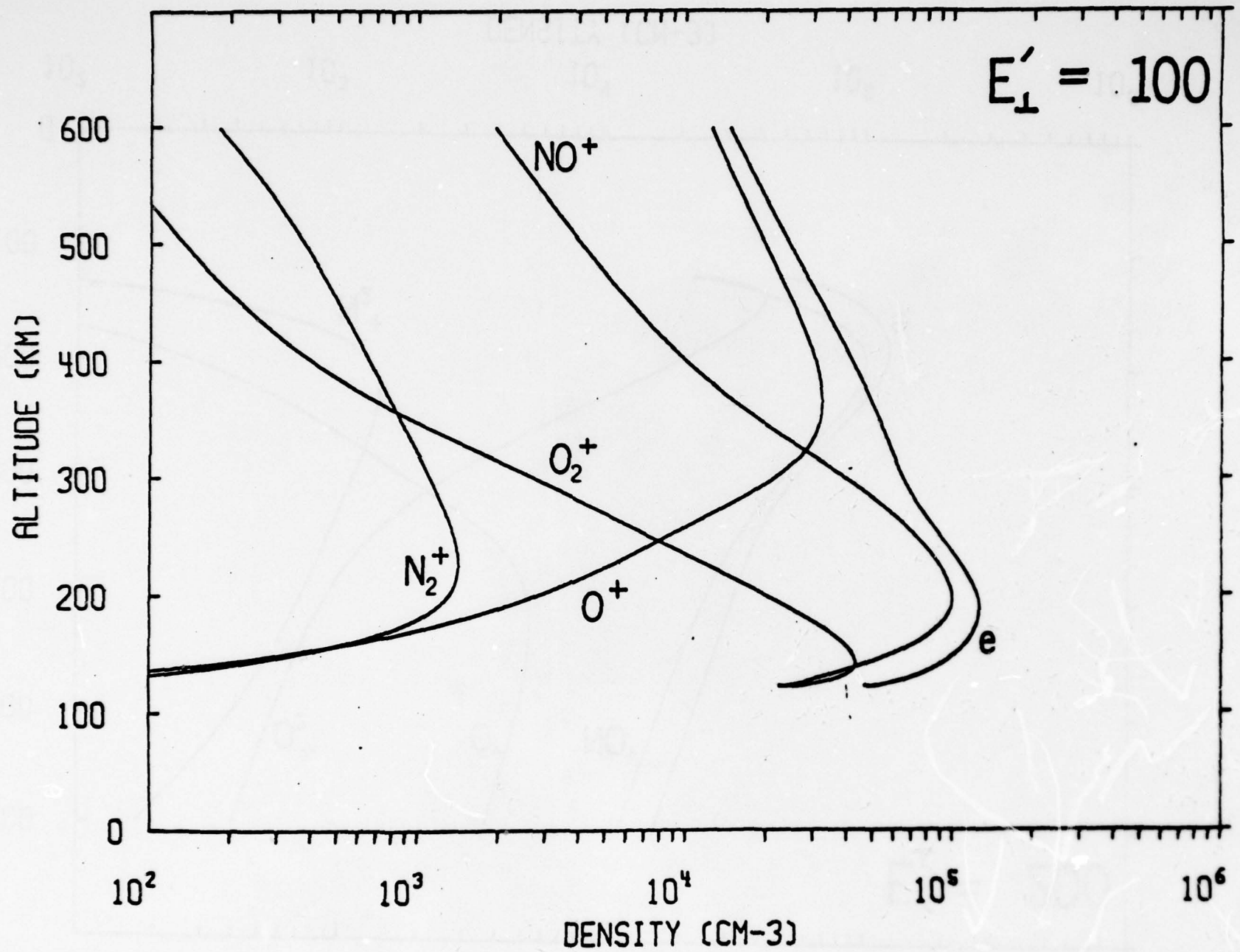
$E'_\perp$ = 100
600
500
400
300
200
100
0
ALTITUDE (KM)
NO^+
O_2^+
N_2^+
O^+
e
10^2
10^3
10^4
10^5
10^6
DENSITY (CM-3)

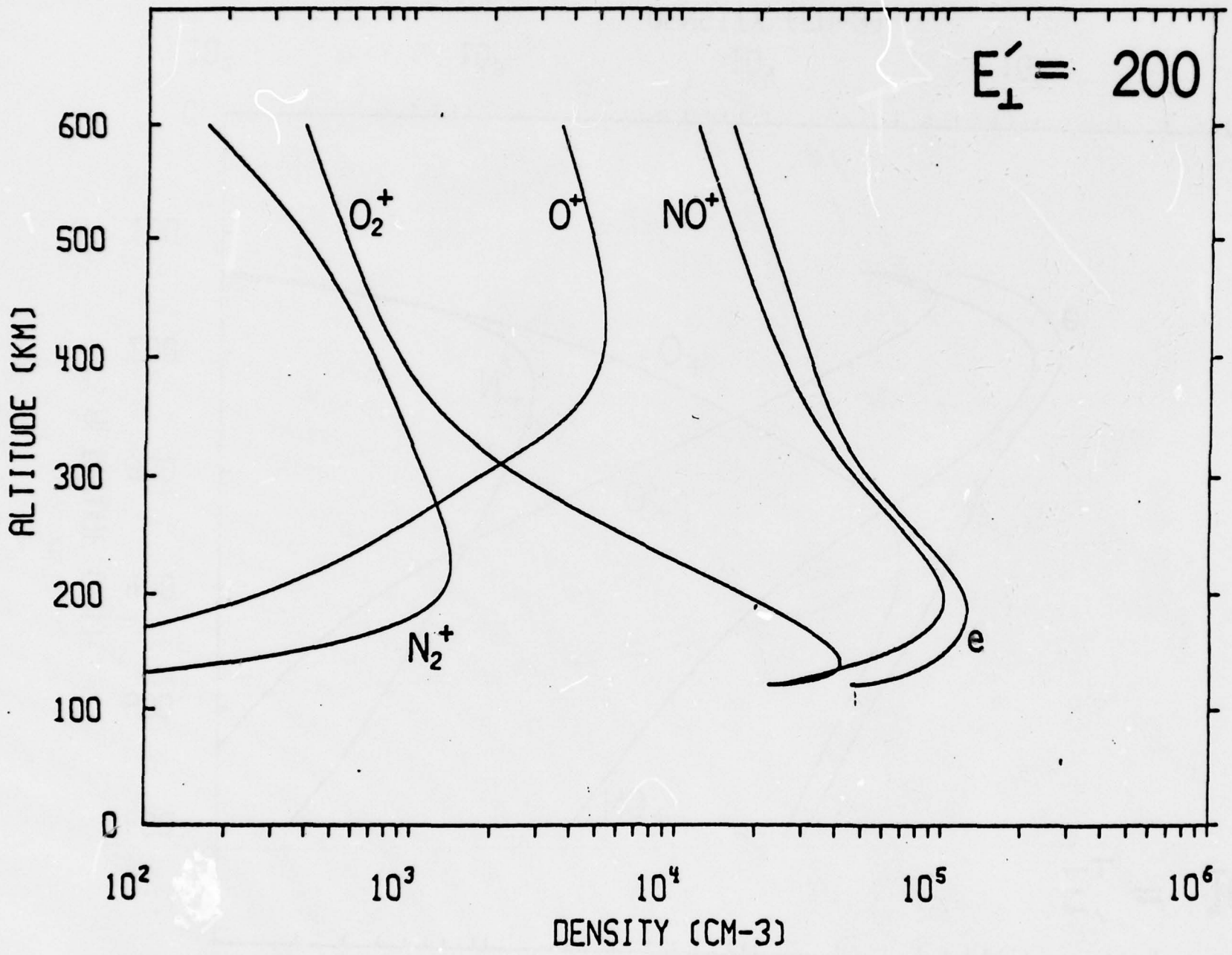
$E_\perp' = 200$
600
500
400
300
200
100
0
ALTITUDE (KM)
O_2^+
O^+
NO^+
N_2^+
e
10^2
10^3
10^4
10^5
10^6
DENSITY (CM-3)

SLIDE 8

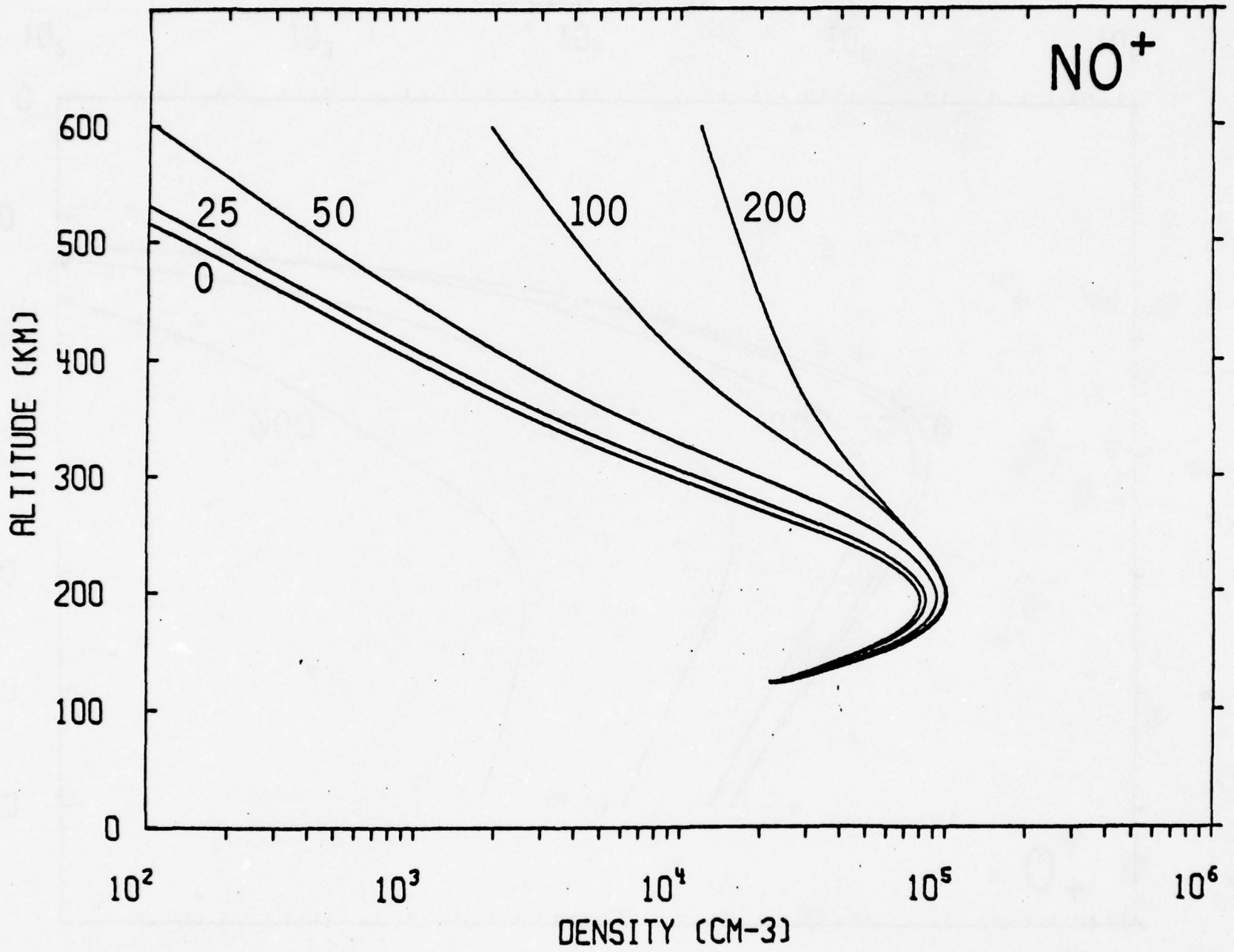
NO+
600
500
400
300
200
100
0
ALTITUDE (KM)
25
50
100
200
0
10^2
10^3
10^4
10^5
10^6
DENSITY (CM-3)

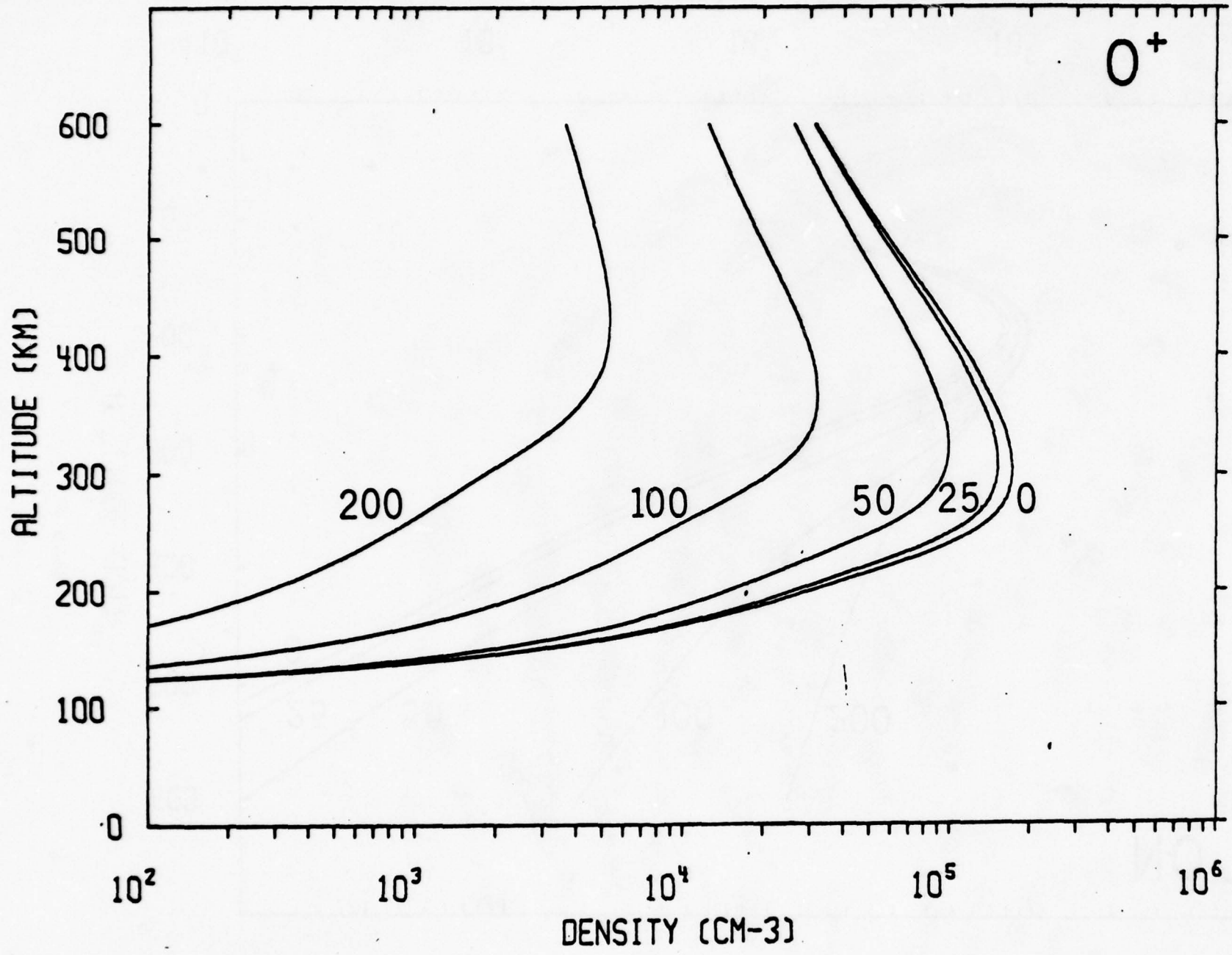
O+
600
500
400
300
200
100
0
ALTITUDE (KM)
200
100
50
25
0
10^2
10^3
10^4
10^5
10^6
DENSITY (CM-3)

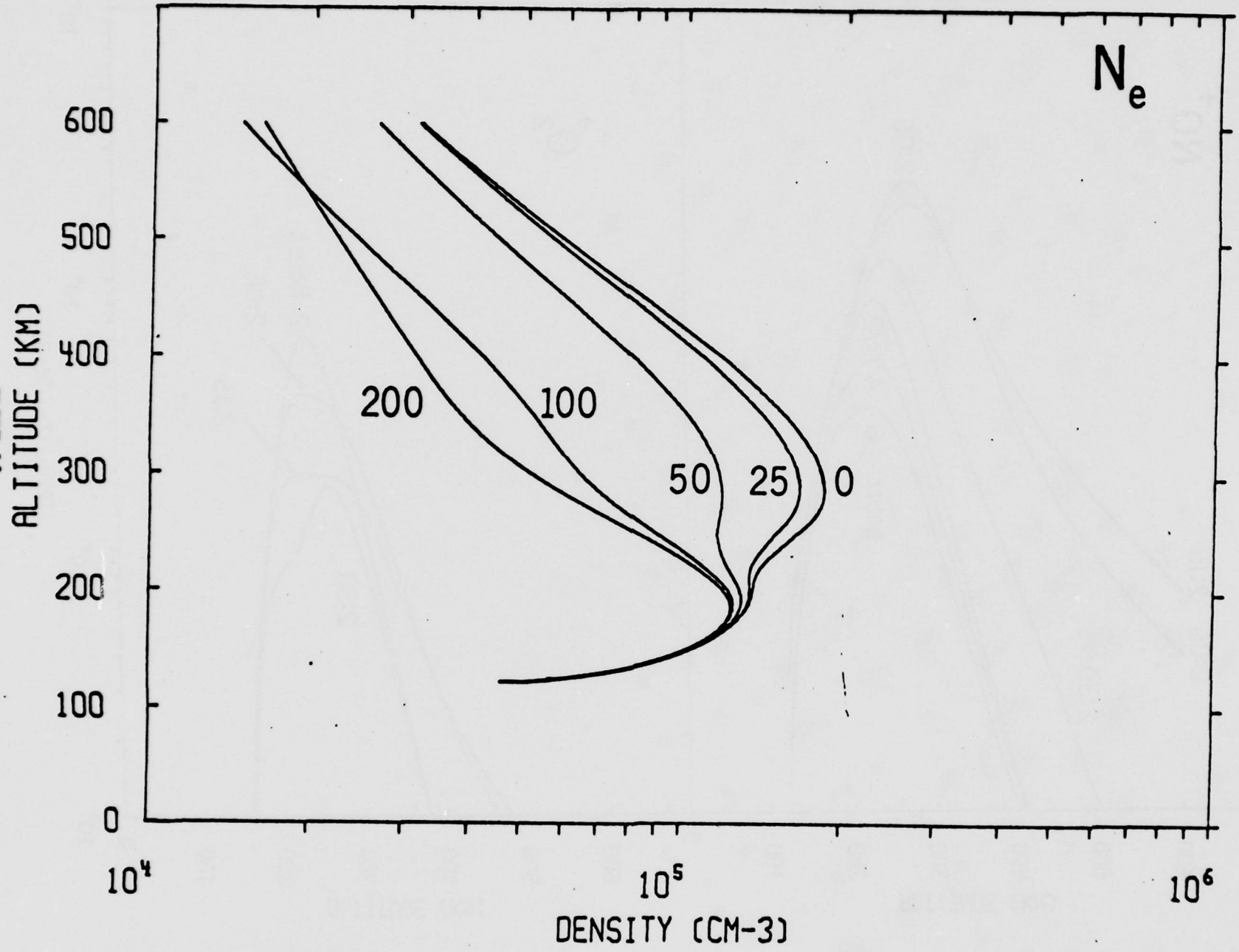
N_e
600
500
400
300
200
100
0
ALTITUDE (KM)
200
100
50
25
0
10^4
10^5
10^6
DENSITY (CM-3)

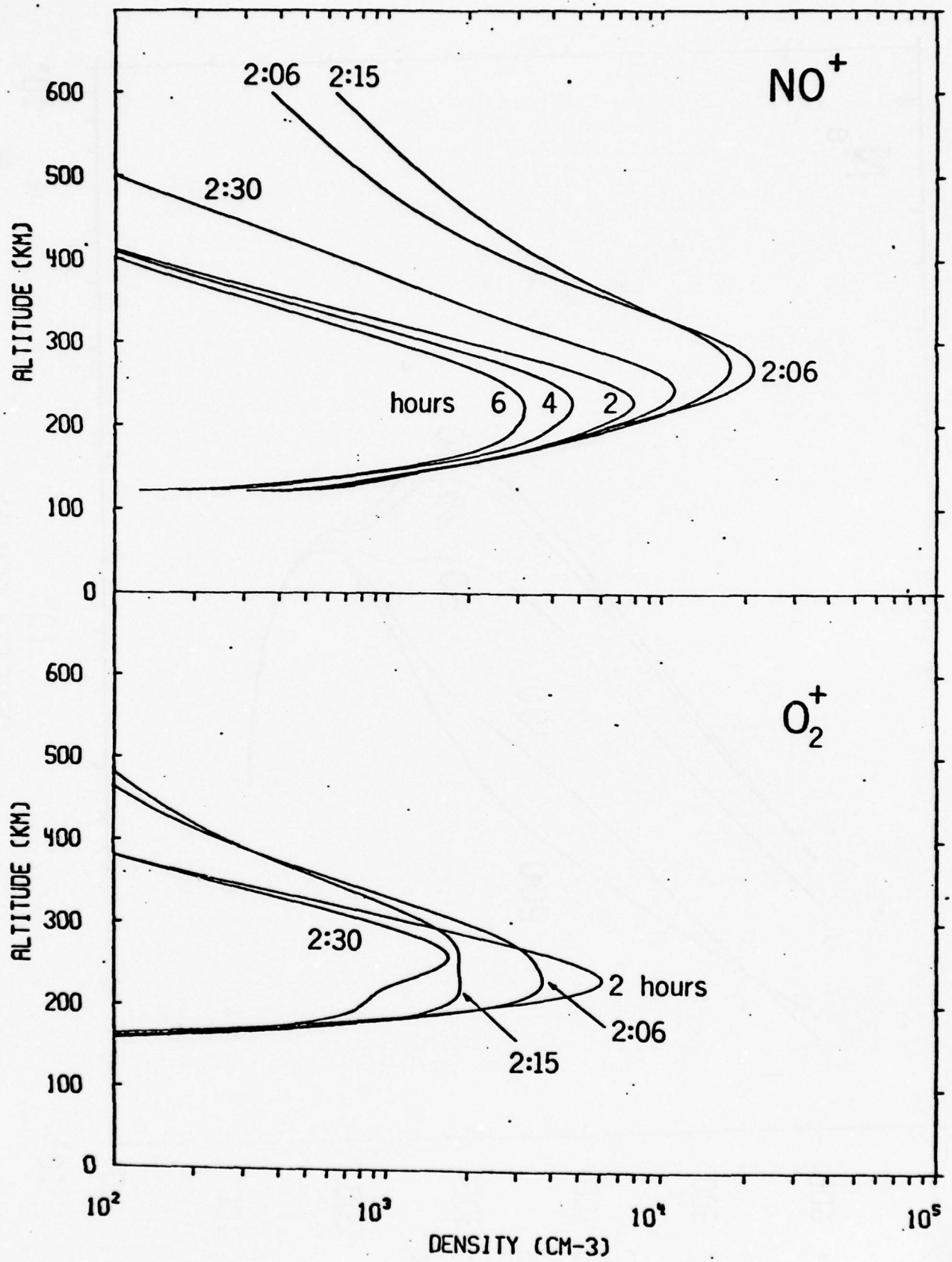
2:06
2:15
NO+
2:30
2:06
hours 6 4 2
ALTITUDE (KM)
600
500
400
300
200
100
0
O2+
2:30
2 hours
2:06
2:15
10²
10³
10⁴
10⁵
DENSITY (CM-3)

SLIDE 11

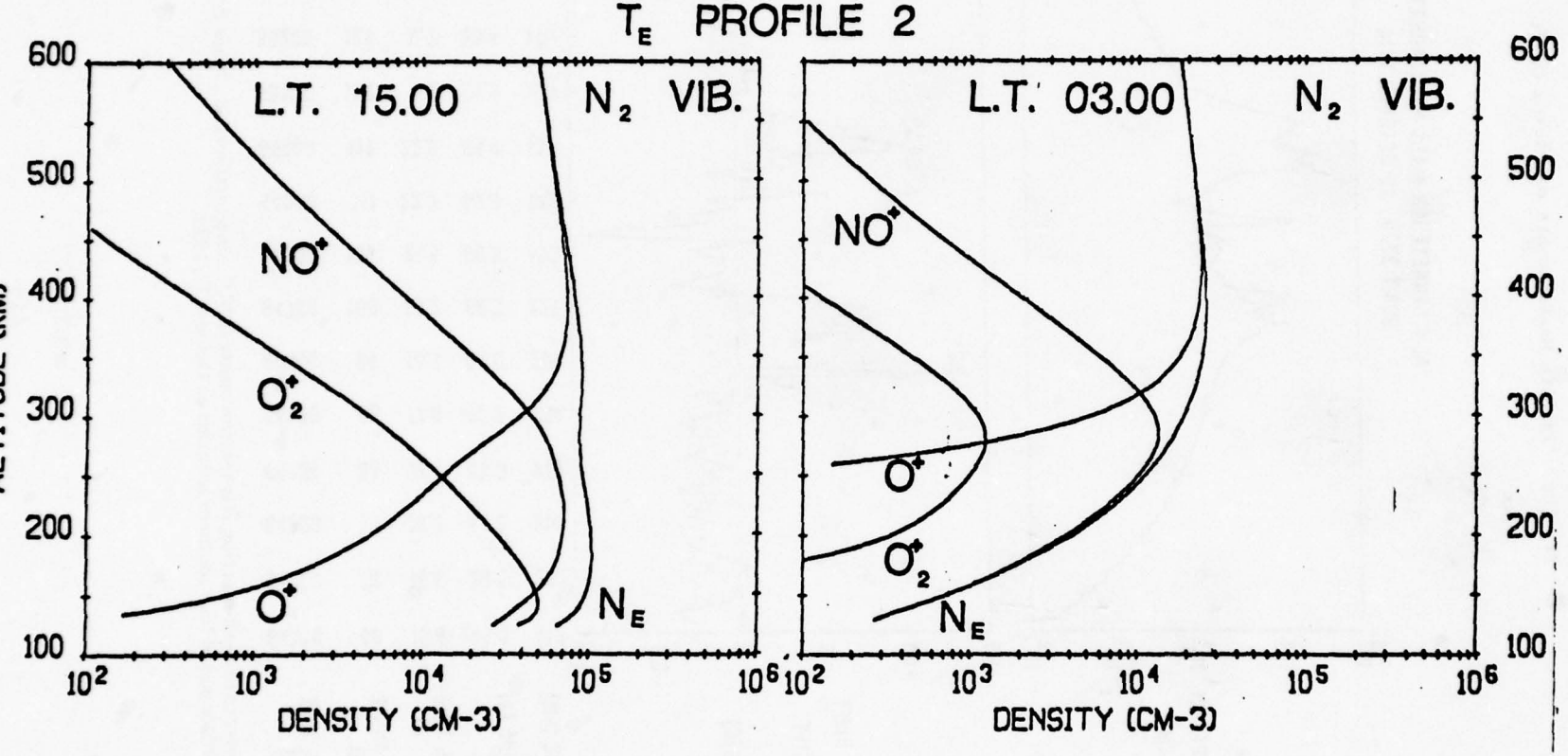
T_E PROFILE 2
L.T. 15.00
N_2 VIB.
L.T. 03.00
N_2 VIB.
NO^+
O_2^+
O^+
N_E
ALTITUDE (KM)
DENSITY (CM-3)
600
500
400
300
200
100
10^2
10^3
10^4
10^5
10^6

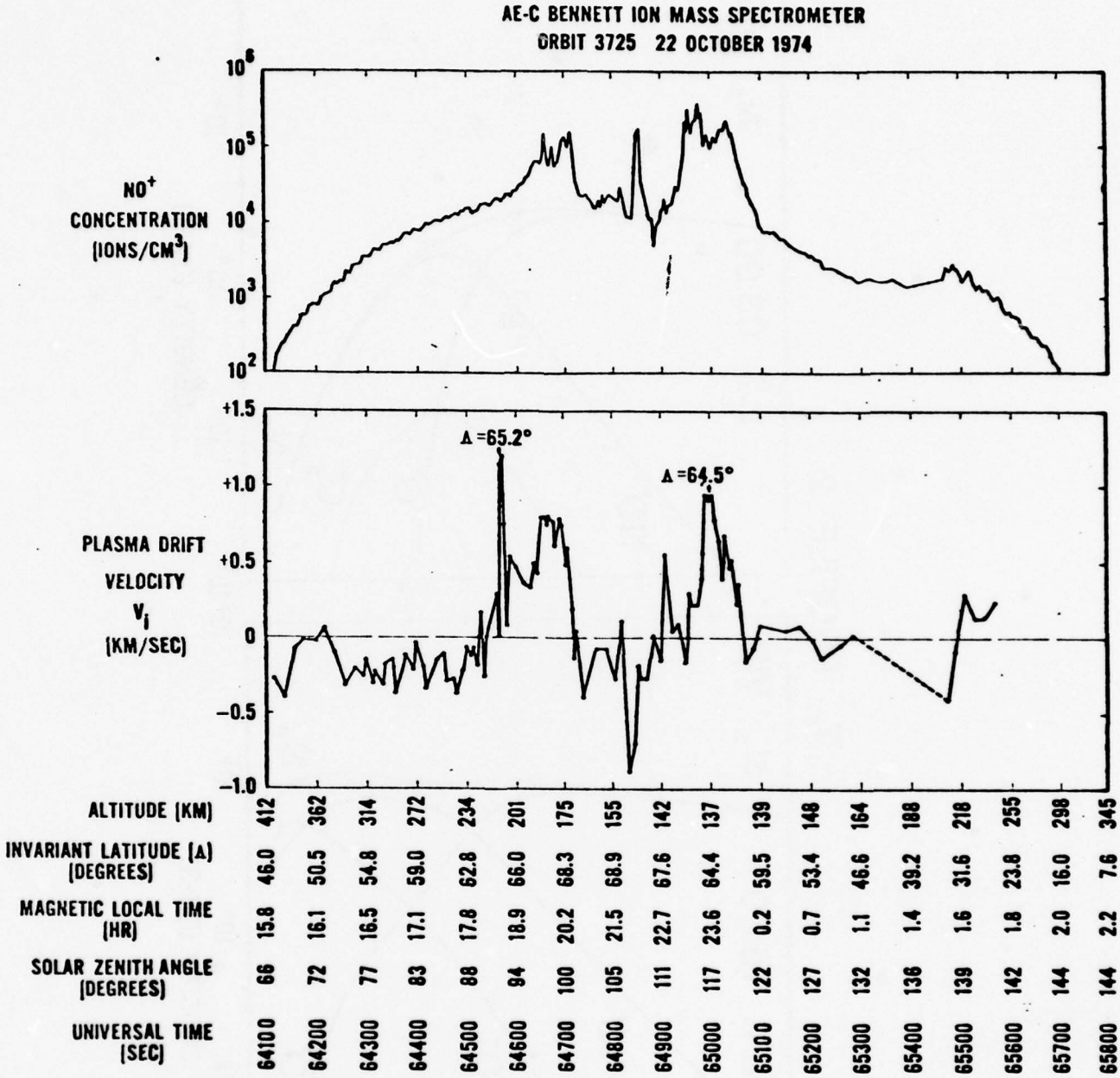

Figure 3. Simultaneous Bennett spectrometer measurements of NO^+ concentration and plasma drift velocity. The data were obtained during a perigee pass at high southern latitudes on October 22, 1974.

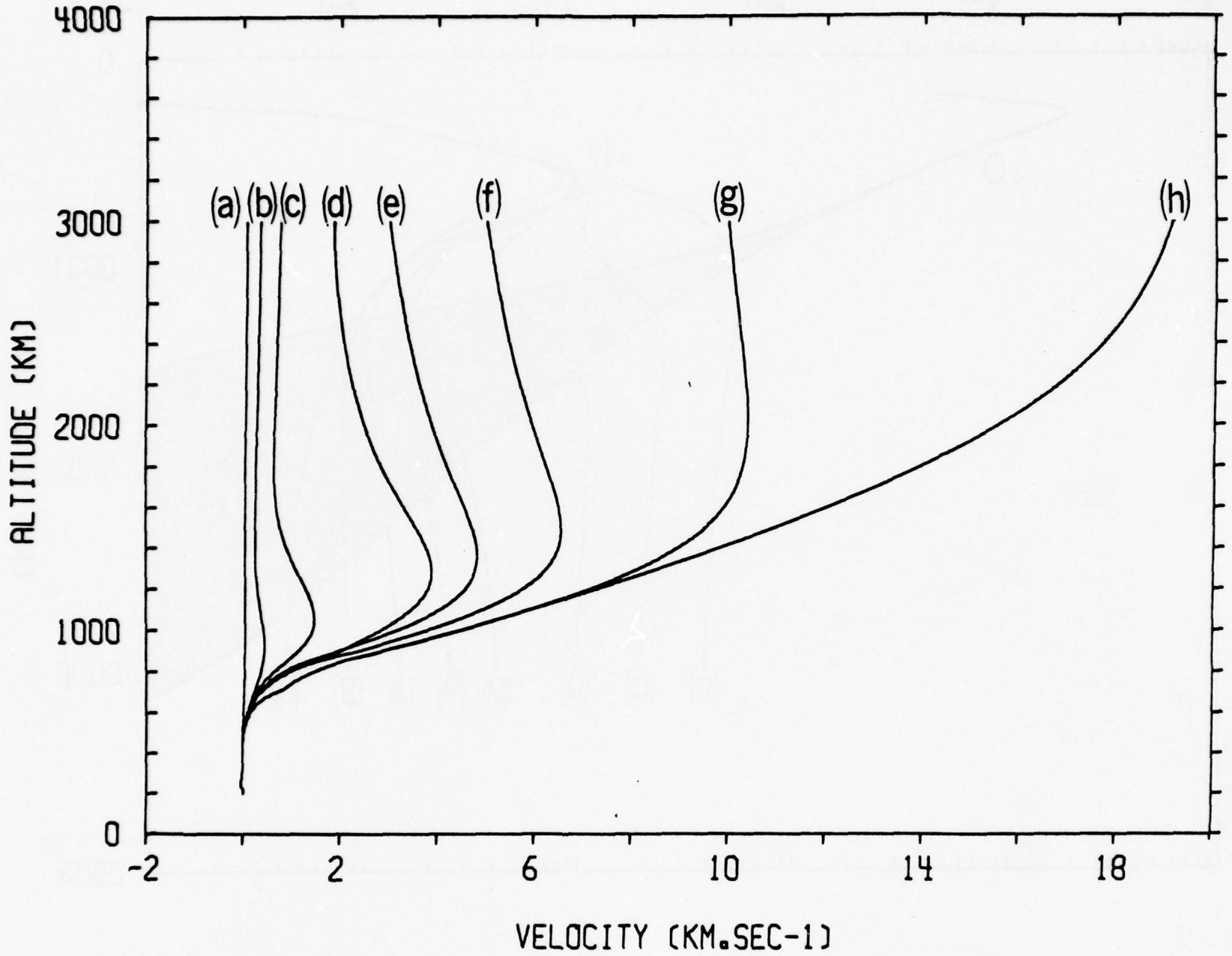
4000
3000
2000
1000
0
ALTITUDE (KM)
(a)
(b)
(c)
(d)
(e)
(f)
(g)
(h)
-2
2
6
10
14
18
VELOCITY (KM.SEC-1)

SLIDE 14
-45-

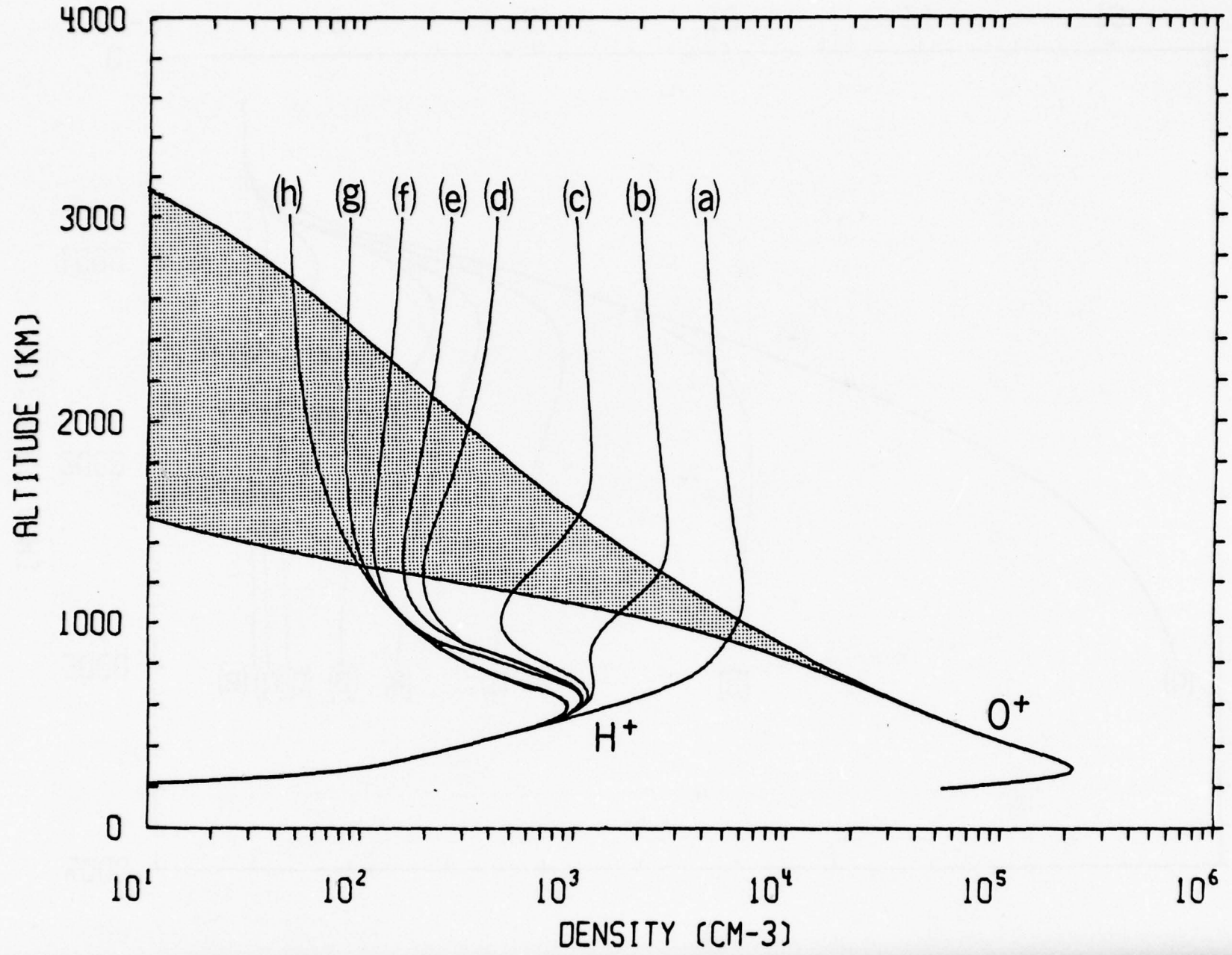
4000
3000
2000
1000
0
ALTITUDE (KM)
(h)
(g)
(f)
(e)
(d)
(c)
(b)
(a)
H+
O+
10^1
10^2
10^3
10^4
10^5
10^6
DENSITY (CM-3)

SLIDE 15
-46-

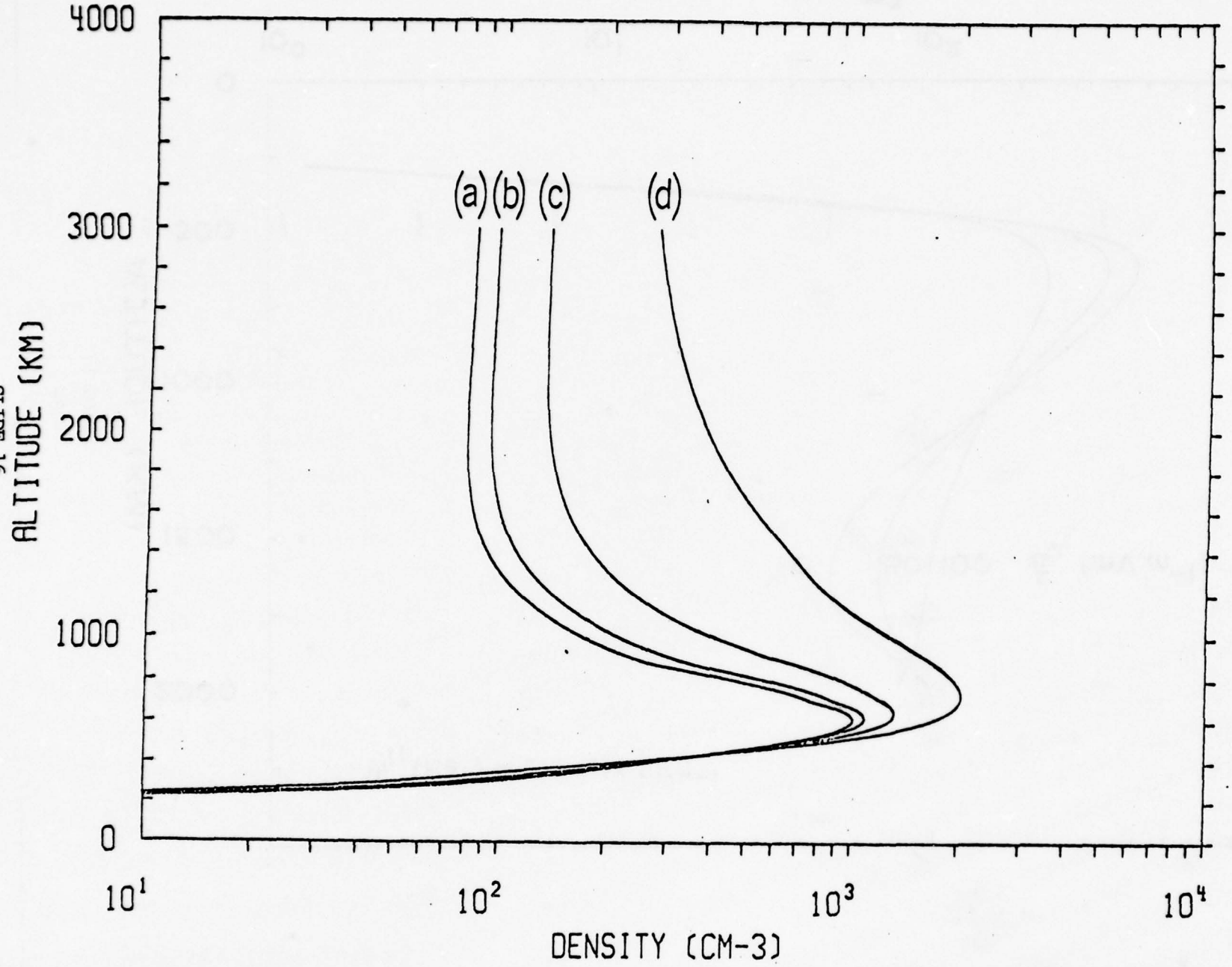
4000
3000
2000
1000
0
ALTITUDE (KM)
(a)
(b)
(c)
(d)
10^1
10^2
10^3
10^4
DENSITY (CM-3)

SLIDE 16
-47-

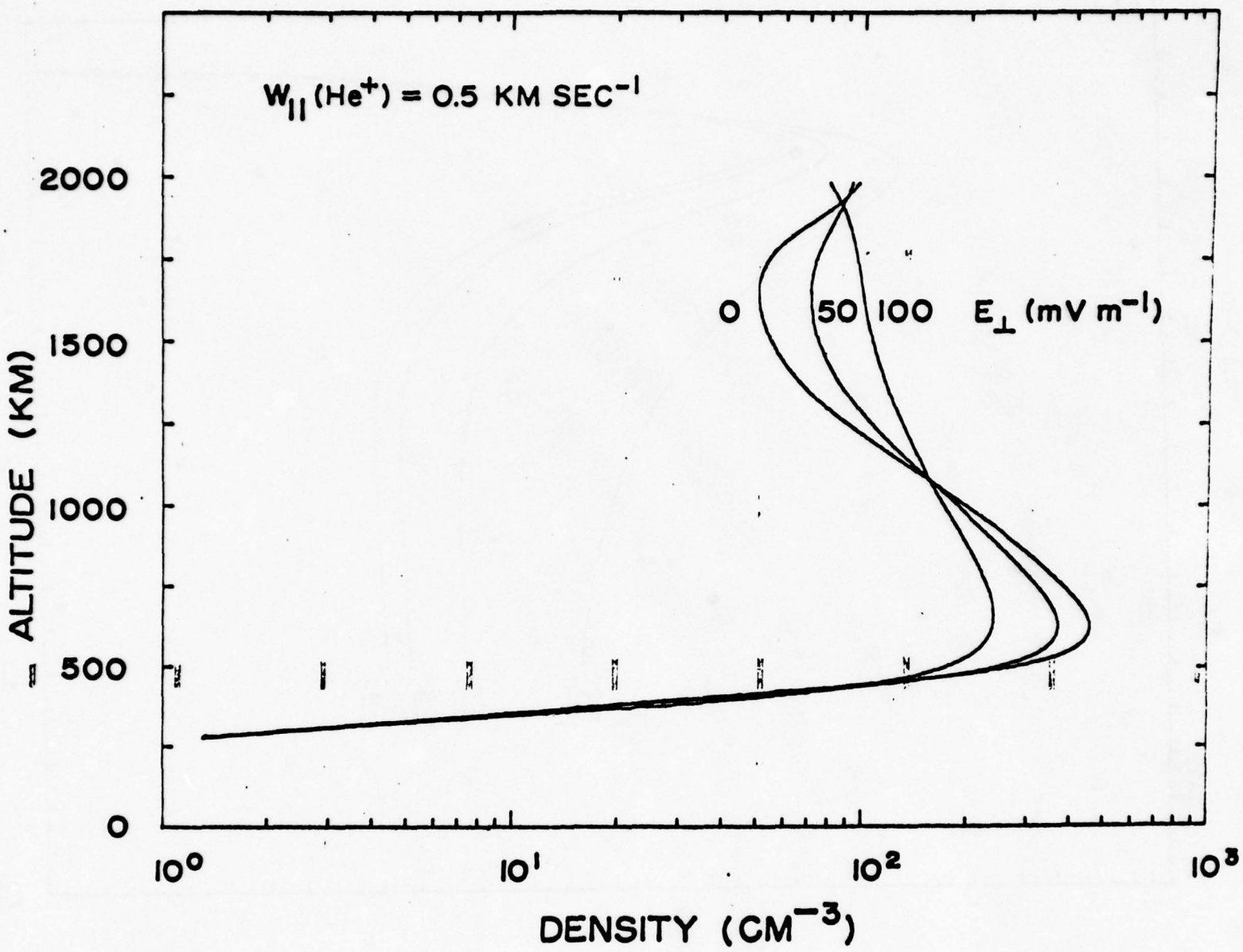
$W_{||}(He^+) = 0.5$ KM SEC^{-1}
0
50
100
$E_\perp$ (mV m^{-1})
ALTITUDE (KM)
2000
1500
1000
500
0
10^0
10^1
10^2
10^3
DENSITY (CM^{-3})

SLIDE 18

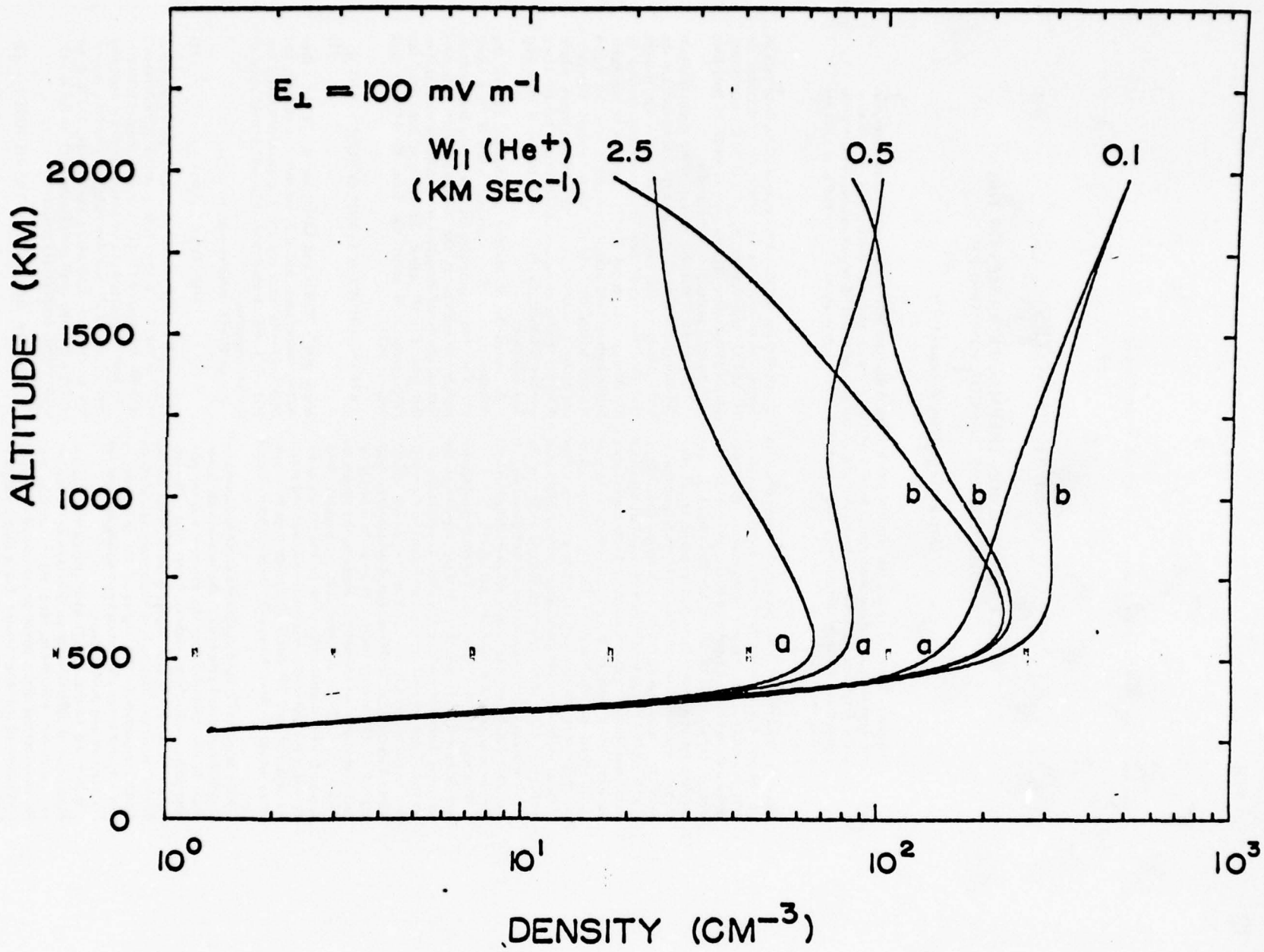
$E_\perp = 100$ mV m^{-1}
$W_{||}$ (He^+)
(KM SEC^{-1})
2.5
0.5
0.1
a
b
2000
1500
1000
500
0
ALTITUDE (KM)
10^0
10^1
10^2
10^3
DENSITY (CM^{-3})

Planet. Space Sci., Vol. 26, pp. 189 to 191. Pergamon Press, 1978. Printed in Northern Ireland

RESEARCH NOTES

EFFECT OF DIFFUSION–THERMAL PROCESSES ON THE HIGH-LATITUDE TOPSIDE IONOSPHERE

(*Received in final form* 8 *August* 1977)

Abstract—We have studied the extent to which diffusion–thermal heat flow affects H^+ temperatures in the high-latitude topside ionosphere. Such a heat flow occurs whenever there are H^+–O^+ relative drifts. From our study we have found that at high-latitudes, where H^+ flows up and out of the topside ionosphere, diffusion–thermal heat flow acts to reduce H^+ temperatures by 500–600 K at altitudes above about 900 km.

Recently, Schunk (1975) has presented a general system of transport equations for the Earth's upper atmosphere and ionosphere. This system of equations, which was derived using Grad's formulation (Grad, 1949, 1958) and Burgers (1969) collision terms, has the advantage over previous systems in that the separate species are allowed to have separate flow velocities and separate temperatures. In a subsequent paper, St.-Maurice and Schunk (1977) applied this general system of transport equations to the mid-latitude topside ionosphere. From their study a number of new transport effects have emerged. In particular, these authors found that for a gas composed of two major ions and electrons: (1) a temperature gradient in either of the major ion gases causes thermal diffusion in both gases; (2) a temperature gradient in either of the major ion gases causes heat to flow in both gases; and (3) a relative drift between the major ion gases induces a heat flow in both gases (diffusion–thermal effect).

With regard to the diffusion–thermal effect, St.-Maurice and Schunk (1977) pointed out three regions of the terrestrial ionosphere where this effect is potentially important. These regions are: (1) at midlatitudes, the transition region between the F-region and the protonosphere, where Vickery *et al.* (1976) measured geomagnetic field-aligned H^+–O^+ relative drifts as large as 80 m/s; (2) the nocturnal equatorial ionosphere, where model studies by Bailey *et al.* (1973) indicated that geomagnetic field-aligned H^+–O^+ relative drifts of up to 300 m/s are possible due to the asymmetry between the summer and winter hemispheres; and (3) the high-latitude topside ionosphere, where H^+ flows through O^+ at speeds up to several km/s.

Nagy *et al.* (1977) have studied the possible importance of diffusion–thermal processes in the mid-latitude ionosphere in the region between the F-region and the protonosphere, and these authors found that diffusion–thermal processes have a negligibly small effect on the thermal structure. This lack of importance of diffusion–thermal processes in this region of the ionosphere is primarily due to the efficient energy coupling between the ion, electron and neutral gases.

Bailey and Moffett (1977) have studied the possible importance of diffusion–thermal processes in the nocturnal equatorial ionosphere, and they conclude that diffusion–thermal effects should be considered for precise calculations of ion temperatures. For a dipole magnetic field line that crosses the equatorial plane at approximately 800 km and for a local time of 2200, these authors found that diffusion–thermal effects act to decrease the H^+ and O^+ temperatures by 50 and 30 K, respectively. Larger temperature decreases are expected on field lines with higher equatorial crossing points.

The purpose of this note is to study the extent to which diffusion–thermal processes affect H^+ temperatures in the high-latitude topside ionosphere. Initially it was thought that the "low-speed" heat flow equations derived by St.-Maurice and Schunk (1977) would not be applicable to the high-latitude topside ionosphere, since this region is characterized by large H^+ Mach numbers. However, our study indicates that at the altitude region where diffusion–thermal processes are important the H^+ Mach number is sufficiently low to justify the use of these heat flow equations.

As noted by St.-Maurice and Schunk (1977), the diffusion–thermal effect is greatest when H^+ is a minor ion. Since this is generally the case in the high-latitude topside ionosphere at the altitudes where diffusion–thermal effects are important, we restrict our discussion to this limit. For H^+ minor, the H^+ heat flow along the geomagnetic field takes the form (St.-Maurice and Schunk, 1977)

$$\mathbf{q}(H^+) = -\lambda(H^+)\nabla T(H^+) + \delta(H^+, O^+)[\mathbf{U}(H^+) - \mathbf{U}(O^+)], \tag{1}$$

where $\mathbf{q}(H^+)$, $T(H^+)$ and $\mathbf{U}(H^+)$ are the H^+ heat flow vector, temperature, and drift velocity, respectively, and $\mathbf{U}(O^+)$ is the O^+ drift velocity. The quantities $\lambda(H^+)$ and $\delta(H^+, O^+)$ are thermal and diffusion–thermal conductivities, respectively.

For an H^+–O^+ mixture with H^+ minor,

$$\delta(H^+, O^+) = 1.13p(H^+), \tag{2}$$

where $p(H^+) = n(H^+)kT(H^+)$ is the H^+ partial pressure, $n(H^+)$ is the H^+ number density, and k is Boltzmann's constant. In equation (2), $\delta(H^+, O^+)$ has units of pressure.

In deriving equation (1), we have ignored the negligibly small amount of H^+ heat flow induced by an O^+ temperature gradient (cf. St.-Maurice and Schunk, 1977). If we further ignore the small contribution of O^+ to the H^+–O^+ relative drift, equation (1) reduces to

$$\mathbf{q}(H^+) = -\lambda(H^+)\nabla T(H^+) + 1.13p(H^+)\mathbf{U}(H^+), \tag{3}$$

where we have used equation (2) to eliminate $\delta(H^+, O^+)$.

As far as the H^+ thermal structure is concerned, it is the divergence of $\mathbf{q}(H^+)$ that is important. Assuming a vertical magnetic field and neglecting gradients of density and temperature perpendicular to geomagnetic field lines, $\nabla \cdot \mathbf{q}(H^+)$ can be expressed in the form

$$\nabla \cdot \mathbf{q}(H^+) = -\frac{\partial}{\partial S}\left[\lambda(H^+)\frac{\partial T(H^+)}{\partial S}\right] + 1.13kT(H^+)\frac{\partial}{\partial S}[n(H^+)U(H^+)] + 1.13n(H^+)U(H^+)k\frac{\partial T(H^+)}{\partial S}, \quad (4)$$

where S is the vertical coordinate. The first term in equation (4) is the term generally considered in studies of H^+ thermal structure, while the two additional terms are due to the inclusion of diffusion–thermal effects. When expressed in this form, the diffusion–thermal process adds a term proportional to advection and another proportional to the divergence of the H^+ flux.

With regard to O^+ heat flow, we note that an H^+ temperature gradient induces a negligibly small amount of O^+ heat flow when H^+ is a minor ion (cf. St.-Maurice and Schunk, 1977). At the altitudes where H^+ is major (typically above 2000 km), thermal conduction dominates the H^+ energy balance, and this yields a negligibly small H^+ temperature gradient. We also note that diffusion–thermal heat flow is unimportant for O^+ when H^+ is a minor ion (St.-Maurice and Schunk, 1977). At the altitudes where H^+ is major, diffusion–thermal heat flow cannot compete with ordinary O^+ thermal conduction. Consequently, in our models the O^+ heat flow vector is governed by ordinary O^+ thermal conduction.

To determine the importance of diffusion–thermal heat flow, we obtain steady state solutions of the coupled continuity, momentum, and energy equations for H^+, O^+ and electrons. Our basic theoretical model is described by Raitt *et al.* (1975, 1977). Briefly, in this model account is taken of the velocity dependence of ion–neutral, ion–ion, and ion–electron collision frequencies. Ion and electron interactions with the neutrals N_2, O_2, O, He and H are considered. In the H^+ momentum equation, parallel stress and nonlinear acceleration terms are retained. In the H^+ energy equation, account is taken of advection, convection, thermal conduction, frictional heating due to convection electric fields, and energy exchange with O^+, electrons, and the different neutrals. To this basic model we add diffusion–thermal heat flow, as given by equation (4).

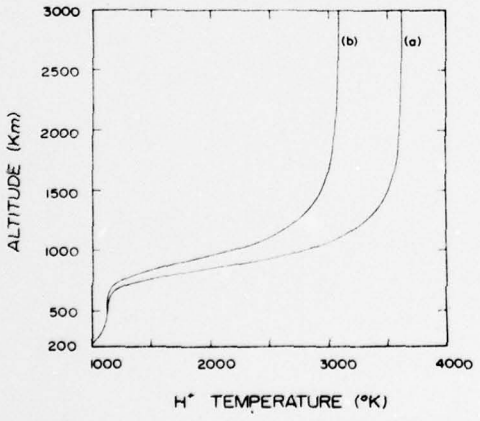

FIG. 1. THEORETICAL H^+ TEMPERATURE PROFILES CALCULATED WITHOUT (CURVE a) AND WITH (CURVE b) ALLOWANCE FOR DIFFUSION–THERMAL HEAT FLOW.

For these calculations, the H^+ velocity at 3000 km was set equal to 10 km/s and the convection electric field was set equal to zero.

TABLE 1. UPPER BOUNDARY H^+ TEMPERATURES (K) CALCULATED WITH AND WITHOUT ALLOWANCE FOR DIFFUSION–THERMAL HEAT FLOW

$U(H^+)$ (km/s)	5		10	
$E_\perp$ (mVm^{-1})	0	50	0	50
Without	3775	4632	3614	4583
With	3267	4064	3077	3943

In Fig. 1 we present H^+ temperature profiles calculated without (curve a) and with (curve b) allowance for diffusion–thermal heat flow. For these calculations, the H^+ velocity at 3000 km was set equal to 10 km/s and the convection electric field was set equal to zero. Further details of the temperature and density structure of the ionospheric plasma can be found in Raitt *et al.* (1975, 1977) for the case where diffusion–thermal heat flow is neglected. It is apparent from Fig. 1 that at high-latitudes, where H^+ flows up and out of the topside ionosphere, diffusion–thermal heat flow acts to cool the H^+ gas. For the case shown in Fig. 1, the H^+ temperature above 900 km is reduced by approximately 600 K when diffusion–thermal heat flow is included.

In order to cover a range of H^+ flow conditions, we considered upper boundary H^+ outflow velocities of 5 and 10 km/s in combination with convection electric fields, $E_\perp$, of 0 and 50 mVm^{-1}. For all combinations, the comparison of H^+ temperature profiles calculated with and without allowance for diffusion–thermal effects is similar to that shown in Fig. 1. These results are summarized in Table 1, where we present the upper boundary H^+ temperatures for the cases considered. It can be seen that diffusion–thermal effects act to reduce the H^+ temperature by 500–600 K for a range of plasma conditions.

Finally, we note that both of the terms in the expression for $\nabla \cdot \mathbf{q}(H^+)$ that are a consequence of diffusion–thermal effects act to cool the H^+ gas (see equation 4). For the case shown in Fig. 1, the cooling rate associated with the term proportional to the divergence of the H^+ flux peaks at about 700 km, while the cooling rate associated with the term proportional to advection peaks at about 900 km. At these altitudes, the H^+ Mach number is 0.08 and 0.34, respectively. These Mach numbers are sufficiently low to justify the use of the "low-speed" heat flow equations of St.-Maurice and Schunk (1977). We further note that the case shown in Fig. 1 corresponds to our worst case with regard to the applicability of the low-speed heat flow equations, since for the other cases summarized in Table 1 the H^+ Mach numbers are lower due to either electric field heating or lower upper-boundary H^+ outflow velocities.

In summary, we have found that diffusion–thermal processes have an important influence on H^+ temperatures in

the high-latitude topside ionosphere. The diffusion–thermal effect results in H^+ temperature decreases of typically 500–600 K at altitudes above about 900 km.

Acknowledgements—This research was supported by NSF Grant ATM76-19792, Air Force Contract F19628-77-C-0011, and NASA Grant NGR23-005-015.

R. W. Schunk
W. J. Raitt
A. F. Nagy

Center for Research in Aeronomy,
Utah State University,
Logan,
UT 84322,
U.S.A.

REFERENCES

Bailey, G. J. and Moffett, R. J. (1977). Diffusion–thermal effects in the topside of the nocturnal equatorial ionosphere. *J. geophys. Res.* To be published.

Bailey, G. J., Moffett, R. J., Hanson, W. B. and Sanatani, S. (1973). Effects of interhemisphere transport on plasma temperatures at low latitudes. *J. geophys. Res.* **78,** 5597.

Burgers, J. M. (1969). *Flow Equations for Composite Gases.* Academic Press, New York.

Grad, H. (1949). On the kinetic theory of rarefied gases. *Comm. pure appl. Math.* **2,** 331.

Grad, H. (1958). Principles of the kinetic theory of gases. *Handbuch Physik.* **XII,** 205.

Nagy, A. F., Roble, R. G., Swartz, W. E. and Vickrey, J. F. (1977). The role of relative ion flows on the thermal structure of the ionosphere. *Planet. Space Sci.* **25,** 1085.

Raitt, W. J., Schunk, R. W. and Banks, P. M. (1975). A comparison of the temperature and density structure in high and low speed thermal proton flows. *Planet. Space Sci.* **23,** 1103.

Raitt, W. J., Schunk, R. W. and Banks, P. M. (1977). The influence of convection electric fields on thermal proton outflow from the ionosphere. *Planet. Space Sci.* **25,** 291.

St.-Maurice, J.-P. and Schunk, R. W. (1977). Diffusion and heat flow equations for the mid-latitude topside ionosphere. *Planet. Space Sci.* **25,** 921.

Schunk, R. W. (1975). Transport equations for aeronomy. *Planet. Space Sci.* **23,** 437.

Vickrey, J. F., Swartz, W. E. and Farley, D. T. (1976). Incoherent scatter measurements of ion counterstreaming. *Geophys. Res. Lett.* **3,** 217.

Planet. Space Sci., Vol. 26, pp. 255 to 268. Pergamon Press, 1978. Printed in Northern Ireland

HELIUM ION OUTFLOW FROM THE TERRESTRIAL IONOSPHERE

W. J. RAITT, R. W. SCHUNK and P. M. BANKS
Center for Research in Aeronomy and Department of Physics,
Utah State University, Logan, UT 84322, U.S.A.

(*Received* 14 *August* 1977)

Abstract—Extensive calculations have been made of the behaviour of He^+ for situations where ion outflow occurs from the topside ionosphere. For these circumstances, steady state solutions for the He^+ continuity, momentum and energy equations have been obtained self-consistently, yielding density, velocity and temperature profiles of He^+ from 200 to 2000 km altitude. To model the high latitude topside ionosphere, a range of background $H^+ - O^+$ ionospheres was considered with variations in the H^+ outflow velocity, the presence of a perpendicular electric field and different peak O^+ densities. In addition, the atmospheric density of neutral helium was chosen to model typical observed winter and summer densities. From our studies we have found that: (a) The outflowing He^+ has density profiles of similar shape to those of H^+, for basically different reasons; (b) The effect of the perpendicular electric field differs considerably for H^+ and He^+. This difference stems from the fact that an electric field acts to alter significantly the O^+ density at high altitudes and this, in turn, changes the H^+ escape flux through the $O^+ + H$ charge exchange reaction. A similar situation does not occur for He^+ and therefore the He^+ escape flux exhibits a negligibly small change with electric field; (c) The fractional heating of He^+ due to the $He^+ - O^+$ relative flow is not as effective in heating He^+ as the $H^+ - O^+$ relative flow is in heating H^+; (d) During magnetospheric disturbances when the N_2 density at the altitude of the He^+ peak (600 km) can increase by a factor as large as 50, the He^+ peak density decreases only by approximately a factor of 2; and (e) The He^+ escape flux over the winter pole is approximately a factor of 20 greater than the He^+ escape flux over the summer pole. Consequently, on high latitude closed field lines there could be an interhemispheric He^+ flux from winter to summer.

1. INTRODUCTION

Early theoretical studies of the distribution of helium ions in the topside ionosphere were restricted to diffusive equilibrium, and predictions of regions where He^+ would be either dominant or significant were shown to be dependent on the ion temperature (Mange, 1960; Hanson, 1962; Bauer, 1963, 1966; Kockarts and Nicolet, 1962; Angeramie and Thomas, 1964).

The work of Banks and Holzer (1969) showed that at mid to high latitudes both H^+ and He^+ ions were likely to exist in a state of dynamic equilibrium with an outflow of ions from the ionosphere along geomagnetic field lines. Banks and Holzer (1969) solved the continuity and momentum equations for both H^+ and He^+ and were able to predict much lower topside He^+ densities for outflow compared to diffusive equilibrium. There have been few studies of He^+ dynamics since this initial work. Lemaire (1972) constructed a collisionless model of the polar wind including He^+, but no altitude profiles of He^+ were presented. Mayr *et al.*, (1972) studied interhemispheric transport and included He^+ in their model, but this study was concerned only with low-speed flows.

There is a growing interest in the theoretical distribution of helium ions in the vicinity of the earth since resonantly scattered 304 Å radiation from He^+ ions can be used as a tracer to experimentally map the He^+ distribution. Within the plasmasphere we expect a transition from near diffusive equilibrium at equatorial latitudes to subsonic/transonic flow at the poleward boundaries. At higher latitudes, in the trough and the polar caps, we expect there to be high speed outflow of the He^+ ions, particularly on open field lines. A further interest in He^+ outflow stems from the problem of the terrestrial helium budget for the two isotopes He^3 and He^4. It has been suggested (Axford, 1968; Johnson and Axford, 1969) that He^+ outflow is an important loss process in the budget. It is, therefore, important to study the limiting outward flux of He^+ under various geophysical conditions.

The behaviour of He^+ in the topside ionosphere is substantially different from H^+ since the two ions are subject to different sources and sinks. The prime production and loss mechanism for H^+ is the $H^+ + O \rightleftarrows H + O^+$ charge exchange reaction. He^+, in contrast, is produced by direct photoionization of He and lost by dissociative charge transfer to O_2 and N_2, the latter reaction being dominant above 300 km where $n(N_2) \gg n(O_2)$. The effects of changing the production and loss processes on the He^+

density distribution and outward flux are discussed later. The importance of the loss process of He^+ to N_2 molecules lies in the observed increases in N_2 density which occur during periods of magnetic disturbance. For example, Jacchia *et al.* (1977) predicts average high latitude increases of N_2 by a factor of 50 at 600 km over the undisturbed atmosphere, based on 1972–73 measurements from the ESRO-4 gas analyser. For these conditions the He density decreases by a factor of about 3 at 600 km. Both of these changes act to significantly reduce the He^+ density.

In the present study we have extended the work of Banks and Holzer (1969) to include a self-consistent solution of the He^+ energy equation in addition to the continuity and momentum equations under steady state conditions. We have included the non-linear acceleration term and parallel stress in the momentum equation, and velocity dependent factors in the collision frequencies. We have also included the effect of convection electric fields on the He^+ ion properties. In all of the present studies we have only concerned ourselves with conditions under which He^+ is a minor ion and as such makes only a small contribution to the electron density. This is consistent with the aims of this study to investigate the outflow of He^+ from the high latitude terrestrial ionosphere. We recognize, however, that there are conditions when He^+ can become a dominant ion (cf. Shepherd *et al.*, 1976) in the polar cap. This is most likely to occur when the He^+ ions are in diffusive equilibrium or even subjected to downflow. The techniques used to study the properties of outflowing He^+ used in the present analysis are not appropriate to this situation.

We have used background $H^+ - O^+$ ionospheres computed previously, details of which have been described by Raitt *et al.* (1977). Within these background ionospheres typical of polar wind conditions, we have considered a range of upper boundary He^+ outflow velocities from 0.1 to 2.5 km s^{-1}. We have also considered a change in the neutral He density typical of the change from the winter to summer pole conditions. Our final variation was to consider the case when the O^+ peak density was reduced by a factor of 10 to simulate conditions existing within the mid-latitude trough.

It is unfortunate that He^+ has not been experimentally studied as widely as H^+ and O^+ in the topside ionosphere. However, a number of latitudinal profiles of He^+ density have been reported (Taylor *et al.*, 1968; Taylor, 1972; Hoffman *et al.*, 1974; Breig and Hoffman, 1975) which clearly show a light ion trough structure for He^+ indicating the transition from a low latitude region of diffusive equilibrium to a mid-high latitude region where a dynamic equilibrium exists.

There have been fewer direct measurements of the latitude profiles of He^+, however the radar backscatter technique has yielded profiles at Arecibo at night which show characteristics of He^+ flow even at low latitudes (Hagen and Hsu, 1974). A further *in situ* observation of the altitude variation of He^+ was obtained from satellite measurements over a period long enough for significant precession of perigee (Brinton *et al.*, 1971). This again showed the characteristic profile of He^+ outflow.

We have not been able to locate published reports of any He^+ temperature measurements, but there should be a rich source of these and other He^+ data available at mid to high latitudes from the AE series of satellites. We look forward to the publication of these results.

II. THEORETICAL FORMULATION

The situation we investigated is the steady state flow of He^+ through a convecting topside polar ionosphere composed of O^+, H^+, electrons and the neutrals N_2, O_2, O, He and H. The neutral atmosphere was assumed to be stationary, and for N_2, O_2, O and He we adopted the atmospheric model of Jacchia (1964), as modified by Walker (1965). In Walker's model the altitude distributions of the neutral temperature and densities are determined by specifying the temperature and densities at 120 km and the exospheric temperature. At 120 km, the N_2, O_2, O and He densities were taken to be 4×10^{11} cm^{-3}, 7.5×10^{10} cm^{-3}, 7.6×10^{10} cm^{-3} and 3.4×10^{7} cm^{-3}, respectively. The neutral temperature at 120 km was taken to be 350 K, while the exospheric temperature was assumed to be 1000 K. For neutral atomic hydrogen, we adopted the values tabulated by Banks and Kockarts (1973) in Table B2(a).

For the electrons and H^+ and O^+ ions, we adopted the density, drift velocity, and temperature profiles calculated by Raitt *et al.* (1975, 1977). These profiles were obtained by solving a system of continuity, momentum, and energy equations for the major ions and electrons. In the transport equations, account was taken of the velocity dependence of ion–neutral, ion–ion, and ion–electron collision frequencies. In addition, parallel stress and non-linear acceleration terms were retained in the H^+ momentum equation, thus allowing for both subsonic and supersonic thermal proton outflows. Furthermore, the frictional heating associated with

convection electric fields was also included. The complete details of the basic ionospheric model is given by Raitt *et al.* (1975, 1977) and a description of the specific H^+, O^+, and electron profiles adopted for the present investigation is given in the next section.

Because we have adopted previously computed H^+, O^+ and electron density profiles, we can only consider situations for which He^+ is a minor ion. To model the behaviour of He^+ in the topside polar ionosphere, we solved the following continuity, momentum (parallel to **B**), and energy equations:

He^+ *continuity*

$$\frac{d}{ds}[N(He^+)W_{\parallel}(He^+)] = P(He^+) - \beta(He^+)N(He^+). \tag{1}$$

He^+ *momentum*

$$W_{\parallel}(He^+) + \frac{1}{\nu(He^+)}\left[W_{\parallel}(He^+)\frac{dW_{\parallel}(He^+)}{ds} + \frac{d\tau_{\parallel}(He^+)/ds}{N(He^+)M(He^+)}\right]$$
$$= \frac{\nu(He^+, H^+)\Phi(He^+, H^+)W_{\parallel}(H^+)}{\nu(He^+)} - D(He^+)$$
$$\times\left\{\frac{1}{N(He^+)}\frac{dN(He^+)}{ds} + \frac{T_e/T(He^+)}{N_e}\frac{dN_e}{ds} + \frac{M(He^+)g_{\parallel}}{kT(He^+)}\right.$$
$$\left. + \frac{1}{T(He^+)}\frac{d}{ds}[T(He^+) + T_e]\right\}. \tag{2}$$

He^+ *energy*

$$\tfrac{3}{2}N(He^+)kW_{\parallel}(He^+)\frac{dT(He^+)}{ds}$$
$$+\tfrac{3}{2}kT(He^+)\frac{d}{ds}[N(He^+)W_{\parallel}(He^+)]$$
$$+N(He^+)kT(He^+)\frac{dW_{\parallel}(He^+)}{ds} - \frac{d}{ds}\left[K(He^+)\frac{dT(He^+)}{ds}\right]$$
$$= N(He^+)\nu(He^+, e)3k[T_e - T(He^+)]\Psi(He^+, e)$$
$$+\frac{N(He^+)M(He^+)\nu(He^+, H^+)}{M(He^+) + M(H^+)}$$
$$\times\{3k[T(H^+) - T(He^+)]\Psi(He^+, H^+)$$
$$+M(H^+)\Phi(He^+, H^+)[W_{\parallel}(H^+) - W_{\parallel}(He^+)]^2\}$$
$$+\frac{N(He^+)M(He^+)\nu(He^+, O^+)}{M(He^+) + M(O^+)}$$
$$\times\{3k[T(O^+) - T(He^+)]\Psi(He^+, O^+)$$
$$+M(O^+)\Phi(He^+, O^+)W_{\parallel}^2(He^+)\}$$
$$+\sum_j\frac{N(He^+)M(He^+)\nu(He^+, j)}{M(He^+) + M(j)}$$
$$\times\{3k[T_n - T(He^+)]\Psi(He^+, j)$$
$$+M(j)\Phi(He^+, j)[W_{\parallel}^2(He^+) + W_{\perp}^2]\}, \tag{3}$$

where the summation in equation (3) is over the neutrals N_2, O_2, O, He and H.

In equations (1)–(3) and subsequent equations the symbols have the following meaning:

$N(H^+)$, $N(O^+)$, $N(He^+)$, N_e—H^+, O^+, He^+ and electron densities; $N_e = N(O^+) + N(H^+)$

$M(H^+)$, $M(O^+)$, $M(He^+)$, M_e—H^+, O^+, He^+ and electron masses

$W_{\parallel}(H^+)$, $W_{\parallel}(O^+)$, $W_{\parallel}(He^+)$, $W_{\parallel_e}$—H^+, O^+, He^+ and electron flow velocities along the magnetic field; $N_e W_{\parallel_e} = N(O^+)W_{\parallel}(O^+) + N(H^+)W_{\parallel}(H^+)$

$N(j)$, $M(j)$—density and mass of neutral species j

$T(H^+)$, $T(O^+)$, $T(He^+)$, T_e, T_n—H^+, O^+, He^+, electron and neutral temperatures

$P(He^+)$—He^+ production rate

$\beta(He^+)$—He^+ loss frequency

$\nu(He^+)$—He^+ total collision frequency

$D(He^+)$—He^+ diffusion coefficient

$\tau_{\parallel}(He^+)$—parallel component of the He^+ stress tensor

$K(He^+)$—He^+ thermal conductivity

$\nu(i, j)$—momentum transfer collision frequency for species i and j

$\Phi(i, j)$, $\psi(i, j)$—velocity dependent correction factors for species i and j

s—spatial coordinate parallel to the magnetic field, which is assumed to be vertical

$g_{\parallel}$—component of gravitational acceleration parallel to the magnetic field

k—Boltzmann's constant

$\mathbf{W}_{\perp}$—plasma convection velocity

$\mathbf{E}_{\perp}$—convection electric field

B—geomagnetic field

c—speed of light.

Helium ions are produced by photoionization of neutral He and lost in reactions with N_2 (cf. Banks and Kockarts, 1973),

$$P(He^+) = 8.16\times10^{-8}N(He)\,cm^{-3}\,s^{-1}, \tag{4}$$

$$\beta(He^+) = 1.5\times10^{-9}N(N_2)\,s^{-1}. \tag{5}$$

The He^+ diffusion coefficient, the parallel component of the He^+ stress tensor, and the He^+ thermal conductivity can be obtained from the equations presented by Schunk (1975).

$$D(He^+) = \frac{kT(He^+)}{M(He^+)\nu(He^+)}, \tag{6}$$

$$\tau_{\parallel}(He^+) = -\frac{10}{9}\frac{N(He^+)kT(He^+)}{\nu'(He^+)}\frac{dW_{\parallel}(He^+)}{ds}, \tag{7}$$

$$K(He^+) = \frac{5}{2}\frac{N(He^+)k^2T(He^+)}{M(He^+)\nu''(He^+)}, \tag{8}$$

where

$$\nu(\mathrm{He}^+) = \nu(\mathrm{He}^+, \mathrm{N}_2) + \nu(\mathrm{He}^+, \mathrm{O}_2) + \nu(\mathrm{He}^+, \mathrm{O}) + \nu(\mathrm{He}^+, \mathrm{H}) + \nu(\mathrm{He}^+, \mathrm{He})\Phi(\mathrm{He}^+, \mathrm{He}) + \nu(\mathrm{He}^+, \mathrm{O}^+)\Phi(\mathrm{He}^+, \mathrm{O}^+) + \nu(\mathrm{He}^+, \mathrm{H}^+)\Phi(\mathrm{He}^+, \mathrm{H}^+), \quad (9)$$

$$\nu'(\mathrm{He}^+) = 1.08\nu(\mathrm{He}^+, \mathrm{N}_2) + 1.07\nu(\mathrm{He}^+, \mathrm{O}_2) + 1.13\nu(\mathrm{He}^+, \mathrm{O}) + 1.25\nu(\mathrm{He}^+, \mathrm{He}) + 1.53\nu(\mathrm{He}^+, \mathrm{H}) + 1.53\nu(\mathrm{He}^+; \mathrm{H}^+) + 1.13\nu(\mathrm{He}^+, \mathrm{O}^+). \quad (10)$$

$$\nu''(\mathrm{He}^+) = 0.99\nu(\mathrm{He}^+, \mathrm{N}_2) + 0.99\nu(\mathrm{He}^+, \mathrm{O}_2) + 1.02\nu(\mathrm{He}^+, \mathrm{O}) + 1.48\nu(\mathrm{He}^+, \mathrm{He}) + 2.22\nu(\mathrm{He}^+, \mathrm{H}) + 1.21\nu(\mathrm{He}^+, \mathrm{O}^+) + 2.23\nu(\mathrm{He}^+, \mathrm{H}^+). \quad (11)$$

The momentum transfer collision frequencies and the velocity dependent correction factors are given in the Appendix.

At the altitudes of interest in the present study (200–2000 km), the effect of a convection electric field is to cause the ionospheric plasma to drift in a direction perpendicular to the geomagnetic field with a velocity $\mathbf{W}_\perp$ given by

$$\mathbf{W}_\perp = c(\mathbf{E}_\perp \times \mathbf{B})/B^2. \quad (12)$$

In deriving equation (12) from the charged particle perpendicular momentum equations, we have neglected the effects of neutral collisions (valid above 200 km), ion pressure gradients perpendicular to **B**, and horizontal gradients in plasma velocity. In addition, we have assumed a vertical magnetic field, the absence of neutral atmospheric winds, and we have neglected changes in magnetic flux tube volume and area.

Additional simplifying assumptions are implicit in equations (1)–(11). We did not allow for He^+ thermal diffusion and diffusion-thermal effects (Walker, 1967; Schunk and Walker, 1969, 1970; St. Maurice and Schunk, 1977) or production and loss collision terms in the He^+ momentum and energy equations, since the appropriate expressions have not yet been derived. An estimate of the effect that these processes may have on the density, drift velocity, and temperature profiles has been presented by Banks *et al.* (1974) for the case of H^+ outflow.

Further simplifying assumptions were involved in the calculation of the parallel component of the He^+ stress tensor (7) and the He^+ thermal conductivity (8). These expressions were obtained from low-speed, collision-dominated stress and heat flow equations. A more rigorous procedure would be to obtain the He^+ heat flow and stress components directly from generalized flow equations such as the 13-moment system presented by Schunk (1975). Unfortunately, the high-speed collision terms for these generalized equations are complex and are currently not available (cf. Schunk, 1975).

Because of the above limitations, our model of He^+ outflow cannot be accepted as a completely accurate description of the He^+ flow process. However, the present results should serve as a useful guide to the behaviour of He^+ outflow until the more accurate set of equations can be developed and solved.

Solutions to the coupled system of equations that we have adopted have been obtained using iterative methods applied to linearized finite difference equations. The accuracy of the results has been determined through checks on particle, momentum and energy conservation. At our lower boundary (200 km), transport processes are not important and, consequently, $N(He^+)$ was obtained by equating local production and loss rates and $T(He^+)$ was obtained by equating local heating and cooling rates. At our upper boundary (2000 km), we selected the He^+ velocity as a parameter which could be varied to investigate the effects of different He^+ escape fluxes. Since the He^+ escape flux reached its limiting value for most of our studies, we could just as well have chosen the He^+ density as the boundary parameter. In the absence of experimental observations we also set $dT(He^+)/ds = 0$; that is, we neglected He^+ heat sources above 2000 km.

In computing our profiles it was assumed that the frame of reference followed the convecting flux tube, and that the time constant to reach a steady state solution is small compared with times to drift over distances where the overall boundary conditions change significantly. *Post facto* comparisons of He^+ fluxes, collision times and densities indicate this.

III. DISCUSSION OF RESULTS

III.1 *Background ionosphere*

As we discussed earlier, the He^+ density, velocity, and temperature profiles were computed in the presence of $H^+ - O^+$ model ionospheres derived from previous model calculations. The $H^+ - O^+$ models consist of H^+ flowing out through an O^+ background, the whole plasma drifting when subjected to convection (perpendicular) electric fields.

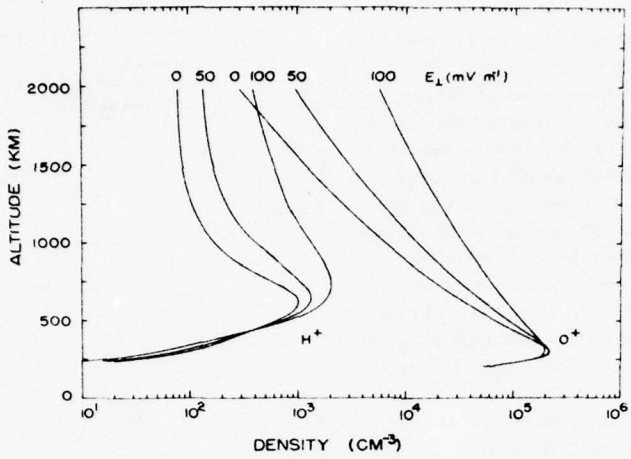

FIG. 1(a). THEORETICAL H^+ AND O^+ DENSITY PROFILES AS A FUNCTION OF ALTITUDE FOR THE STANDARD BACKGROUND IONOSPHERE.

The H^+ outflow velocity at the upper boundary is fixed at 10 km s^{-1}, while the perpendicular electric field varies between 0 and 100 mVm^{-1}.

The $H^+ - O^+$ model is described fully by Raitt *et al.* (1977).

Of the many models available from the former calculations we adopted one set of profiles as a standard set and then studied the effects of deviations from these standard background ionospheres. The general characteristics of our standard ionosphere were an O^+ density at the F_2 peak of 2.1×10^5 cm^{-3} and an H^+ outflow velocity at 3000 km of 10 km s^{-1}. The standard H^+ and O^+ density profiles are shown in Fig. 1(a), where the ion density is plotted against altitude for both the O^+ and H^+ ions and for three values of the perpendicular electric field; 0, 50 and 100 mVm^{-1}. As expected, an increasing electric field acts to increase both the H^+ and O^+ ion densities in the region above the ion peak densities where diffusion dominates over chemical processes. The O^+ densities in all cases were such that He^+ remained a minor ion at all altitudes, as is required by the formulation given in Section 2.

The H^+, O^+ and electron temperature profiles of our standard model for each of the electric field cases are shown in Fig. 1(b). Particle temperature is

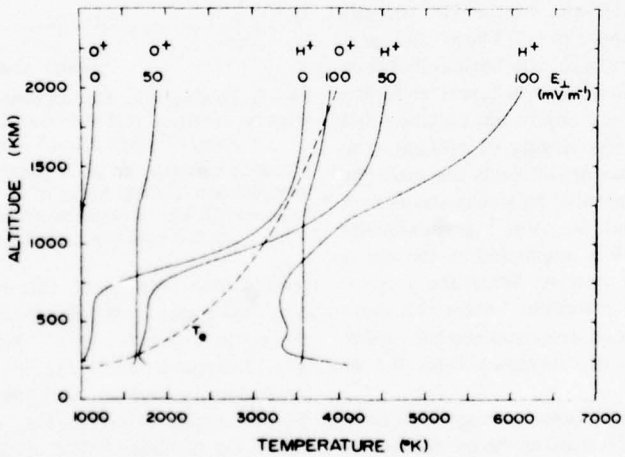

FIG. 1(b). THEORETICAL TEMPERATURE PROFILES AS A FUNCTION OF ALTITUDE FOR ELECTRONS (BROKEN LINES), H^+ AND O^+ IONS.

For the ions the boundary conditions are the same as for Fig. 1(a). The electron temperature profile corresponds to that for a perpendicular electric field of 50 mVm^{-1}.

plotted as a function of altitude, the H^+ and O^+ temperature profiles being represented by solid lines and the electron temperature profile by the broken line. Again, three sets of ion temperature profiles are presented corresponding to the three perpendicular electric fields adopted as standard. The electron temperature profile showed negligible change with the perpendicular electric field so only that profile corresponding to $E_\perp = 50\,\mathrm{mVm^{-1}}$ is presented. The heating effect of the perpendicular electric field on both H^+ and O^+ at low altitudes can be seen, together with the additional frictional heating of H^+ as it begins to flow rapidly relative to O^+ above 800 km.

The model background ionospheres shown in Figs. 1(a) and 1(b) were used in most of the He^+ outflow calculations. Deviations from this background plasma were treated as special cases and will be discussed later.

III.2 *Helium ion density profiles*

The He^+ density profiles as a function of altitude for the standard background ionospheres are shown in Fig. 2. These background ionospheres and the He^+ density profiles were calculated for sunlit conditions. For each of the three standard perpendicular electric fields chosen, three He^+ outflow velocities at the upper boundary were chosen. The magnitudes of these outflow velocities were 0.1, 0.5 and 2.5 $\mathrm{km\,s^{-1}}$. The perpendicular electric field used in the He^+ calculation was consistent with that which had been used in deriving the background ionosphere.

The general characteristics of the He^+ density profiles are similar to those of H^+. There is a region below about 600 km where equilibrium between production and loss dominates, whereas at higher altitudes diffusion is more important, resulting in a peak He^+ density in the vicinity of 600 km. The higher He^+ outflow cases qualitatively resemble the flux limited profiles computed by Banks and Holzer (1969). For the 0 and 50 $\mathrm{mVm^{-1}}$ perpendicular electric fields, this peak is unaffected by the upper boundary He^+ outflow velocity. When the perpendicular electric field is 100 $\mathrm{mVm^{-1}}$ there is a slight reduction in the He^+ peak density as the He^+ upper boundary outflow velocity increases from 0.1 to 2.5 $\mathrm{km\,s^{-1}}$.

The reason for this behaviour is a consequence of the increasing ion temperature as the perpendicular electric field increases. The higher ion temperature causes a decreased Mach number for a given outflow at the upper boundary. The result is that the profiles become nearer to diffusive equilibrium

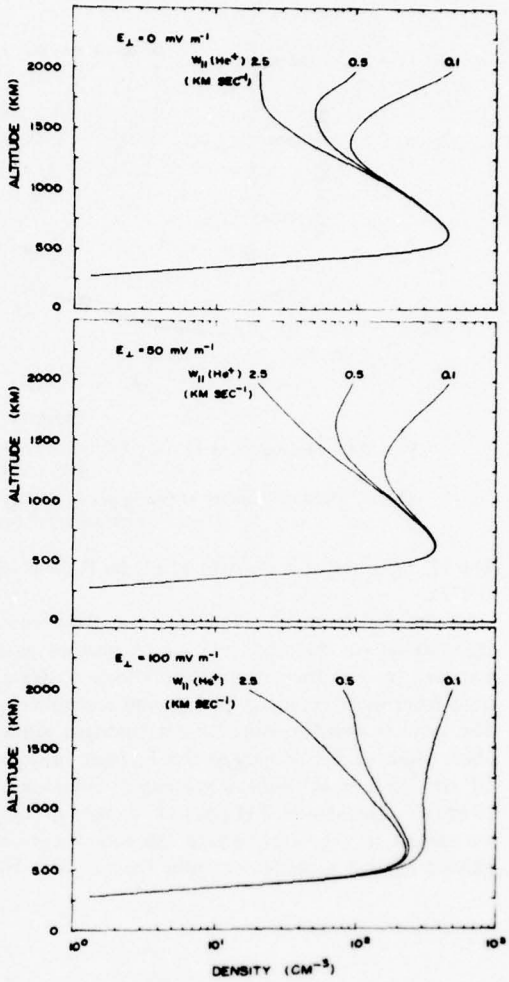

FIG. 2. THEORETICAL He^+ DENSITY PROFILES AS A FUNCTION OF ALTITUDE FOR He^+ UPPER BOUNDARY OUTFLOW VELOCITIES OF 0.1, 0.5 AND 2.5 $\mathrm{km\,s^{-1}}$.

The upper, middle and lower panels show the profiles for perpendicular electric fields of 0, 50 and 100 $\mathrm{mVm^{-1}}$, respectively. The background ionospheres are the standard models shown in Figs. 1a and 1b.

profiles above the peak, this effect being particularly noticeable in the most extreme case of $E_\perp = 100\,\mathrm{mVm^{-1}}$ and 0.1 $\mathrm{km\,s^{-1}}$ He^+ outflow velocity (Fig. 2, bottom panel). For this case the increased peak density and much higher upper boundary density results from the He^+ outward flux being below the saturated flux of $3.8\times10^6\,\mathrm{cm^{-2}\,s^{-1}}$ at $3.2\times10^6\,\mathrm{cm^{-2}\,s^{-1}}$. This again is due to the high ion temperature and the inhibiting effect on the He^+ diffusion coefficient of the higher H^+ and O^+ densities for $E_\perp = 100\,\mathrm{mVm^{-1}}$.

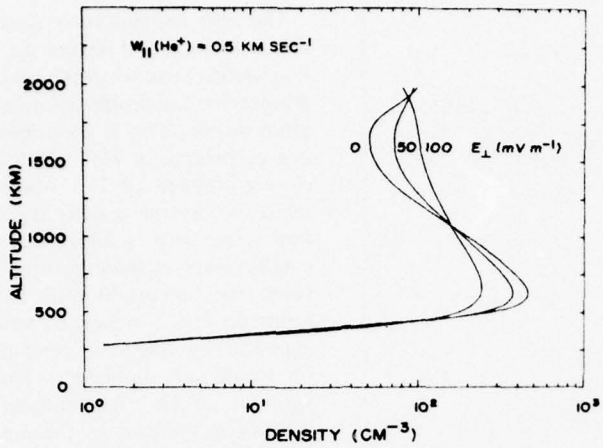

FIG. 3. THEORETICAL He^+ DENSITY PROFILES AS A FUNCTION OF ALTITUDE FOR A FIXED He^+ UPPER BOUNDARY OUTFLOW VELOCITY OF 0.5 km s^{-1} AND THREE PERPENDICULAR ELECTRIC FIELDS OF 0, 50 AND 100 MVm^{-1}.

The background ionospheres are the same as those for Fig. 2.

Figure 3 shows three He^+ density profiles for the same He^+ outflow velocity of 0.5 km s^{-1}, but for each of the three standard perpendicular electric fields of 0, 50 and 100 mVm^{-1}. This figure emphasizes an important difference between He^+ and H^+ outflows as they are affected by the magnitude of the perpendicular electric field. Figure 3 shows the increase in scale height with increasing magnitude of the perpendicular electric field resulting in a redistribution of ions, the density near the peak decreasing and the density above about 1000 km increasing. The upper boundary density shows little variation because the outward flux remains constant at its saturated value. This can be contrasted to the H^+ density profiles shown in Fig. 1(a) where, although the increased scale height above the H^+ peak is evident, the outward flux increases with increasing electric field, as illustrated by the increasing H^+ density at the upper boundary while the H^+ velocity at this boundary remains fixed. The reason for this different behaviour is that the increased O^+ above the F_2 peak acts as an additional source of H^+ ions due to the charge exchange reaction $H + O^+ \rightleftarrows H^+ + O$, while in our present model the source of He^+ is unchanged since it arises solely from photoionization of He.

III.3 *Helium ion velocity profiles*

Profiles of the He^+ velocity parallel to **B** as a function of altitude are shown in Fig. 4. These velocities correspond to the three perpendicular electric fields and the three He^+ boundary outflow velocities used to compute the He^+ density profiles shown in Fig. 2.

The zero perpendicular electric field case is similar in characteristics to the H^+ velocity profiles (Raitt *et al.*, 1977) in that the ion velocity parallel to **B** is negative at low altitudes, becomes positive, then increases to reach a peak value before falling back to the upper boundary value. A notable difference between He^+ and H^+ in the detail of the profiles is that the rapid increase in the He^+ outflow velocity occurs at a higher altitude than for H^+; the He^+ increase occurring at about 1300 km while the H^+ increase occurs around 800 km. This difference is primarily due to the smaller diffusion coefficient for He^+ resulting in production and loss being more important to higher altitudes for He^+ than for H^+.

In comparing the velocity profiles for increasing perpendicular electric fields it can be seen that at higher altitudes, above about 1000 km, there is a decrease in the He^+ outflow velocity. This is a result of the flux limited condition for all but the extreme case of $E_\perp = 100$ mVm^{-1} and 0.1 km s^{-1} He^+ outflow boundary velocity. The increased scale height results in increased number densities at these altitudes and since the outward flux ($N(He^+)W_{\parallel}(He^+)$) is constant $W_{\parallel}(He^+)$ must be lower.

At lower altitudes, around 300 km, there is a marked increase in the downward velocity as the perpendicular electric field is increased. This is a result of the increase in the ion–ion diffusion coefficient, $D \sim T_i^{5/2}/N_i$. The O^+ density changes only

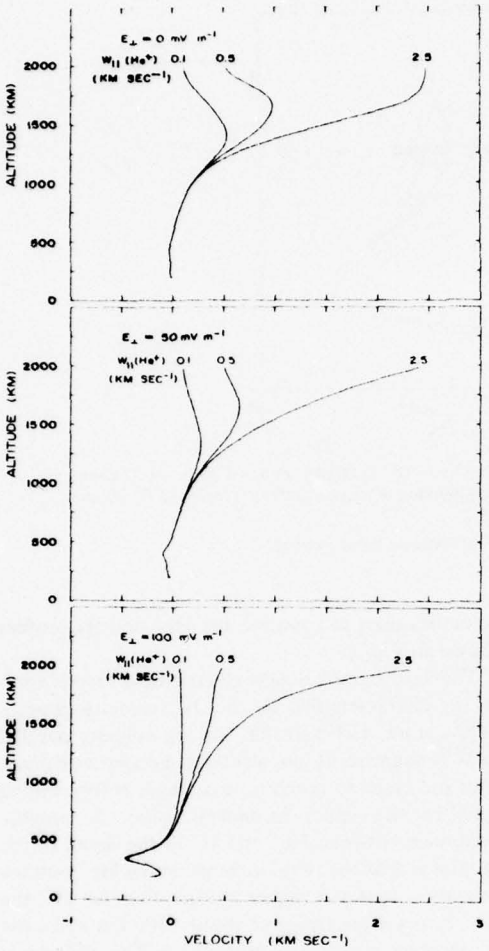

FIG. 4. THEORETICAL He^+ VELOCITY PROFILES AS A FUNCTION OF ALTITUDE FOR He^+ UPPER BOUNDARY VELOCITIES OF 0.1, 0.5 AND 2.5 km s^{-1}.

The upper, middle and lower panels correspond to perpendicular electric fields of 0, 50 and 100 mVm^{-1}, respectively. The background ionospheres are the same as those for Fig. 2.

slightly with increasing $E_\perp$, from 0 to 100 mVm^{-1}, but $T(O^+)$ increases by a factor of about 3.5; hence D increases by a factor of approximately 25. The net result of the various competing processes is an increase in the downward velocity by a factor of 16.

III.4 *Helium ion temperature profiles*

The He^+ temperature profiles as a function of altitude for the same background ionospheres and He^+ outflow velocities at the upper boundary used to calculate the density and velocity profiles of Figs. 2 and 4 are shown in Fig. 5.

The zero perpendicular electric field case shows that below about 1300 km the boundary He^+ outflow velocity has very little effect on the He^+ temperature and the profile is similar to the O^+ temperature profile. This is confirmed by a study of the energy balance of He^+ which shows it to be very closely coupled to O^+. Above 1300 km a more rapid increase in velocity occurs, which results in flow terms such as advection, convection, thermal conduction, and Joule heating by collision with O^+ being more important in the energy balance. These terms do not, however, dominate the energy balance and coupling to O^+ remains an important term up to the top boundary. This prevents a large variation of He^+ temperature with He^+ outflow velocity in contrast to the marked affect for H^+ ions. The main reason for the small effect of frictional heating is that the He^+ velocity shows a rapid increase only above 1300 km, while for H^+ the rapid increase in outflow velocity begins at about 800 km. At 1300 km the O^+ density is typically a factor of 5 lower than at 800 km and the Joule heating is consequently reduced. It should be noted, however, that the behaviour of the Joule heating agrees with that observed for H^+ in that the subsonic–transonic cases of 0.1 and 0.5 km s^{-1} outflow velocity show an increase in upper boundary temperature, while the supersonic outflow case of 2.5 km s^{-1} shows a reduction. This can be attributed to the same reason as that for H^+ temperatures, a reduction in the velocity dependent collision frequency factor $\Psi(He^+, O^+)$ as the Mach number significantly exceeds unity.

The groupings of the families of He^+ temperature profiles for different He^+ outflow velocities for each of the three standard perpendicular electric fields shows that this latter parameter has the strongest influence on the He^+ temperature. The increase in frictional heating of He^+ ions near the lower boundary by collisions with the neutral gas as $E_\perp$ increases can be seen. This frictional heating rapidly declines with altitude as the neutral gas density decreases until the strong coupling to the O^+ ions takes over. Like the zero perpendicular electric field case the effect of the He^+ outflow is minimal until about 1300 km when the flow, conduction, and $He^+ - O^+$ frictional heating terms become significant.

The upper boundary temperatures for the 50 mVm^{-1} case show the same pattern of increase followed by decrease as the He^+ outflow velocity increases that was shown by the zero-field case. At 100 mVm^{-1}, however, there is a continual decrease in $T(He^+)$ at the top boundary. This results from

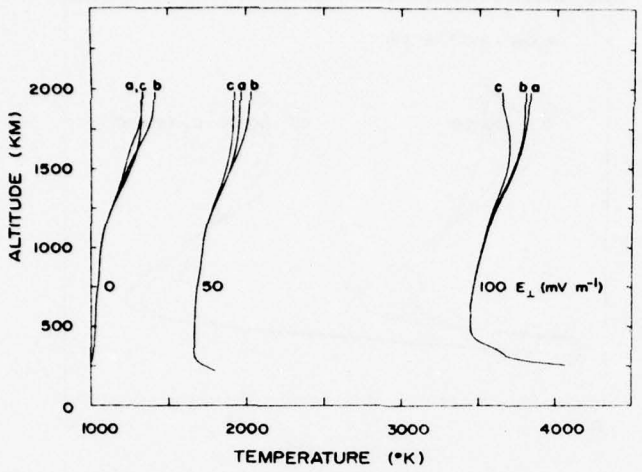

FIG. 5. THEORETICAL He^+ TEMPERATURE PROFILES AS A FUNCTION OF ALTITUDE FOR He^+ UPPER BOUNDARY VELOCITIES OF: (a) 0.1, (b) 0.5 AND (c) 2.5 km s^{-1}.

Each family of curves corresponds to a different perpendicular electric field as is indicated by the labels. The background ionospheres are the same as those for Fig. 2.

the effect of the convection term in the energy balance switching from a heat source to a heat sink. This is confirmed by reference to the He^+ velocity profiles shown in Fig. 4 where it can be seen that the 0.1 and 0.5 km s^{-1} outflow cases for 0 and 50 mVm^{-1} have negative slopes near the upper boundary, while the slopes are near zero or positive for the 100 mVm^{-1} case.

III.5 *Change of background ionosphere* H^+ *outflow*

In order to study the effect of the H^+ outflow velocity on the He^+ ion profiles the same three perpendicular electric field cases and the same three He^+ upper boundary outflow velocities were used to compute He^+ profiles for an H^+ upper boundary outflow velocity of 5 km s^{-1}. It was found that none of the He^+ density, velocity or temperature profiles differed significantly when the H^+ outflow velocity was 5 km s^{-1} compared to the standard background ionosphere when the H^+ outflow velocity was 10 km s^{-1}. This is emphasized in Table 1 which summarizes the upper boundary He^+ temperatures for the standard background ionosphere and for the lower H^+ outflow velocity model.

TABLE 1. He^+ TEMPERATURES (K) AT THE UPPER BOUNDARY OF THE MODEL (2000 km) AS A FUNCTION OF H^+ AND He^+ OUTFLOW VELOCITIES AND PERPENDICULAR ELECTRIC FIELD. IN ALL CASES THE O^+ PEAK DENSITY WAS 2.1×10^5 cm^{-3}

$W_{\parallel}(He^+)$ (km s^{-1})	0.1		0.5		2.5	
	$W_{\parallel}(He^+)$, km s^{-1}					
$E_{\perp}$ (mVm^{-1})	5	10	5	10	5	10
0	1350	1328	1417	1410	1338	1332
50	2006	1963	2056	2026	1939	1920
100	3858	3831	3816	3798	3648	3643

The reason for the insensitivity of He^+ to H^+ outflow is that it is the O^+ density rather than the H^+ density which has the major effect on both the He^+ outflow velocity and the He^+ temperature. In changing the H^+ upper boundary outflow velocity from 10 km sec^{-1} to 5 km s^{-1} there is a negligible change in the O^+ density profile for a given perpendicular electric field.

III.6 *Change of neutral helium gas density*

The neutral atmospheric structure used in our model contains a helium density profile which is in good agreement with the measured winter hemisphere density of Mauersberger *et al.* (1976a, b). In order to test the effect of a neutral helium density profile more typical of the summer hemisphere we reduced the neutral helium density by a factor of 20 at all altitudes. We then computed He^+ profiles for our standard background ionospheres and with a fixed He^+ upper boundary outflow velocity of 0.5 km s^{-1}.

The He^+ density profiles with the reduced neutral helium density are compared in Fig. 6(a) to the He^+ density profiles for the standard background ionospheres and with the same He^+ outflow

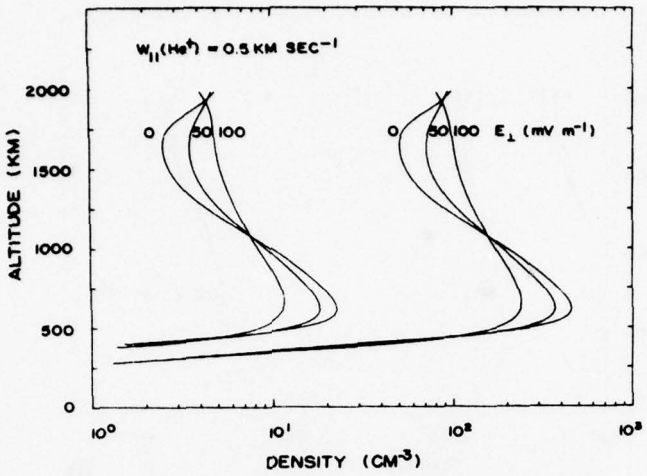

FIG. 6(a). THEORETICAL He^+ DENSITY PROFILES AS A FUNCTION OF ALTITUDE FOR A FIXED He^+ UPPER BOUNDARY VELOCITY OF 0.5 km s^{-1} AND PERPENDICULAR ELECTRIC FIELDS OF 0, 50 AND 100 mVm^{-1}, AS LABELLED.

The right-hand family of curves corresponds to neutral He densities typical of the winter hemisphere, while the left-hand family corresponds to a reduction in n(He) by a factor of 20 at all altitudes.

velocity of 0.5 km s^{-1}. It can be seen that the densities at all altitudes are reduced by a factor of 20 and since the upper boundary He^+ outflow velocities are the same the escape flux is also reduced by a factor of 20. The linear scaling is a consequence of the source of He^+ being photoionization of He, thus reducing He by a factor of 20 reduces the available He^+ ions in the same proportion.

A comparison of the He^+ temperature structure for the standard neutral helium density and the reduced density is shown in Fig. 6(b), where the He^+ temperature is plotted as a function of altitude. There is also a small change in $T(He^+)$ when the neutral He is varied by a factor of 20. The slightly higher temperature profile when N(He) is reduced results from lower collisional cooling between He^+ and He. This effect is most pronounced

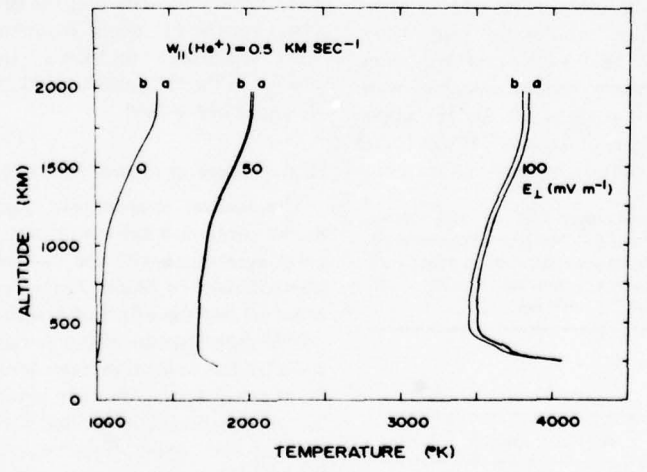

FIG. 6(b). THEORETICAL He^+ TEMPERATURE PROFILES AS A FUNCTION OF ALTITUDE FOR AN UPPER BOUNDARY He^+ VELOCITY OF 0.5 km s^{-1} AND PERPENDICULAR ELECTRIC FIELDS OF 0, 50 AND 100 mVm^{-1}.

Curves (a) and (b) correspond to the standard and reduced neutral helium densities, respectively, described for Fig. 6a.

TABLE 2. He^+ TEMPERATURE (K) AT THE UPPER BOUNDARY OF THE MODEL (2000 km) AS A FUNCTION OF PERPENDICULAR ELECTRIC FIELD AND NEUTRAL He DENSITY. IN ALL CASES OF PEAK O^+ DENSITY WAS $2.1\times10^5\,cm^{-3}$ AND THE He^+ OUTFLOW VELOCITY WAS $0.5\,km\,s^{-1}$

N(He) factor	$E_\perp$(mVm^{-1})		
	0	50	100
1.00	1410	2026	3798
0.05	1414	2040	3870

at the highest perpendicular electric field strength since for that case the difference between $T(He^+)$ and T_n is greatest. The effect on the He^+ temperature of reducing the neutral He density is summarized in Table 2.

III.7 *Change of molecular nitrogen density*

In order to simulate the observed selective changes in molecular nitrogen density profiles which occur during periods of magnetic disturbance (Jacchia *et al.*, 1977), we increased the N_2 density profile to that for an exospheric temperature of 1500 K while maintaining the remaining neutral species at densities corresponding to 1000 K. The result of this change was to increase the N_2 density by a factor of 50 at 600 km and by larger factors above this altitude.

Our model He^+ profile was then computed for the standard background ionosphere with zero perpendicular electric field, but with the enhanced N_2 density. The result of increasing the loss to N_2 was to increase the height of the He^+ peak by approximately 150 km, reduce the peak density by a factor of 2, and reduce the limiting He^+ escape flux by about a factor of 1.5. The relatively small effect on the He^+ density and escape flux of the enhanced loss to N_2 results from the fact that the greatest increases in the loss rate occur at and above the altitude of the He^+ peak. At these altitudes He^+ production and diffusion are the dominant processes affecting the density profile. This is in contrast to the situation at the altitude of the H^+ peak density, where loss is competitive with production and diffusion.

III.8 *Change of F_2 peak O^+ density*

In order to study situations more typical of the mid-latitude trough, we computed He^+ profiles for a background ionosphere with a peak O^+ density of $2.1\times10^4\,cm^{-3}$, which is a factor of 10 lower than our standard value. Such trough-like O^+ densities are often associated with strong perpendicular electric fields, so we studied the effect of changing the O^+ peak density for the case of a $100\,mVm^{-1}$ perpendicular electric field.

The He^+ density profiles are shown in Fig. 7(a), where $N(He^+)$ for O^+ peak densities of $2.1\times10^5\,cm^{-3}$ and $2.1\times10^4\,cm^{-3}$ are shown for He^+ outflow velocities of 0.1, 0.5 and $2.5\,km\,s^{-1}$. At altitudes above the He^+ peak the fractional reduction in $N(He^+)$ as the O^+ peak density is reduced

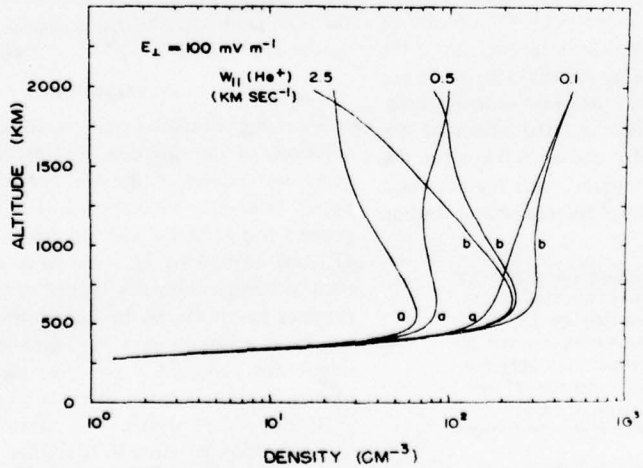

FIG. 7(a). THEORETICAL He^+ DENSITY PROFILES AS A FUNCTION OF ALTITUDE FOR UPPER BOUNDARY He^+ VELOCITIES OF 0.1, 0.5 AND $2.5\,km\,s^{-1}$ AND FOR A PERPENDICULAR ELECTRIC FIELD OF $100\,mVm^{-1}$. The profiles labelled (a) correspond to a peak O^+ density of $2.1\times10^4\,cm^{-3}$, while those labelled (b) correspond to the standard value of $2.1\times10^5\,cm^{-3}$ for the O^+ peak density. In all cases the H^+ outflow velocity was $10\,km\,s^{-1}$.

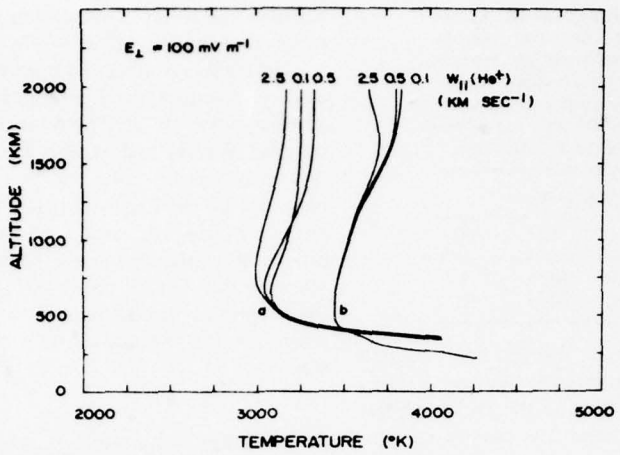

FIG. 7(b). THEORETICAL He$^+$ TEMPERATURE PROFILES AS A FUNCTION OF ALTITUDE FOR THE SAME He$^+$ UPPER BOUNDARY CONDITIONS AND IONOSPHERIC PARAMETERS AS FIG. 7(a).
The profiles labelled (a) correspond to the lower peak O$^+$ density.

increases with increasing He$^+$ outflow velocity. When $N(O^+)$ is reduced the outflowing He$^+$ meets less resistance and the altitude at which diffusion dominates moves lower. This results in a larger He$^+$ outflow velocity and, since the flow is flux limited, a reduced He$^+$ density. However, we have imposed fixed upper boundary He$^+$ velocities and therefore, the slight difference in upper boundary He$^+$ densities reflects the insensitivity of the He$^+$ escape flux to the background O$^+$ density profile.

The corresponding He$^+$ temperature profiles are shown in Fig. 7(b) where $T(He^+)$ is plotted against altitude for both the standard peak O$^+$ density of 2.1×10^5 cm^{-3} and the reduced density of 2.1×10^4 cm^{-3}. At all altitudes above 400 km the lower peak O$^+$ density results in lower He$^+$ temperatures. The shapes of the profiles and the effect of the outflow velocity also differ above 500 km for the low peak O$^+$ density compared with the standard ionosphere. This results from the collisional cooling to O$^+$ being lower, and the influence of the flow terms and thermal conduction being greater for the reduced O$^+$ density. It should be noted that Joule heating due to He$^+$ outflow is still not a significant heat source.

Below 400 km the He$^+$ temperature is higher for the reduced O$^+$ density. In this region much of the heating of the He$^+$ ions comes from frictional heating with the neutral atmosphere. When O$^+$ is lower in density this reduces an important cooling term and so the He$^+$ ions settle at a higher temperature.

The effect on the He$^+$ temperature of reducing the O$^+$ peak density by a factor of 10 is summarized in Table 3.

TABLE 3. He$^+$ TEMPERATURES (K) AT THE UPPER BOUNDARY OF THE MODEL (2000 km) AS A FUNCTION OF O$^+$ PEAK DENSITY AND He$^+$ OUTFLOW VELOCITY. IN ALL CASES THE PERPENDICULAR ELECTRIC FIELD WAS 100 mVm^{-1} AND THE H$^+$ OUTFLOW VELOCITY WAS 10 km s^{-1}

$N(O^+)$ peak (cm^{-3})	$W_{||}$(He$^+$), km s^{-1}		
	0.1	0.5	2.5
2.1×10^5	3831	3798	3643
2.1×10^4	3265	3340	3178

IV. CONCLUSION

We have obtained self-consistent steady state solutions of the coupled He$^+$ continuity, momentum, and energy equations for a range of He$^+$ upper boundary velocities and a range of background ionospheres with an ionic composition of O$^+$ and outflowing H$^+$. We have also considered neutral helium densities typical of both winter and summer hemispheres. In formulating the equations we have assumed that He$^+$ is a minor ion, and under this assumption we have identified the following features related to outflowing He$^+$ ions:

(i) The shape of the He$^+$ density profile as a function of altitude is similar to that for H$^+$, showing a peak density at about 600 km.
(ii) The He$^+$ density, velocity and temperature profiles are negligibly affected by a change in the H$^+$ outflow velocity from 10 km s^{-1} to 5 km s^{-1}.

(iii) The effect of changing the perpendicular electric field is quite different for He^+ compared to H^+. Changes in O^+ density results only in changes in the diffusion velocity for He^+, while for H^+ the outward flux is also changed as a result of O^+ being a source for H^+ ions through the change exchange reaction $O^+ + H \rightleftarrows H^+ + O$.

(iv) The rapid increase in He^+ outflow velocity occurs at about 1300 km compared to about 800 km for H^+ ions.

(v) As a consequence of (iv) Joule heating for the outflowing He^+ is much less significant than for H^+, resulting in lower He^+ ion temperatures and less dependence on the He^+ outflow velocity.

(vi) The He^+ ion temperature is most strongly controlled by the O^+ ion temperature, particularly below about 1300 km.

(vii) The effect of reducing neutral helium densities from winter to summer hemisphere values is to scale the He^+ density linearly. The effect on He^+ temperature profiles is minimal.

(viii) The effect on the He^+ density profile of an enhancement in the N_2 density of a factor of 50 at 600 km, as observed during substorms, is to reduce the peak He^+ density by a factor of 2 and decrease the limiting He^+ escape flux by approximately a factor of 1.5.

(ix) The effect of reducing the peak O^+ ion density by a factor of 10 is to increase He^+ outflow velocities and consequently decrease He^+ densities in the altitude range where diffusion is dominant. At most altitudes the He^+ ions receive less heat as a result of the reduced O^+ densities, which results in lower He^+ temperatures. At the lower boundary where heating due to perpendicular electric fields is more effective, the smaller O^+ cooling results in higher He^+ temperature.

(x) The limiting He^+ escape flux is little affected by a change in the peak O^+ density by a factor of 10. A decrease in neutral helium densities by a factor of 20 at all altitudes resulted in a factor of 20 reduction in the limiting He^+ escape flux.

The limiting He^+ escape flux of 5×10^6 cm $^{-2}$ s $^{-1}$ that we have computed for winter hemisphere conditions is consistent with the escape fluxes computed by Banks and Holzer (1969) using a much more restricted theoretical treatment. Since the original studies of terrestrial He loss by Axford (1968) and Johnson and Axford (1969) were based upon the Banks and Holzer (1969) He^+ escape fluxes, the seasonal change in the limiting He^+ escape flux that we have calculated should have great impact on these studies.

The large seasonal variation in neutral helium density at high latitudes suggests that further direct measurements of the properties of He^+ ions in the topside ionosphere would be useful to increase our understanding of seasonal changes in ionsopheric composition. In particular, a direct measurement of the temperature of both He^+ and H^+ ions at latitudes where outflow is occurring would be helpful in testing the theoretical results presented in this paper.

Acknowledgement—This research was supported by Air Force Contract F19628-77-C-0011, NSF Grant ATM76-19792, and NASA Grant NSG-7289.

REFERENCES

Angerami, J. J. and Thomas, J. O. (1964). Studies of planetary atmospheres: 1. The distribution of electrons and ions in the Earth's exosphere. *J. geophys. Res.* **69,** 4537.

Axford, W. I. (1968). The polar wind and the terrestrial helium budget. *J. geophys. Res.* **73,** 6855.

Banks, P. M. and Holzer, T. E. (1969). High-latitude plasma transport: The polar wind. *J. geophys. Res.* **74,** 6317.

Banks, P. M. and Kockarts, G. (1973). *Aeronomy.* Academic Press, New York.

Banks, P. M., Schunk, R. W. and Raitt, W. J. (1974). Temperature and density structure of thermal proton flows. *J. geophys. Res.* **79,** 4691.

Bauer, S. J. (1963). Helium ion belt in the upper atmosphere. *Nature, Lond.* **197,** 36.

Breig, E. L. and Hoffman, R. A. (1975). Variations in ion composition at middle and low latitudes from Isis 2 satellite. *J. geophys. Res.* **80,** 2207.

Brinton, H. C., Grebowsky, J. M. and Mayr, H. G. (1971). Altitude variation of ion composition in the mid-latitude trough region: Evidence for upward plasma flow. *J. geophys. Res.* **76,** 3738.

Hagen, J. B. and Hsu, P. Y. (1974). The structure of the protonosphere above Arecibo. *J. geophys. Res.* **79,** 4269.

Hanson, W. B. (1962). Upper atmosphere helium ions. *J. geophys. Res.* **67,** 183.

Hoffman, J. H., Dodson, W. H., Lippincott, C. R. and Hammack, H. D. (1974). Initial ion composition results from the ISIS 2 satellite. *J. geophys. Res.* **79,** 4246.

Jacchia, L. G. (1964). Static diffusion models of the upper atmosphere with empirical temperature profiles. *Res. Space Sci.* (Smithson. Astrophys. Obs. Spec. Rep.) **170,** 53.

Jacchia, L. G., Slowey, J. W. and von Zahn, U. (1977). Temperature, density, and composition in the disturbed thermosphere from ESRO 4 gas analyzer measurements: A global model. *J. geophys. Res.* **82,** 684.

Johnson, H. E. and Axford, W. I. (1969). Production and loss of He^3 in the Earth's atmosphere *J. geophys. Res.* **74,** 2433.

Kockarts, G. and Nicolet, M. (1963). L'Hélium et l'hydrogèn atomique au cours d'un minimum d'activite solaire. *Ann. Geophys.* **19,** 370.
Lemaire, J. (1972). O^+, H^+ and He^+ ion distributions in a new polar wind model. *J. atmos. terr. Phys.* **34,** 1647.
Mange, P. (1960). The distribution of minor ions in electrostatic equilibrium in the high atmosphere. *J. geophys. Res.* **65,** 3833.
Mauersberger, K., Kayser, D. C., Potter, W. E. and Nier, A. D. (1976a). Seasonal variation of neutral thermospheric constituents in the northern hemisphere. *J. geophys. Res.* **81,** 7.
Mauersberger, K., Potter, W. E. and Kayser, D. C. (1976b). A direct measurement of the winter helium bulge. *Geophys. Res. Lett.* **3,** 269.
Mayr, H. G., Fontheim, E. G., Brace, L. H., Brinton, H. C. and Taylor, H. A. (1972). A theoretical model of the ionosphere dynamics with interhemispheric coupling. *J. atmos. terr. Phys.* **34,** 1659.
Raitt, W. J., Schunk, R. W. and Banks, P. M. (1975). A comparison of the temperature and density structure in high and low speed thermal proton flows. *Planet. Space Sci.* **23,** 1103.
Raitt, W. J., Schunk, R. W. and Banks, P. M. (1977). The influence of convection electric fields on thermal proton outflow from the ionosphere. *Planet. Space Sci.* **25,** 291.
St-Maurice, J.-P. and Schunk, R. W. (1977). Diffusion and heat flow equations for the mid-latitude topside ionosphere. *Planet. Space Sci.* **25,** 907.
Schunk, R. W. (1975). Transport equations for aeronomy. *Planet. Space Sci.* **23,** 437.
Schunk, R. W. and Walker, J. C. G. (1969). Thermal diffusion in the topside ionosphere for mixtures which include multiply-charged ions. *Planet. Space Sci.* **17,** 853.
Schunk, R. W. and Walker, J. C. G. (1970). Thermal diffusion in the *F*2-region of the ionosphere. *Planet. Space Sci.* **18,** 535.
Shepherd, G. G., Whitteker, J. H., Winningham, J. D., Hoffman, J. H., Maier, E. J., Brace, L. H., Burrows, J. R. and Cogger, L. L. (1976). The topside magnetospheric cleft ionosphere observed from the ISIS 2 spacecraft. *J. geophys. Res.* **81,** 6092.
Taylor, H. A., Jr. (1972). The light ion trough. *Planet. Space Sci.* **20,** 1593.
Taylor, H. A., Brinton, H. C., Pharo, M. W., III and Rahman, N. K. (1968). Thermal ions in the exosphere; evidence for solar and geomagnetic control. *J. geophys. Res.* **73,** 5521.
Walker, J. C. G. (1965). Analytic representation of upper atmosphere densities based on Jacchia's static diffusion models. *J. atmos. Sci.* **22,** 462.
Walker, J. C. G. (1967). Thermal diffusion in the topside ionosphere. *Planet. Space Sci.* **15,** 1151.

APPENDIX

The momentum transfer collision frequencies (s^{-1}) are given by (Schunk, 1975).

$$\nu(He^+, N_2) = 1.60\times 10^{-9} N(N_2)$$

$$\nu(He^+, O_2) = 1.53\times 10^{-9} N(O_2)$$

$$\nu(He^+, O) = 1.01\times 10^{-9} N(O)$$

$$\nu(He^+, H) = 4.72\times 10^{-10} N(H)$$

$$\nu(He^+, He) = 6.46\times 10^{-11} N(He)[T(He^+)+T_n]^{1/2} \times [1.00 - 0.09\log_{10}(T(He^+)+T_n)]^2$$

$$\nu(He^+, H^+) = 0.285\frac{N(H^+)}{T^{3/2}(He^+, H^+)}$$

$$\nu(He^+, O^+) = 0.569\frac{N(O^+)}{T^{3/2}(He^+, O^+)}$$

$$\nu(He^+, e) = 0.008\frac{N_e}{T_e^{3/2}}.$$

The momentum transfer collision frequencies satisfy the relation $N(i)M(i)\nu(i,j) = N(j)M(j)\nu(j,i)$.

The velocity dependent correction factors are given by:

Non-resonant ion–neutral interactions

$$\Phi(i,j) = \Psi(i,j) = 1.$$

Resonant ion–neutral interactions

$$\Phi(i,j) = \frac{3\sqrt{\pi}}{8}\left[\varepsilon(i,j) + \frac{1}{\varepsilon(i,j)} - \frac{1}{4\varepsilon^3(i,j)}\right]\mathrm{erf}\,[\varepsilon(i,j)] + \frac{3}{8}\left[1 + \frac{1}{2\varepsilon^2(i,j)}\right]\exp[-\varepsilon^2(i,j)]$$

$$\Psi(i,j) = \frac{\sqrt{\pi}}{2}\left[\varepsilon(i,j) + \frac{1}{2\varepsilon(i,j)}\right]\mathrm{erf}\,[\varepsilon(i,j)] + \tfrac{1}{2}\exp[-\varepsilon^2(i,j)].$$

Coulomb

$$\Phi(i,j) = \frac{3\sqrt{\pi}}{4}\frac{\mathrm{erf}\,[\varepsilon(i,j)]}{\varepsilon^3(i,j)} - \frac{3}{2}\frac{\exp[-\varepsilon^2(i,j)]}{\varepsilon^2(i,j)}$$

$$\Psi(i,j) = \exp[-\varepsilon^2(i,j)],$$

where

$$\varepsilon(He^+, He) = \frac{[W_\parallel^2(He^+) + W_\perp^2]^{1/2}}{\left[\dfrac{2k(T(He^+)+T_n)}{M(He^+)}\right]^{1/2}}$$

$$\varepsilon(He^+, O^+) = \frac{|W_\parallel(He^+)|}{\left[\dfrac{5kT(He^+, O^+)}{2M(He^+)}\right]^{1/2}}$$

$$\varepsilon(He^+, H^+) = \frac{|W_\parallel(He^+) - W_\parallel(H^+)|}{\left[\dfrac{10kT(He^+, H^+)}{M(He^+)}\right]^{1/2}}$$

$$\varepsilon(He^+, e) = \frac{|W_{\parallel e} - W_\parallel(He^+)|}{(2kT_e/M_e)^{1/2}},$$

and

$$T(He^+, O^+) = [4T(He^+) + T(O^+)]/5$$

$$T(He^+, H^+) = [T(He^+) + 4T(H^+)]/5.$$

The velocity dependent correction factors are symmetric so that $\Phi(i,j) = \Phi(j,i)$ and $\psi(j,i) = \psi(i,j)$.

QUANTITATIVE CALCULATIONS OF HELIUM ION ESCAPE FLUXES FROM THE POLAR IONOSPHERES

W. J. Raitt, R. W. Schunk, and P. M. Banks

Center for Research in Aeronomy, Utah State University, Logan, Utah 84322

Abstract. Recent experimental measurements of He^+ outward fluxes have been obtained for winter and summer hemispheres. The observed fluxes indicate an average He^+ escape flux of 2×10^7 cm^{-2} s^{-1} in the winter hemisphere and a factor of 10-20 lower in the summer hemisphere. Earlier theoretical calculations had yielded winter fluxes a factor of 4 lower than the measured values and summer fluxes a further factor of 20 below the winter fluxes. We have attempted to reduce this discrepancy between our earlier theoretical model and the experimental observations by improving our theoretical model in the following ways. The helium photoionization cross sections used are accurate to 10%, the latest solar EUV fluxes measured by the Atmosphere Explorer satellites have been incorporated, and the most recent MSIS model of the neutral atmosphere is contained in the model. A range of conditions covering solar cycle, seasonal, and geomagnetic conditions were studied. The results show a maximum He^+ escape flux of 1.4×10^7 cm^{-2} s^{-1} for solar maximum, winter, low magnetic activity conditions, which is within the scatter of the measured fluxes. The computed summer He^+ escape flux is a factor of 20 lower than the winter value, a result which is in reasonable agreement with the summer experimental observations. Possible reasons for the slight discrepancy between theory and experiment in summer are discussed.

1. Introduction

The dynamics of He^+ ions in the F region of the terrestrial ionosphere and the resulting density, velocity, and temperature distributions were studied for a variety of ionospheric and atmospheric conditions in an earlier paper [Raitt et al., 1978], hereafter referred to as RSB. The motivation for making the earlier study was discussed in some detail by RSB; in summary, we felt that the inclusion of the temperature structure was important in predicting more accurate density distributions for help in mapping the plasmasphere by He^+ 304-Å resonantly scattered sunlight and also in updating the predictions of He^+ escape flux as an improvement

to understanding the terrestrial helium budget [Axford, 1968; Johnson and Axford, 1969].

The outcome of the RSB study was that the limiting He^+ escape flux was about 5×10^6 cm^{-2} s^{-1} in all of our winter models, and this was reduced by a factor of 20 for summer models. The summer/winter variation reflected the change in neutral helium density between the seasons, the so-called 'winter helium bulge,' which was neglected in earlier studies [Banks and Holzer, 1969].

Subsequent to our previous studies we were made aware of some recently analyzed measurements of He^+ outward flux from data taken on the Isis 2 satellite (J. H. Hoffman, private communication, 1977). These measurements of He^+ escape flux indicate an average value of 2×10^7 cm^{-2} s^{-1} at the winter pole and a factor of 6 lower at the summer pole. Thus a discrepancy of a factor of 4 exists between the earlier theoretical predictions and the recent experimental observations for the winter hemisphere, and an even larger discrepancy for the summer hemisphere.

In the present study we have improved our ionospheric-atmospheric model in an attempt to get better quantitative estimates of the behavior of He^+ at high latitudes. In the work of RSB it was shown that the H^+ outflow velocity and perpendicular electric field had little effect on the He^+ escape flux. Thus in this study we adopt a fixed background H^+-O^+ ionosphere with an H^+ outflow velocity of 10 km s^{-1}, typical of high-speed polar wind conditions, and no perpendicular electric field. The neutral atmospheric model has been improved by using the latest MSIS model atmosphere [Hedin et al., 1977a, b]. Helium photo-ionization cross sections accurate to 10% have been incorporated into the model as well as solar EUV fluxes measured on the Atmosphere Explorer satellites. In addition, we have taken into account the solar zenith angle change from summer to winter. Details of the improvements to the model are specified in more detail later.

The study covers a range of atmospheric-ionospheric conditions allowing for variations of geomagnetic activity, F_2 peak density, season, and solar cycle. Results for the He^+ escape flux as a function of these parameters are given in terms of typical velocity and density profiles. Temperature profiles for He^+ are not presented, since the results obtained are consistent with our previous study which showed that ion temperature changes with outflow velocity and other parameters are not as marked for He^+ as for H^+.

2. Atmosphere-Ionosphere Model

Basic Model

The basic features of the ionospheric model used are described fully by RSB. We assume an ionosphere of H^+, He^+, and O^+ ions and electrons with a background neutral atmosphere of H, He, O, O_2, and N_2. The H^+-O^+ ionospheric component is taken from a previous model [Raitt et al., 1977], and the He^+ properties are obtained from a steady state solution of the coupled continuity, momentum, and energy hydrodynamic equations for the case of outflow when He^+ is a minor ion. Account is taken of the velocity dependence of ion-neutral, ion-ion, and ion-electron collision frequencies. Nonlinear acceleration and parallel stress terms are retained in the He^+ momentum equation, and provision is made for the effect of perpendicular electric fields in the equations. We will not repeat the detailed formulation of the H^+-O^+ and He^+ ionospheric models but refer the reader to Raitt et al. [1977] and RSB, respectively.

Improvements to Basic Model

Helium ions are produced by photo-ionization of neutral He and lost in reactions with N_2:

$$He + h\nu \rightarrow He^+ + e \qquad (1)$$

$$He^+ + N_2 \rightarrow N^+ + N + He \qquad (2a)$$

$$He^+ + N_2 \rightarrow N_2^+ + He \qquad (2b)$$

In our initial study (RSB) the production rate $P(He^+)$ was assumed to be proportional to $N(He)$, and a proportionality constant of 8.16×10^{-8} s^{-1} was adopted from Banks and Kockarts [1973]. In the present study the He^+ production rate is calculated using the He photo-ionization cross section calculated by Stewart and Webb [1963], which agrees with the experimentally determined cross section of Baker et al. [1961] to within 10%, and by using the latest solar EUV fluxes obtained from the Atmosphere Explorer satellites [Hinteregger et al., 1978]. Additional details concerning the calculation of photo-ionization rates are given by Schunk and Walker [1973], as are the absorption cross sections for N_2, O_2, and O. As in our initial study, the rate coefficient for reaction (2) is taken to be $k_2 = 1.5 \times 10^{-9}$ cm^3 s^{-1} [Lindinger et al., 1974].

Our earlier He^+ theoretical model is further improved by the adoption of the MSIS model of the

neutral atmosphere [Hedin et al., 1977a, b]. This atmospheric model, which is based upon data obtained from five satellites and four incoherent scatter radar stations, produces neutral density profiles for a wide range of conditions, including solar cycle, seasonal, and geomagnetic variations.

The dependence of the solar zenith angle χ on the declination of the sun ζ, the geographic latitude ϕ, and local time is given by

$$\cos\chi = \sin\zeta \sin\phi + \cos\zeta \cos\phi \cos[2\pi(H-12)/24] \quad (3)$$

where H is the local time in decimal hours.

Range of Parameters Used

The solutions for the He^+ density, velocity, and temperature profiles were obtained for the steady state condition at noon local time and at a geographic latitude of 80^o. The magnetic field dip angle was assumed to be 90^o.

The range of magnetic activities used was defined by the index Ap, which was varied between 0 and 70 on the internationally established scale. These values are used in the determination of the MSIS atmospheric model and affect the neutral gas temperature, resulting in N_2 density changes of more than a factor of 100 at altitudes near the He^+ peak density. Since N_2 provides the dominant loss process for He^+, such a change might be expected to have a significant effect on the limiting He^+ escape flux. The F_2 peak density was allowed to change by a factor of 10 from 2×10^5 cm^{-3}, representing normal high-latitude values, to 2×10^4 cm^{-3} for an ionospheric trough condition. The seasonal effect from summer to winter was specified by choosing day 1 as winter and day 183 as summer to enable the MSIS model to compute the appropriate neutral species densities. We also changed the solar declination from 23^o to -23^o to allow for the change in solar zenith angle from summer to winter. Finally, we performed our calculations for both solar minimum and solar maximum conditions. The solar activity was specified by the 10.7-cm solar flux, which was set to vary from $F_{10.7} = 60 \times 10^{-22}$ W m^{-2} Hz^{-1} for solar minimum to $F_{10.7} = 150 \times 10^{-22}$ W m^{-2} Hz^{-1} for solar maximum. This parameter again affects the neutral atmosphere in the MSIS model. We also speculatively ran some cases with a change in the solar EUV flux by a factor of 2 from solar minimum to solar maximum.

We consider that these are limiting cases and bracket the range of He^+ escape fluxes which should be observed. The limits represent the boundaries with the most recent knowledge of the neutral atmosphere, EUV fluxes, and photoionization cross sections.

As is indicated above, most of the parameters act to change the neutral atmosphere. To illustrate the effects for the solar cycle, seasonal, and magnetic activity changes, Figures 1-2 show altitude profiles of the atmospheric species controlling the production and loss of He^+, where N(He) and $N(N_2)$ are plotted as functions of altitude. Figure 3 shows plots of the resulting He^+ production rate as a function of altitude. In all three figures the summer profiles are shown by dashed curves, and the winter profiles by solid curves; the labels 'high' and 'low' refer to the magnetic activity levels specified earlier.

It can be seen from Figure 1 that the greatest influence on the He density results from the seasonal effect, while Figure 2 shows that the solar cycle and magnetic activity changes have a large influence on the N_2 density. The effects on He^+ densities are folded into the production rate of He^+ shown in Figure 3. The groupings of the curves again indicate that the seasonal influence dominates near the winter peak production rate altitude; however, at high altitudes, particularly at solar minimum, the seasonal effect is equally important. The falloff in He^+ production at altitudes below about 300 km in the winter is due to the solar zenith angle effect attenuating and eventually cutting off the solar EUV flux.

3. Calculated He^+ Escape Fluxes

The fixed background H^+-O^+-electron ionosphere used in all the calculations except the trough case was a model with an F_2 peak density of 2×10^5 cm^{-3} and an H^+ outflow velocity of 10 km s^{-1} at 3000 km; the profiles of density and temperature for the background ionosphere are shown in Figure 1 of RSB.

It was found in our previous study (RSB) that the He^+ escape flux was not sensitive to perpendicular electric fields in the range 0-100 mV m^{-1}, so in order to reduce the number of parameters in this study we only considered the case for zero perpendicular electric field

The small effect of H^+ outflow velocity and F_2 peak density on the He^+ escape flux, as shown in our previous study, prompted us to keep the same background ionosphere for both solar maximum

and solar minimum and for both winter and summer. The results presented later for a reduced F_2 peak density were run more as a check on the effect of ionospheric troughs on the He^+ parameters than to reflect any solar cycle or seasonal effects.

As in the work of RSB, we computed the He^+ profiles over the altitude range 200-2000 km. We defined upper boundary velocities of 0.1, 0.5, and 2.5 km s^{-1} and assumed chemical equilibrium at the lower boundary. In all cases considered, we found that the escape flux had saturated by the time the upper boundary velocity was 0.5 km s^{-1} and so we will only present results for this boundary condition.

Standard Cases

The He^+ density and He^+ velocity profiles for our standard cases are shown in Figures 4 and 5, respectively. In both figures the convention of winter profiles having solid curves and summer profiles having dashed curves is again adopted. The He^+ density profiles in Figure 4 show that the seasonal effect dominates over the effect of magnetic activity. There is, however, still a significant change in He^+ density as the magnetic activity varies over the range discussed earlier. There is very little difference between solar maximum and solar minimum as far as the peak He^+ densities are concerned. The main solar cycle effect can be seen in the larger scale height above the peak at solar maximum. This is a consequence of the generally hotter atmosphere at solar maximum.

The He^+ velocity profiles in Figure 5 show very little change with any of the parameters we have considered. Thus the variation in He^+ density at the upper boundary closely reflects the changes in the He^+ outward flux.

The He^+ limiting fluxes computed for the standard background ionosphere are tabulated in Table 1. It can be seen that at low magnetic activity in winter during solar maximum we predict an He^+ escape flux as high as 1.35×10^7 cm^{-2} s^{-1} and as low as 0.99×10^5 cm^{-2} s^{-1} in summer at high magnetic activity during solar minimum. The ratios between winter and summer He^+ escape fluxes vary from 32 to 36 for high magnetic activity and from 23 to 25 for low magnetic activity. The He^+ escape fluxes during solar maximum are 1.5-2.0 times greater than those for solar minimum.

Effect of Doubling Solar EUV Flux

The solar EUV flux values used in the model calculations from the Atmosphere Explorer satellites [Hinteregger et al., 1978] were measured near solar minimum. Ionospheric modeling studies [Roble, 1976; Swartz and Nisbet, 1973] have shown that in order for their theoretical predictions to correspond to ionospheric experimental observations at solar maximum, the solar EUV fluxes should be doubled in comparison with the solar minimum fluxes.

We have repeated our solar maximum runs with the solar EUV fluxes doubled, and the He^+ escape fluxes resulting from this model are shown in Table 2. The He^+ outward flux does not increase linearly with solar EUV flux but increases by factors varying from 1.4 to 1.8 depending on the season and magnetic activity. The winter to summer ratios vary from 25 to 35 as the magnetic activity changes from low to high, that is, with the same magnitude as for the standard cases.

Effect of Changing N_mF_2

A reduction in the F_2 peak density from 2×10^5 cm^{-3} to 2×10^4 cm^{-3} in our background ionosphere while still maintaining an H^+ outflow velocity at the upper boundary of 10 km s^{-1} resulted in the He^+ outward fluxes shown in Table 3.

The relative He^+ outward fluxes in these cases are more complex than for other deviations from the standard model. For high magnetic activity the He^+ outward flux is decreased by factors from 0.8 to 0.9 for both seasonal and solar cycle conditions, while for low magnetic activity the outward flux is increased by factors from 1.08 to 2.06 for the same range of seasonal and solar cycle conditions.

Importance of Transport

The changing atmospheric and solar zenith angle effects for the range of conditions studied in the standard cases (Table 1) result in the peak of the He^+ density profile occurring at different altitudes. The actual peak altitudes are summarized in Table 4. There is a wide range of peak altitudes, varying from the lowest value of 460 km to the highest value of 820 km.

A study of the balance of terms in the continuity equation confirmed the result reported by RSB that the peak is determined by competition between He^+ production and He^+ transport processes. At the peak altitudes the loss to N_2

is insignificant in all cases. This is in contradiction to earlier suggestions [cf. Banks and Kockarts, 1973] that at the peak density, production and loss are essentially equal.

It is for this reason that while the He/N_2 density ratio at 300 km shows a variation of 3 orders of magnitude over extreme conditions of season, solar cycle, and magnetic activity, the variation in He^+ outward flux over the same conditions is only a factor of 25. At altitudes above 300 km the loss process to N_2 becomes of less and less importance, and large changes in N_2 density in response to atmospheric temperature changes following substorms and solar cycle changes do not have a proportionate effect on the He^+ outward flux.

Another feature worth noting about the mass transport of He^+ is that in all of our model calculations for the 0.5 km s^{-1} upper boundary outflow velocity the flow was subsonic at all altitudes. The maximum Mach number occurred in the altitude range 1600-1630 km and varied between 0.55 and 0.61.

4. Summary and Discussion of Results

We have improved the ionospheric model for computing the He^+ ion density, velocity, and temperature profiles over that presented by RSB by including the most recent values of atmospheric density and composition, solar EUV fluxes, and He photo-ionization cross sections. In addition, we have allowed for the different solar zenith angle effect between summer and winter. We have also utilized the result found by RSB that the He^+ outward flux is insensitive to perpendicular electric field strength and to the background H^+-O^+ ionosphere, to limit our present study to zero perpendicular electric field and to two background ionospheric models; one representative of the normal, high-latitude, daytime F region and the other representative of an ionospheric trough.

The predicted He^+ limiting escape flux shows a variation of about 2 orders of magnitude over the range of conditions studied, which encompassed extreme solar cycle, seasonal, and geomagnetic variations. The He^+ escape flux varies from a low value of 0.99×10^5 cm^{-2} s^{-1} for solar minimum, summer, high magnetic activity conditions to a maximum of $1\text{-}2 \times 10^7$ cm^{-2} s^{-1} for solar maximum, winter, low magnetic activity conditions. The variations are due primarily to changes in the neutral helium density. At the He^+ density profile peak the loss process to N_2

is not a significant term in the balance of the continuity equation, and so geophysical effects selectively changing the N_2 density in the 300- to 700-km altitude range do not have a large effect on the He^+ escape flux.

In comparing our theoretical values of the He^+ escape flux with recent experimental data (J. H. Hoffman, private communication, 1977) we find that good agreement is obtained between Hoffman's winter pole measurements of 1-2 x 10^7 cm^{-2} s^{-1} and our winter pole predictions for solar maximum and low magnetic activity. Hoffman's data were taken for a range of magnetic activities with $Kp \geq 0$ being the only specification. The time frame of 1972 was during the declining phase of a solar cycle, although there was a minor peak in solar activity in 1972. However, encouraging as the agreement of the theoretical and experimental He^+ escape fluxes is, we feel that more work needs to be done to extract average values of the escape flux to smooth out day to day variations which are no doubt influenced by day to day variations of the high-latitude neutral atmosphere.

The summer pole measurements made by Hoffman do not agree quite so well with the theoretical predictions. Hoffman measures summer He^+ escape fluxes of about 1 x 10^6 cm^{-2} s^{-1} during quiet magnetic conditions, while we predict escape fluxes of about 6 x 10^5 cm^{-2} s^{-1} for comparable conditions. Our result shows a reduction of a factor of about 20 in the He^+ escape flux from winter to summer, which is roughly in agreement with the measured ratio of neutral helium density at altitudes in the range 300-700 km between the summer and winter hemispheres. All of our calculations in this paper and those by RSB have indicated that the He^+ escape flux varies linearly with the neutral He density at low altitudes. It is possible that the remaining discrepancy between the theoretical predictions and experimental observations is due to differences in local time between the two sets of results.

We find the exospheric temperatures computed by the MSIS model to be generally in accord with experimentally observed values at appropriate combinations of solar cycle, season, and magnetic activity for which the experimental data have been published [cf. Kayser and Potter, 1976; Hedin et al., 1977a]. The only case in question is for solar minimum, winter, magnetically quiet conditions when the model predicts exospheric temperatures of about 500°K. However, this is not one of our bracketing cases for the range of He^+ escape fluxes in our predictions. Apart

from running the MSIS model atmosphere to its extreme limits, we feel that since the He^+ model incorporates the latest atmospheric, solar flux, and photo-ionization cross sections, the He^+ escape fluxes predicted represent the best values available at this time.

Acknowledgements. We thank A. E. Hedin for a computer code which calculates the neutral densities, and we thank A. F. Nagy for useful discussions concerning the He photo-ionization cross section. This research was supported by Air Force contract F19628-77-C-0011, NSF grant ATM76-19792, and NASA grant NSG-7289.

The Editor thanks T. E. Holzer and J. H. Hoffman for their assistance in evaluating this paper.

References

Axford, W. I., The polar wind and the terrestrial helium budget, J. Geophys. Res., 73, 6855-6859, 1968.

Baker, D. J., D. E. Bedo, and D. H. Tomboulian, Phys. Rev., 124, 1471, 1961.

Banks, P. M., and T. E. Holzer, High-latitude plasma transport: The polar wind, J. Geophys. Res., 74, 6317-6332, 1969.

Banks, P. M., and G. Kockarts, Aeronomy, Academic, New York, 1973.

Hedin, A. E., J. E. Salah, J. V. Evans, C. A. Reber, G. P. Newton, N. W. Spencer, D. C. Kayser, D. Alcaydé, P. Bauer, L. Cogger, and J. P. McClure, A global thermospheric model based on mass spectrometer and incoherent scatter data, MSIS 1, N_2 density and temperature, J. Geophys. Res., 82, 2139-2147, 1977a.

Hedin, A. E., C. A. Reber, G. P. Newton, N. W. Spencer, H. C. Brinton, H. G. Mayr, and W. E. Potter, A global thermospheric model based on mass spectrometer and incoherent scatter data, MSIS 2, Composition, J. Geophys. Res., 82, 2148-2156, 1977b.

Hinteregger, H. E., D. E. Bedo, J. E. Manson, and D. B. Stillman, EUV flux variations with solar rotation observed during 1974-1976 from AE satellites, C, D, and E, Space Res., 17, in press, 1978.

Johnson, H. E., and W. I. Axford, Production and loss of He^3 in the earth's atmosphere, J. Geophys. Res., 74, 2433-2438, 1969.

Kayser, D. C., and W. E. Potter, Molecular oxygen measurements at 200 km from AE-D near winter solstice, 1975, Geophys. Res. Lett., 3, 455-458, 1976.

Lindinger, W., F. C. Fehsenfeld, A. L. Schmeltekopf, and E. E. Ferguson, Temperature dependence of some ionospheric ion-neutral reactions from 300°-900°K, J. Geophys. Res., 79, 4753-4756, 1974.

Raitt, W. J., R. W. Schunk, and P. M. Banks, The influence of convection electric fields on thermal proton outflow from the ionosphere, Planet. Space Sci., 25, 291-301, 1977.

Raitt, W. J., R. W. Schunk, and P. M. Banks, Helium ion outflow from the terrestrial ionosphere, Planet. Space Sci., 26, 255-268, 1978.

Roble, R. G., Solar EUV flux variation during a solar cycle as derived from ionospheric modeling considerations, J. Geophys. Res., 81, 265-269, 1976.

Schunk, R. W., and J. C. G. Walker, Theoretical ion densities in the lower ionosphere, Planet. Space Sci., 21, 1875-1896, 1973.

Stewart, A. L., and T. G. Webb, Photo-ionization of helium and ionized lithium, Proc. Phys. Soc. London, 82, 532, 1963.

Swartz, W. E., and J. S. Nisbet, Incompatibility of solar EUV fluxes and incoherent scatter measurements at Arecibo, J. Geophys. Res., 78, 5640, 1973.

(Received February 27, 1978;
revised May 12, 1978;
accepted May 23, 1978.)

Fig. 1. Profiles of He density versus altitude for solar maximum and solar minimum, for summer (dashed curves) and winter (solid curves), and for high and low geomagnetic activity. These density profiles were calculated from the MSIS model of the neutral atmosphere [Hedin et al., 1977a, b].

Fig. 2. Profiles of N_2 density versus altitude for solar maximum and solar minimum, for summer (dashed curves) and winter (solid curves), and for high and low geomagnetic activity. These density profiles were calculated from the MSIS model of the neutral atmosphere [Hedin et al., 1977a, b].

Fig. 3. Profiles of the He^+ production rate versus altitude for solar maximum and solar minimum, for summer (dashed curves) and winter (solid curves), and for high and low geomagnetic activity.

Fig. 4. Theoretical He^+ density profiles as a function of altitude for solar maximum and solar minimum, for summer (dashed curves) and winter (solid curves), and for high and low geomagnetic activity. For all cases the He^+ outflow velocity at the upper boundary was set equal to 0.5 km s^{-1}.

Fig. 5. Theoretical He^+ velocity profiles as a function of altitude for solar maximum and solar minimum, for summer (dashed curves) and winter (solid curves), and for high and low geomagnetic activity. These He^+ velocity profiles correspond to the He^+ density profiles shown in Figure 4.

TABLE 1. Limiting He^+ Escape Fluxes in Square Centimeters per Second

Geomagnetic Activity	Solar Maximum		Solar Minimum	
	Summer	Winter	Summer	Winter
High	1.61(5)	5.07(6)	0.99(5)	3.54(6)
Low	5.97(5)	1.35(7)	3.02(5)	7.40(6)

TABLE 2. Limiting He^+ Escape Fluxes in Square Centimeters per Second for Solar Maximum Conditions

Geomagnetic Activity	Summer	Winter
High	2.22(5)	7.87(6)
Low	9.67(5)	2.49(7)

These escape fluxes were calculated by doubling the solar EUV fluxes measured by Hinteregger et al. [1977].

TABLE 3. Limiting He^+ Escape Fluxes in Square Centimeters per Second for a Background Ionosphere With $N_m F_2 = 2 \times 10^4$ cm^{-3}

Geomagnetic Activity	Solar Maximum		Solar Minimum	
	Summer	Winter	Summer	Winter
High	1.34(5)	4.63(6)	7.61(4)	3.19(6)
Low	6.45(5)	1.64(7)	6.21(5)	1.18(7)

TABLE 4. Altitude in Kilometers of the He^+ Peak Density

Geomagnetic Activity	Solar Maximum		Solar Minimum	
	Summer	Winter	Summer	Winter
High	820	680	640	580
Low	630	530	460	460

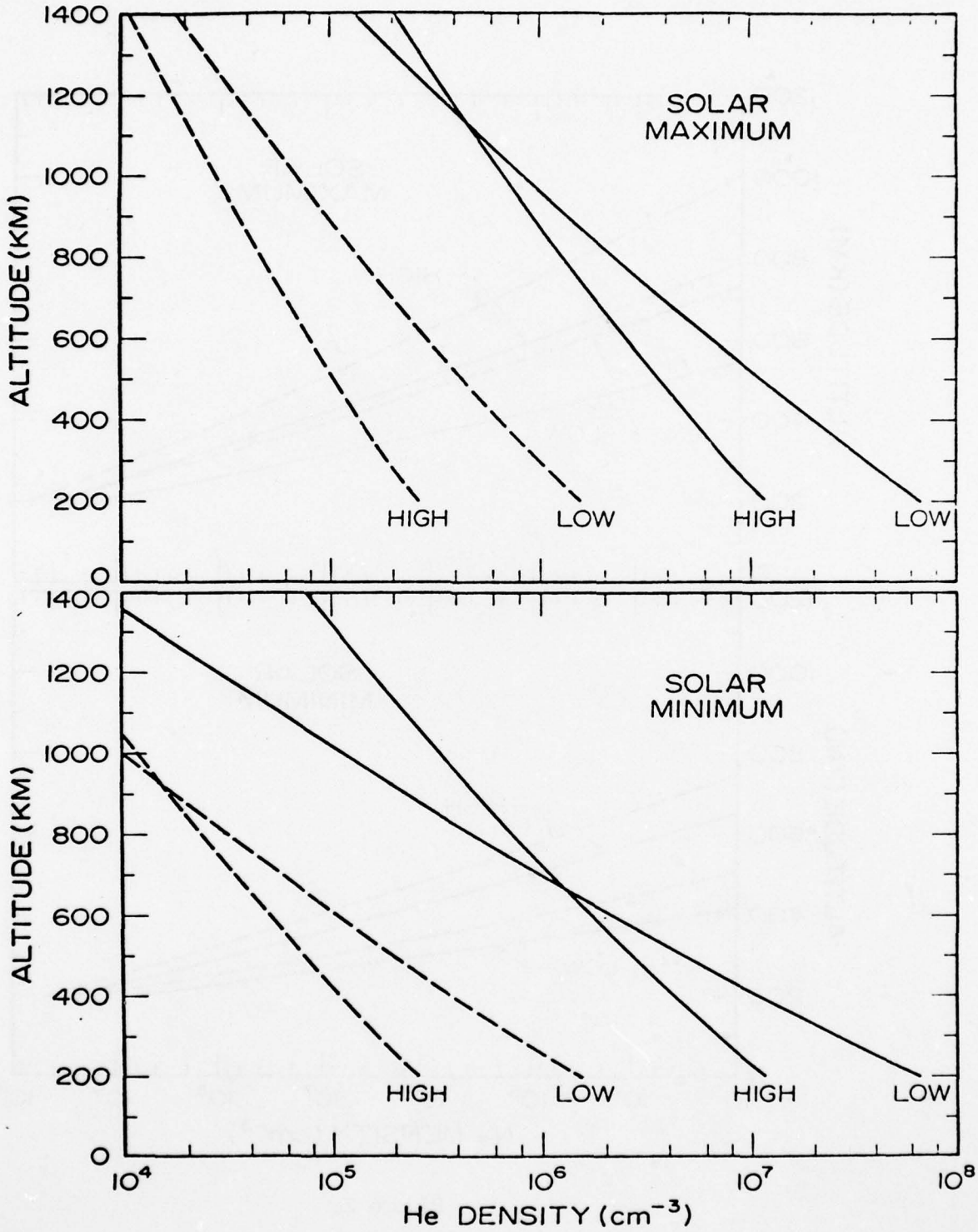
SOLAR
MAXIMUM
HIGH
LOW
HIGH
LOW
SOLAR
MINIMUM
HIGH
LOW
HIGH
LOW
ALTITUDE (KM)
ALTITUDE (KM)
0
200
400
600
800
1000
1200
1400
10^4
10^5
10^6
10^7
10^8
He DENSITY (cm^{-3})

Figure 1

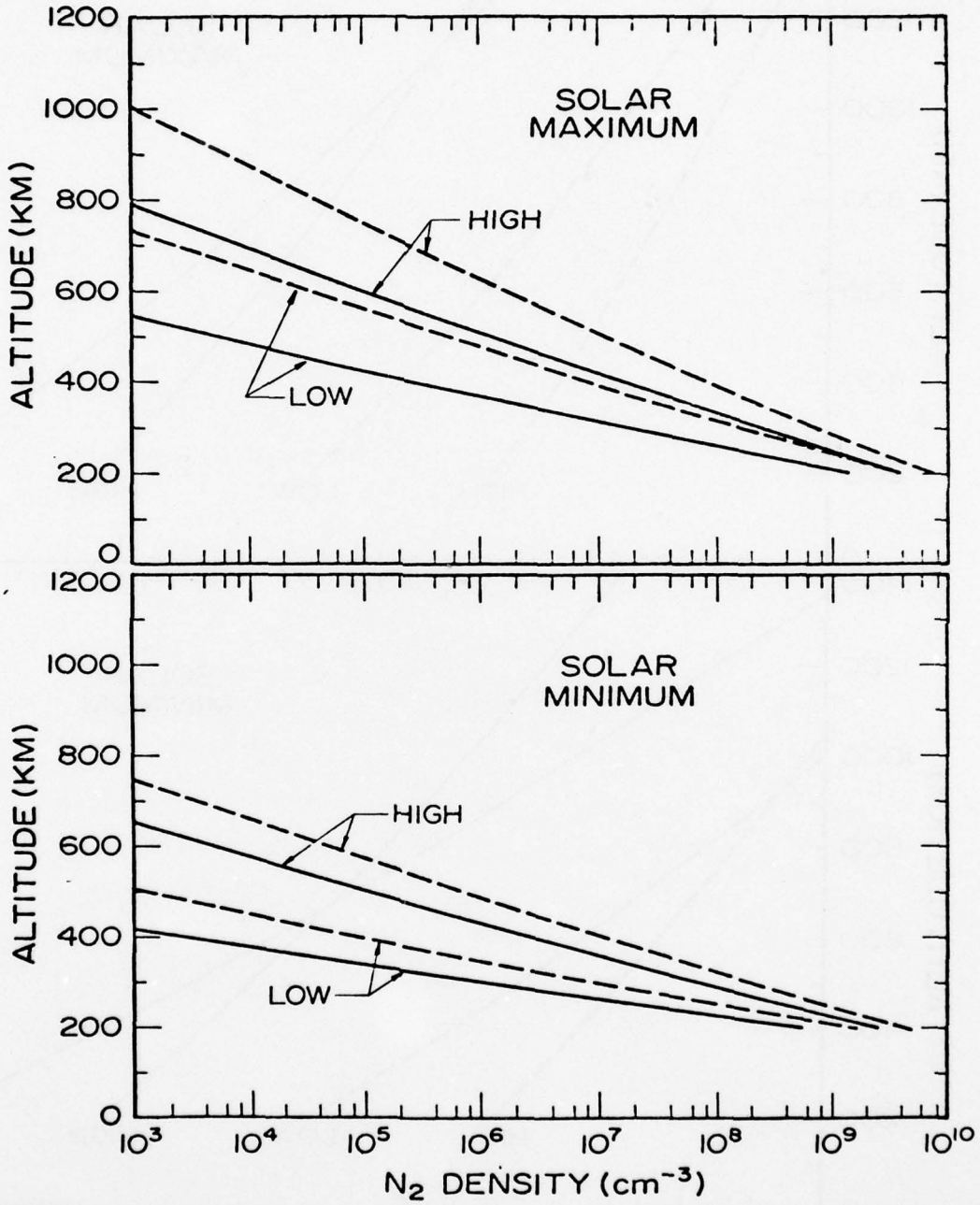
SOLAR
MAXIMUM
HIGH
LOW
ALTITUDE (KM)
1200
1000
800
600
400
200
0
SOLAR
MINIMUM
HIGH
LOW
ALTITUDE (KM)
1200
1000
800
600
400
200
0
10^3
10^4
10^5
10^6
10^7
10^8
10^9
10^{10}
N_2 DENSITY (cm^{-3})

Figure 2

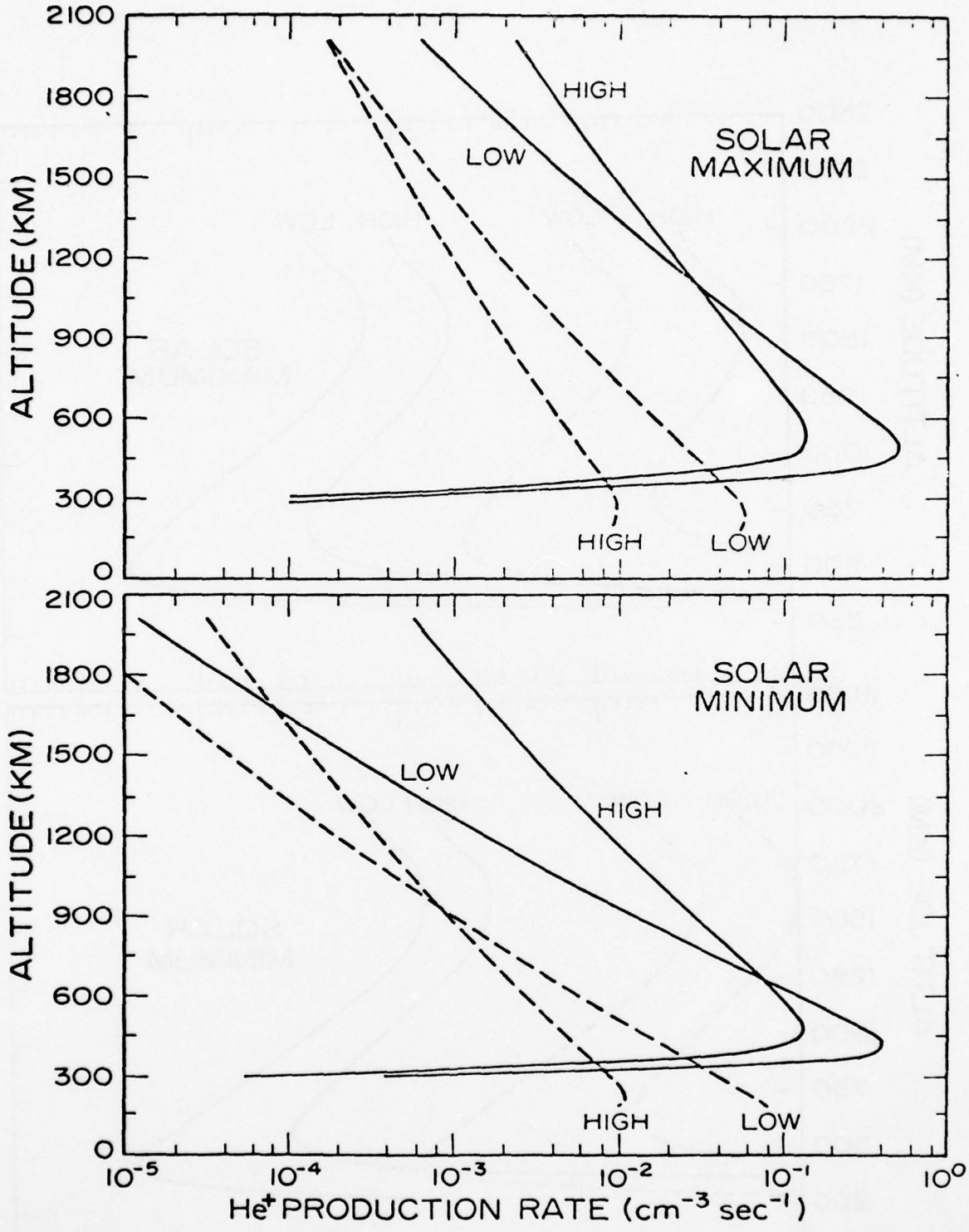
SOLAR MAXIMUM
HIGH
LOW
HIGH
LOW
SOLAR MINIMUM
LOW
HIGH
HIGH
LOW
ALTITUDE (KM)
2100
1800
1500
1200
900
600
300
0
10^{-5}
10^{-4}
10^{-3}
10^{-2}
10^{-1}
10^{0}
He^{+} PRODUCTION RATE (cm^{-3} sec^{-1})

Figure 3

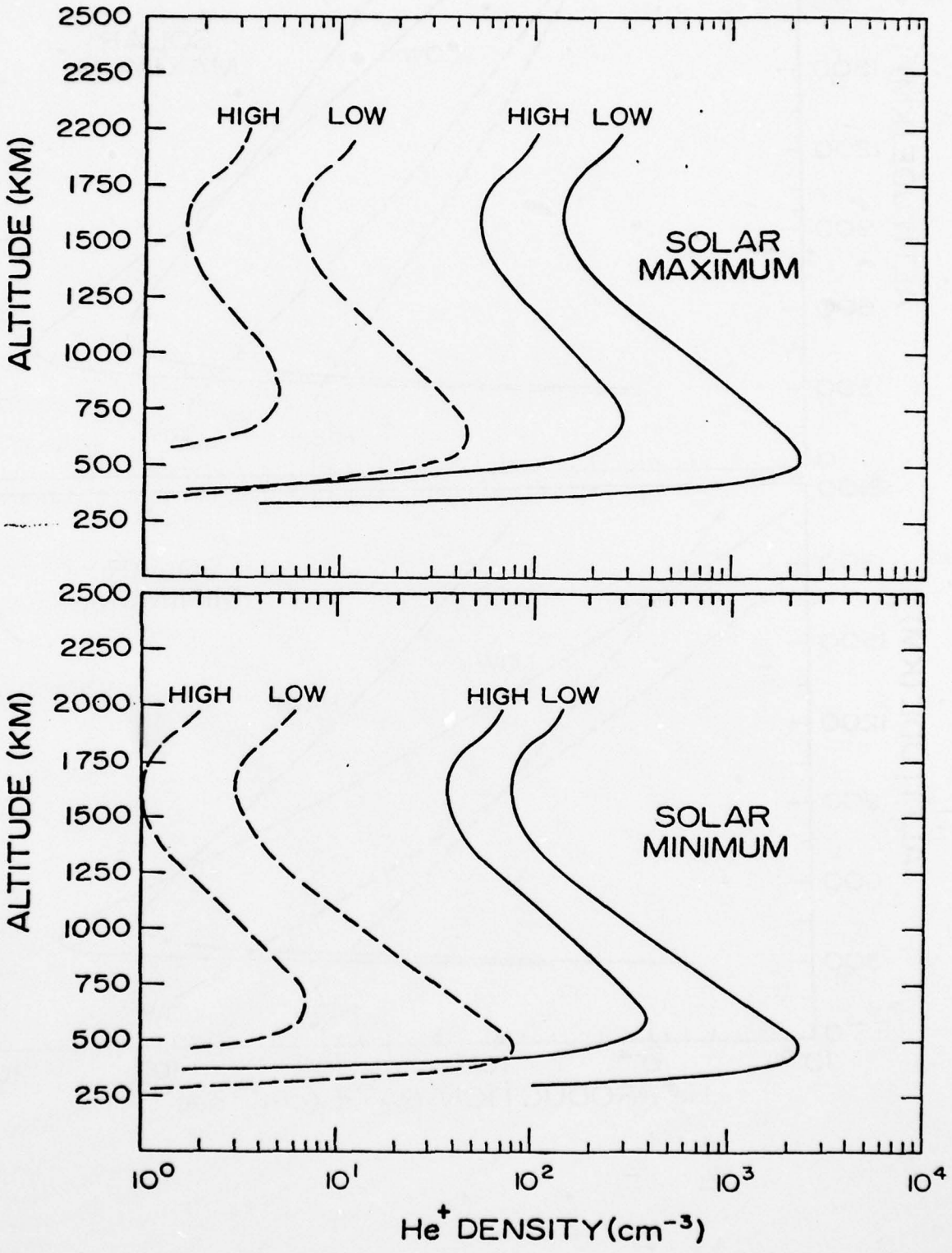
ALTITUDE (KM)
2500
2250
2200
1750
1500
1250
1000
750
500
250
HIGH
LOW
HIGH
LOW
SOLAR
MAXIMUM
ALTITUDE (KM)
2500
2250
2000
1750
1500
1250
1000
750
500
250
HIGH
LOW
HIGH
LOW
SOLAR
MINIMUM
10^0
10^1
10^2
10^3
10^4
He^+ DENSITY (cm^{-3})

Figure 4

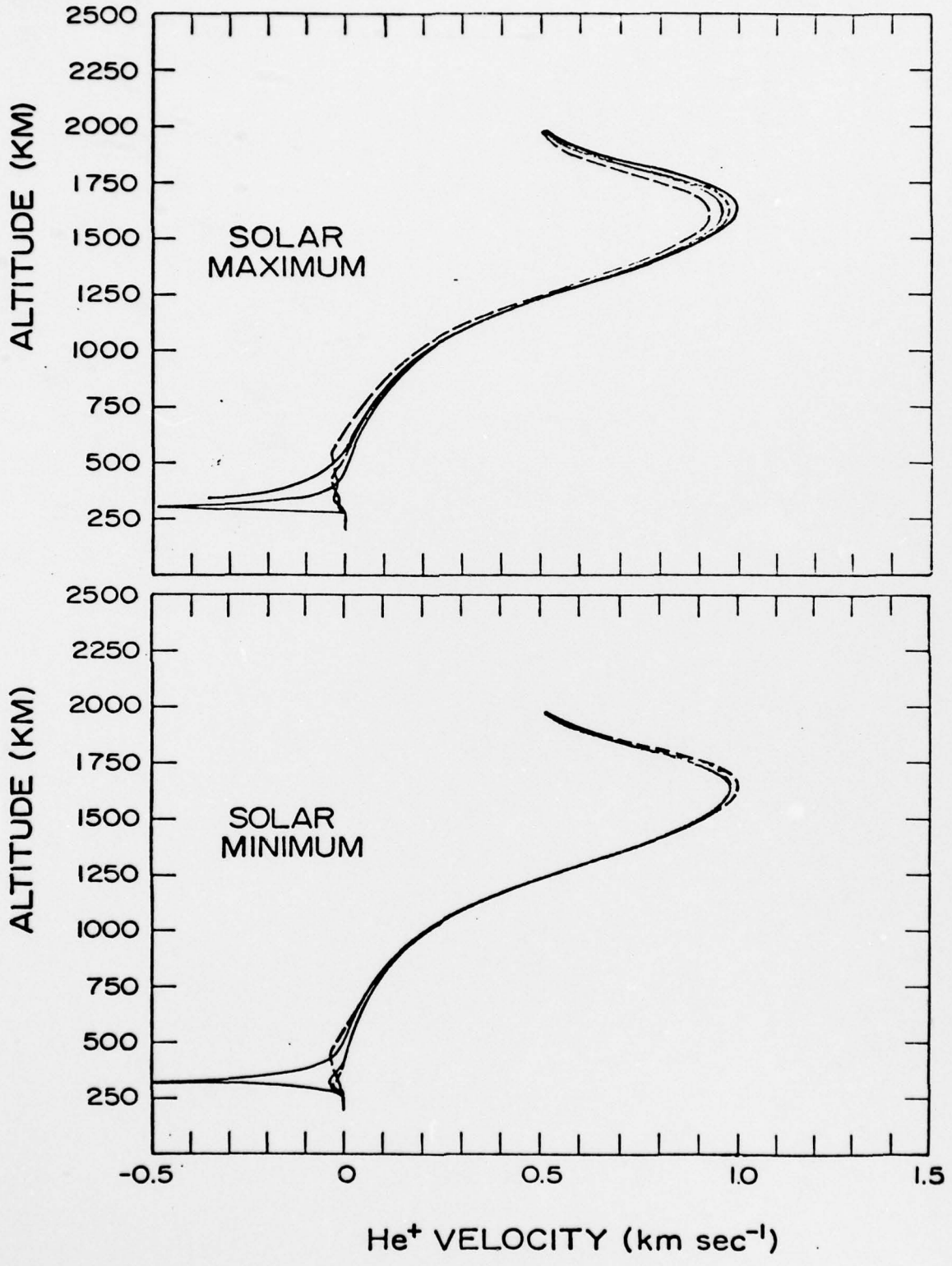
2500
2250
2000
1750
1500
1250
1000
750
500
250
ALTITUDE (KM)
SOLAR
MAXIMUM
SOLAR
MINIMUM
-0.5
0
0.5
1.0
1.5
He+ VELOCITY (km sec-1)

Figure 5